REMOTE SENSING OF TROPICAL COASTAL WATERS: STUDY OF THE BERAU ESTUARY, EAST KALIMANTAN, INDONESIA

Wiwin Ambarwulan

September 2010

Examining Committee:

prof.dr. F.D. van der Meer	University of Twente
prof.dr. A.K. Skidmore	University of Twente
prof.dr. P. Hoekstra	Utrecht University
prof.dr.ir. J. Sopaheluwakan	Indonesian Institute of Sciences

UNIVERSITY OF TWENTE.

ITC FACULTY OF GEO-INFORMATION SCIENCE AND EARTH OBSERVATION

REMOTE SENSING OF TROPICAL COASTAL WATERS: STUDY OF THE BERAU ESTUARY, EAST KALIMANTAN, INDONESIA

DISSERTATION

to obtain
the degree of doctor at the University of Twente,
on the authority of the rector magnificus,
prof.dr. H. Brinksma,
on account of the decision of the graduation committee,
to be publicly defended
on Friday, September 3, 2010 at 16:45 hrs

by

Wiwin Ambarwulan

born in Jakarta, Indonesia
on June 29, 1960

This thesis is approved by

Prof. Dr. Ing. Wouter Verhoef, promotor

Dr. Ir. Chris M.M. Mannaerts, assistant promotor

Acknowledgements

List of Acronyms

ANN	:	Artificial Neural Network
AOP	:	Apparent Optical Property
AATSR	:	Advanced Along-Track Scanning Radiometer
ASAR	:	Advanced Synthetic Aperture Radar
ATSR	:	Along-Track Scanning Radiometer
ATBD	:	Algorithm Theoretical Basis Document
BEAM	:	Basic ENVISAT Toolbox for (A)ATSR and MERIS
Chl-*a*	:	Chlorophyll a pigment
C2R	:	Case-2 Regional
CDOM	:	Colored Dissolved Organic Matter
CZCS	:	Coastal Zone Color Scanner
BAKOSURTANAL	:	*Badan Koordinasi Survei dan Pemetaan Nasional* - National Coordinating Agency for Surveys and Mapping
ERS	:	European Remote Sensing Satellite
BMG	:	*Badan Meteorologi dan Geofisika* - Meteorological and Geophysical Agency
EKP	:	East Kalimantan Program
ENVISAT	:	European Environmental Satellite
ESDM	:	*Energi Sumberdaya Mineal* - Indonesian ministry of Energy and Mineral Resources
ESA	:	European Space Agency
FR	:	Full Resolution
FUB	:	Free University Berlin
FWHM	:	Full-Width at Half Maximum
GF/F	:	Glass Fiber/ Filter
GPS	:	Global Positioning System
GSM	:	Garver-Siegel-Maritorena
HYDROPT	:	HYDROLIGHT OPTimization
ICoMaR	:	Indonesian Consortium on Coastal and Marine Research
IOP	:	Inherent Optical Property

IOCCG	:	International Ocean Color Coordinating Group
IRS-1C		Indian Remote Sensing satellite
ITB.	:	*Institut Teknologi Bandung* - Bandung Institute of Technology -
ITF	:	Indonesia Through-Flow
K-M	:	Kubelka-Munk
KNAW	:	*Koninklijke Nederlandse Academie van Wetenschappen* - Royal Netherlands Academy of Arts and Sciences
LAPAN	:	*Lembaga Penerbangan dan Antariksa Nasional* - National Institute for Aeronautics and Space -
LIPI	:	*Lembaga Ilmu Pengetahuan Indonsia* - Indonesian Institute of Science
LTOA	:	Top-Of-Atmosphere total radiance
LUT	:	Look-Up Table
MERIS	:	Medium Resolution Imaging Spectrometer
MODIS	:	Moderate Resolution Imaging Spectroradiometer
MODTRAN	:	MODerate spectral resolution atmospheric TRANsmittance
MPA	:	The Berau Marine Protected Area
NASA	:	National Space Agency
NIOZ	:	*Koninklijk Nederlands Instituut voor Zeeonderzoek* - Royal Netherlands Institute for Sea Research
NWO	:	NWO-Earth and Life Sciences (ALW),
pH	:	the degree of acidity or basicity of a solution
QAA	:	Quasi Analytical Algorithm
RGB	:	Red Green Blue
RMSE	:	Root Mean Square Error
RR	:	Reduced Resolution
REVAMP	:	Regional Validation of MERIS Chlorophyll products in North Sea coastal waters.
ROFI	:	Region of Fresh water Influence
SDA	:	spectral decomposition algorithm
SIOP	:	Specific Inherent Optical Property
SeaWiFS	:	Sea-viewing Wide Field-of-view Sensor

SMAC	:	Simplified Method for Atmospheric Correction
SRTM	:	Shuttle Radar Topography Mission
SUKM	:	Spectral unmixing with the coupled radiative transfer model and inverse K-M model
6S	:	Second Simulation of the Satellite Signal in the Solar Spectrum
TOW	:	Top-of-Water
TOA	:	Top-of-Atmosphere
TSM	:	Total Suspended Matter
UNESCO.	:	The United Nations Educational, Scientific and Cultural Organization
UNMUL,	:	Universitas Mulawarman - Mulawarman University in Samarinda -
VISAT	:	BEAM's visualisation, analysing and processing application
WOTRO	:	Foundation for the Advancement of Tropical Research
WWF	:	World Wide Fund for Nature

List of Symbols

Symbol	Description
a_{CDOM}	Absorption of CDOM
$a(\lambda)$	Absorption coefficients
$a_w(\lambda)$	Absorption of pure water
a_x^*	Specific absorption spectra of TSM or particle
a_y^*	Specific absorption spectra of CDOM
$a_w(\lambda)$	Absorption and scattering of water molecules,
a_{Chl}^* or a_i^*	Specific absorption spectra of phytoplankton
a_1	Amount of haze above the standard in arbitrary units
a_2	Amount of sediment in arbitrary units
A	Spherical albedo
$b_b(\lambda)$	Backscattering coefficients
$b_{b,w}(\lambda$	Backscattering coefficients of pure water
$b_{b,TSM}$	Backscattering coefficient of particle or TSM
$b_{b,S}^*$	Specific backscattering coefficient of small particles
$b_{b,L}^*$	Specific backscattering coefficient of large particles
$b_{b,TSM}^*$	Specific backscattering coefficient of TSM
C_{Chl} or C_i or C_{ph}	Concentration of phytoplankton
C_{TSM}	Concentration of TSM
C_S	Concentration of small particle
E_u^-	Upward irradiance just beneath the water surface
E_d^-	Downward irradiance just beneath the water surface
E_d^+	Downward irradiance just above the surface water
f	Conversion constant of L_{au} and L_{wu}
F	Fraction diffuse light
G	Gain factor
g_{440}	CDOM absorption at 440 nm
K_d	Diffuse attenuation coefficient
$K_w(490)$	Diffuse attenuation coefficient for pure water at 490 nm,

K_{dw}	Diffuse attenuation coefficient of water molecules
L_{sky}	Radiance of skylight at zenith angle of 42°
L_{au}	The upward radiance above the water at nadir angle of 42°
L_{wu}	The upward radiance just beneath the water
r_{dif}	Fresnel reflectance coefficient of diffuse light
$R(0-)$	Subsurface irradiance reflectance
R_{rs}	Remote sensing reflectance
r_{sky}	Fresnel reflectance coefficient at zenith angle of 42°
r_{Θ}	Fresnel reflectance coefficient for sunlight
S	Spectral slope of CDOM
Q	Conversion coefficient for L_{wu} to E_{wu}
ρ_w	Water reflectance
Z_{SD}	Secchi disc depth
R_{rs}	Remote sensing reflectance
$\boldsymbol{h}$	Spectral vector of increased haze level and zero sediment, relative to $\boldsymbol{r}$
$\boldsymbol{r}$	Reference spectral vector for standard haze level and zero sediment
$\boldsymbol{s}$	Spectral vector of standard haze level and increased sediment, relative to $\boldsymbol{r}$
$\hat{\boldsymbol{p}}$	Modelled TOA radiance spectral vector
$\boldsymbol{\varepsilon}$	Residual error radiance spectral vector

Table of Contents

List of figures

xx

List of tables

CHAPTER 1

INTRODUCTION

1.1. Research background

Coastal zones are important ecological systems and key resources for many nations. The coastal zone is very complex, dynamic and it is the most productive area of the global ocean. It is also the zone for accumulation and transformation of nutrients and sediments derived from terrestrial and atmospheric sources. The area is also crucial for fish nursery and foraging grounds, and home to the majority of ocean fish stocks that compose the fisheries. Approximately 90% of the total of marine fish catch is derived from coastal regions, although the coastal area comprises only less than 8% of the total ocean area (Miller *et al*., 2005).

For humans, the coastal zone has important functions, i.e. primarily as a food supply area, followed by transportation, recreation, biodiversity conservation and even energy supply. These important functions, combined with the beauty of the coastal zone, have caused that approximately 25% of the human population reside in coastal areas. Coastal resources are of utmost importance for food security. The human population density around the globe continues to increase faster along the coast than in inland areas (Miller *et al*., 2005). In Indonesia, more than 60% of the total population lives in the coastal area, with an annual population growth of 1.33%.

The coastal region usually experiences a high intensity of human activities. Human activity can modify the freshwater influx patterns, altering nutrient and sediment fluxes from fluvial and atmospheric sources, and lead to over exploitation of fisheries resources. This impact, combined with the natural ecosystem's fragility, has heavily influenced coastal regions. The result is stress of coastal ocean resources and degradation of water quality, biodiversity and fish abundance at global scale.

Degradation of coastal regions is of direct concern to Indonesia, which is the biggest archipelagic country in the world. The country has more than 17,500 islands, which encompass 81,000 km of coastline, the second longest in the world after Canada. Indonesia's territory includes more than 80,000 km² of

coral reefs. Indonesia is also located in the heart of the Coral Triangle Complex, with an oceanography resulting from deep sea trenches, small island chains, seamounts, and active volcanic islands, which allows for an exchange of nutrients and energy that makes the country one of the most productive marine ecosystems in the world. Its waters hold some of the richest marine biodiversity in the world, including 14 percent of the earth's coral reefs and more than 2,000 coral reef fish species.

With the continuous high intensity of human exploitation, many of the natural resources of Indonesia, including coral reefs and other coastal resources, undergo continuous progressive degradation. Recent estimations show that 40% of Indonesian coral reef is in a poor condition and only 6% is in excellent condition (Nontji, 2000). The main coral reef degradation in coastal areas seems due to anthropogenic processes, rather than natural processes.

One of the major challenges of science is giving a contribution to stopping the continuous decline of natural resources due to increasing human needs. Better understanding of the state and condition of natural resources, including coastal and marine waters, is very important for supporting the sustainability of natural resources. In the field of coastal management, one of the contributions of science deals with continuous monitoring of marine resources in order to better manage these resources in a sustainable way.

Monitoring the coastal waters is a subject which has many countries' attention, including Indonesia. For the Indonesian case, it is difficult to monitor the large coastal zone with only *in situ* observations. The country has a complicated geography with a great number of islands, narrow straits, large river estuaries, strong variations in bathymetry and mainly, a vast and large geographic area. The high costs of operation over large areas make ground operations more difficult. Facing this problem, remote sensing methods give a practical solution as an effective tool for investigating and monitoring Indonesian waters. Remote sensing approaches applied to series of satellite images can provide information on a large area, showing the spatial and temporal development of sea surface features induced by various dynamic processes. For this reason, the usefulness

of field observations, together with laboratory experiments and ocean colour remote sensing data for showing coastal and marine spatio-temporal trends, is subject of this study.

With the large area concerned in Indonesia, the problem of research site location has an important signification. The location selected for the research should present the major important phenomena dealt with the country. For this research, the location chosen was the Berau estuary, East Kalimantan, Indonesia, which is representative of many processes occurring in the Indonesian marine environment.

1.2. Research problems

This study starts from the statement that a technique which allows monitoring the environment in an effective ways is needed in a country with such a large coastal zone as Indonesia. Remote sensing techniques allow monitoring the environment by repetitive observations.

In the domain of remote sensing, standard procedures and algorithms are widely available to measure and map the oceanic waters. Many studies have been done for Case-1 (ocean) waters, where generally reliable estimation of phytoplankton and chlorophyll is being achieved. In contrast, estimation of various water constituents from ocean colour remote sensing data for Case-2 (coastal and inland) waters is often inaccurate, due to poor performance of the standard algorithms (Darecki & Stramski, 2004). In many coastal regions, including those influenced by rivers, the often complex interactions of the physical, chemical and biological processes and lack of knowledge of the optical properties have hampered the routine use of ocean colour remote sensing.

This research was done in the Berau estuary, which is part of Makassar straits that is situated between Kalimantan and Sulawesi. A detailed description of the site location will be given in the next chapter. In this section however, it is necessary to briefly describe the site, in the context of the development of the research problem.

The study area is an excellent site to provide a synoptic view of the situation of Indonesian coastal waters and environment. The coastal ocean that fringes the East Kalimantan coast harbours the Berau barrier reef system and exemplifies a tropical continental shelf area, which is subject to fluvial and oceanographic influences and changes. From the land side, the Berau river accounts for a substantial amount of annual fresh water and sediment input into the coastal zone. From the ocean side, the Indonesian Through-Flow (ITF) from the Pacific to the Indian Ocean plays an important role in the global ocean circulation. ITF affects the predominant along-shore current in East Kalimantan coastal waters in southward direction through the Makassar straits. The area is also influenced by tidal (semi-diurnal), seasonal (monsoon) and intra-annual effects. The Berau outer shelf barrier reef and atolls system is distributed north from the Berau delta in the coast of East Kalimantan (Tomascik, 1997). Thus, studying the coastal dynamics in the Berau estuary is very interesting due to its relative small area, but it is composed of a complex ecosystem and processes.

The Berau river plume may serve as an example to investigate Regions of Freshwater Influence (ROFI) behaviour and impacts of land-based runoff on coastal ecosystems. ROFI's create specific environmental conditions for coastal and marine ecosystems along the East Kalimantan coast that depend on quantities such as salinity, turbidity, temperature, chlorophyll and stratification. In particular, the turbidity and siltation patterns associated to ROFI behaviour influence the zoning and morphology of coral reef systems.

In such an environment, the usefulness of time series of satellite imagery and derived products for showing coastal and marine spatio-temporal trends will therefore be evident. The development of methods to characterize ROFI behaviour in East Kalimantan coastal waters is therefore a challenging topic and requires improved algorithms, built on thorough calibration of image data and under water spectral radiance observations.

One of the problems in remote sensing of the tropical environment is the improvement of accuracy, related to water properties. As known, one of the keys to improve the accuracy of estimation of the seawater constituents from

ocean colour remote sensing is a better understanding of coastal bio-optical properties. In-water optical properties are classified into two main types: inherent optical properties (IOP) and apparent optical properties (AOP) (Preisendorfer, 1976). Until recently, most of the IOP or SIOP (specific inherent optical properties) of the coastal and marine water have been acquired in European (North Atlantic) and US (East Pacific) coastal waters, mainly at higher to mid-latitudes. There is limited IOP research which has been carried out in the tropical equatorial regions, especially in Indonesian waters. In order to fill this gap, one of the studies in this thesis will be focused on estimation of the SIOP from the AOP by using the inversion method of a semi-analytical model.

This research uses Medium Resolution Imaging Spectrometer (MERIS) data as the primary source of satellite images. MERIS is one of the satellite sensors that can be used for open sea water studies and water quality assessment in the coastal zone as well as in freshwater basins. MERIS has 15 bands as described in Table 1.1, and two levels of spatial detail, Full Resolution (FR) and Reduce Resolution (RR). The performance of MERIS for tropical equatorial water quality assessment will be the main question to be addressed.

Table 1.1: Specifications of the 15 MERIS channels

Band.	Band centre (nm)	Bandwidth (nm)	Potential Applications
1	412.5(nm)	10	Yellow substance & detritus pigments
2	442.5	10	Chlorophyll absorption maximum
3	490	10	Chlorophyll and other pigments
4	510	10	Suspended sediment, red tides
5	560	10	Chlorophyll absorption minimum
6	620	10	Suspended sediment
7	665	10	Chlorophyll absorption and fluorescence
8	681.25	7.5	Chlorophyll fluorescence peak
9	708.75	10	Fluorescence, atmospheric corrections
10	753.75	7.5	Vegetation, cloud
11	760.625	3.75	Oxygen absorption R-branch
12	778.75	15	Atmosphere corrections
13	865	20	Vegetation, water vapor reference
14	885	10	Atmosphere corrections
15	900	10	Water vapor, land

One of the goals of ocean colour remote sensing is to derive quantitative information present in the water column, based on variations in the spectral form and magnitude of the ocean colour signal. In this thesis, Total Suspended Matter (TSM) and Chlorophyll-*a* (Chl-*a*) concentration will become the two main parameters that will be derived from remote sensing data.

One of the major problems in applying remote sensing techniques is the presence of parts of the signal which do not come from the target, due to the atmospheric disturbance. Hence, atmospheric correction is really important for retrieving quantitative information from the water column. This applies especially in the context of the tropical Berau environment, where the presence of local haze variations interferes with a reliable image interpretation. For applications over land, a technique called linear spectral unmixing has been found useful for atmospheric correction and quantitative image analysis. In this research, the utility of such a technique applied to remote sensing data of coastal waters will be explored.

1.3. Research objective

The general objective of this thesis is to obtain a better understanding of the dynamics in space and time of several important properties and variables of ocean colour remote sensing in tropical regions. This can be achieved by developing a methodology for quantitative assessment of coastal water quality at the local scale, which is nevertheless representative of many of the processes occurring generally in tropical waters. Such a methodology is applied to investigate the Berau water characteristics. With such a general objective, four more specific objectives are specified below.

1. To estimate the specific inherent optical properties of the Berau water by using *in situ* observations and satellite data.
2. To evaluate the water quality, as derived from MERIS satellite data by using different Case-2 water algorithms.
3. To study TSM concentration in the Case-2 tropical water using different mathematical approaches.

4. To study TSM concentration from MERIS data by using a combination of spectral unmixing with inverse radiative transfer modelling.

1.4. Research context

This research addresses issues of water quality in tropical coastal and marine waters using satellite imagery and *in situ* observations. This research is part of the East Kalimantan Program (EKP) funded by WOTRO, The Netherlands. The EKP is a collaboration project initiated by NWO-Earth and Life Sciences (ALW), NWO-Foundation for the Advancement of Tropical Research (WOTRO), KNAW and the Indonesian Consortium on Coastal and Marine Research (ICoMaR). The EKP aims to enhance and support scientific cooperation in coastal zone research groups from Indonesia and the Netherlands. This collaboration project involves several research institutions from both countries, (Utrecht University, Wageningen University, Delft University of Technology, and NIOZ in the Netherlands, and The Indonesian Institute of Science - LIPI, The Indonesian ministry of Energy and Mineral Resources - ESDM, National Coordinating Agency for Surveys and Mapping - BAKOSURTANAL, National Institute for Aeronautics and Space - LAPAN, Mulawarman University in Samarinda - UNMUL, and Bandung Institute of Technology – ITB in Indonesia).

The EKP has focused its research on the East Kalimantan coast such as the Mahakam delta and the Berau estuary. Both of these two study areas are supposed to be representative for research areas to display the problems occurring in the coastal and land transition zone in Indonesia as well as any tropical region in the world. The Mahakam delta is an example of a delta ecosystem that has been extremely subjected to human pressure, with more than 70% of the mangroves converted into shrimp-ponds between 1980 and 2000. On the other hand, the Berau region is supposed to be still more pristine. The deforestation and mining activities have recently started in this region, and thus, monitoring and controlling human resource exploitation activities in this region is needed.

The Berau Research Cluster, which started a study entitled "From River Basin to Barrier Reef: Physical, Biological and Socio-economic Aspects of the Berau System" focuses on the multi-disciplinary approach, ranging from physical, biological to socio-economical subjects in order to obtain a proper understanding of the dynamics of coastal systems. The main objectives of the research cluster are:

- To analyze and define the interaction of physical, biological, socio-economic as well as cultural processes and developments in a river delta - barrier reef system that is at present characterized by a very large natural variability, including pristine conditions;
- To assess the consequences of environmental change and increasing human activities on the coastal and marine ecosystems and their sustainability;
- To use coral reef ecosystems as a bio-monitor for the ecological status of the system and sustainability of the natural resource. Other indicators for environmental degradation will include, for example, coastal abrasion and mangrove area changes.

In this research context, remote sensing of the Berau coastal waters is the main focus of this PhD research as part of the Berau research cluster. This research is dedicated to contribute the achievement of the cluster objectives, especially in conducting a water quality monitoring and assessment by using MERIS data in the coastal waters.

1.5. Outline of the thesis

The research described in this thesis is organized in seven chapters. The first chapter reviews the introduction including research background, problem and objectives. The objective of this chapter is to give a general understanding about the research to the reader. The description of the study area is given in Chapter 2.

The main subjects dealt with in this thesis are described in Chapters 3 to 6, which are assigned to achieve the research objectives as has been mentioned in the previous section. The Chapter 3 relates to the assessment of water constituents and optical properties in tropical coastal waters from *in situ* observations and MERIS data. In this chapter, the results concerning the apparent optical properties and inherent optical properties of the Berau coastal waters are described first, followed by an evaluation of MERIS data to monitor these properties.

In Chapter 4, retrieval of water quality constituents' concentrations from MERIS data and *in situ* observations is discussed. The objective of this chapter is to evaluate commonly used algorithms and models for estimating water quality in the coastal waters from MERIS data. These are some available regional Case-2 algorithms for estimating water quality in the coastal waters. Moreover, the European Space Agency (ESA) provides a MERIS Level 2 Product that contains both water and land bio-geophysical parameters, derived from sensor data. Thus, an inter-comparison among the Case-2 regional algorithms as well the MERIS L2 product with *in situ* measurements is described in this chapter.

Chapter 5 deals with estimating the total suspended matter from MERIS data by using different mathematical approaches. The objective of this chapter is to test an empirical and a semi-empirical approach, based on the Kubelka-Munk model, for retrieving the TSM concentration. Retrieving quantitative information from the ocean colour data requires proper atmospheric correction, since only around 10% or less of the radiance received by a satellite sensor comes from the water target. In this chapter the atmospheric radiative transfer model MODTRAN is applied by comparing different visibilities (haze levels) and different aerosol optical models.

Chapter 6 deals with atmospheric correction by using a spectral unmixing approach. The objective of this chapter is to derive TSM concentrations by applying spectral unmixing to remove local haze variations and next the inverse Kubelka-Munk model to quantify the sediment. First, the method of how to separate sediment in the water from the haze using spectral unmixing

and selecting endmembers from a look up table of top of atmosphere radiance data is illustrated. Secondly, the spectral unmixing model is applied to MERIS data, followed by atmospheric correction and deriving TSM concentration using the K-M model. Lastly, the result of the new approach proposed in this study is inter-compared with 3 other TSM concentration retrieval algorithms, namely C2R, FUB and MERIS L2.

Finally, Chapter 7 concludes this thesis with a discussion of the main results and findings of all previous chapters and offers suggestions for future research. This chapter synthesizes also the practical information necessary for a better understanding and use of remote sensing in the Berau estuary, as an example of a tropical equatorial region.

CHAPTER 2

STUDY AREA: THE BERAU MARINE PROTECTED AREA

2.1. The Berau Marine Protected Area

In the year of 2005, the local government of the Berau District, Indonesia established a 1.2 million hectare marine protected area (MPA) to protect a coastal zone with one of the highest levels of marine biodiversity in the world (WWF, 2006). The Berau MPA is one of four MPA in Indonesia; these include the Sangihe Talaud, the Bunaken National Park, the Gorontalo and the Berau MPA (*see* Figure 2.1). Those MPAs are located in the Sulawesi Sea and they are part of the Sulu-Sulawesi Marine Ecoregion that stretches across Indonesia, Malaysia and the Philippines.
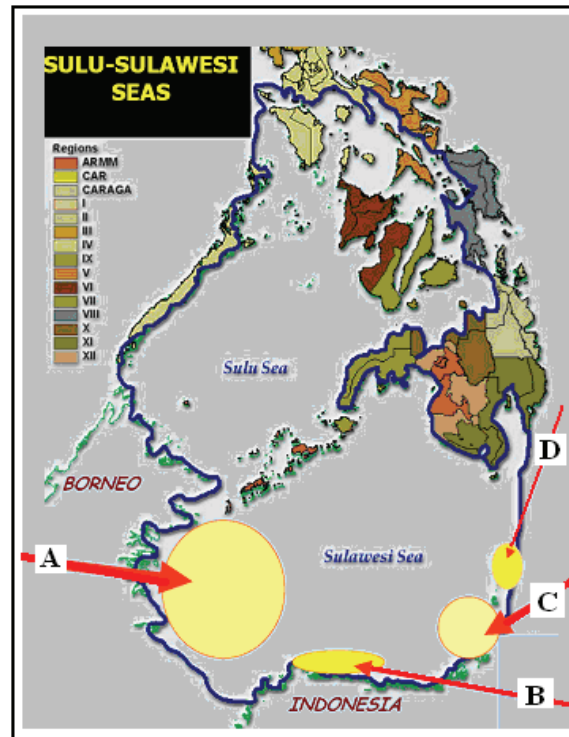
Figure 2.1 :   Marine Protected Area in Indonesia: Berau (A), Gorontalo (B), Bunaken (C) and Sangihe Talaud (D) (source: WWF, 2006)

The Berau MPA which is located in the center of the Coral Triangle has the highest levels of coral reef biodiversity in the world. Based on a survey done by the Indonesian Science Institute (Puslitbang Oseanologi LIPI-Ambon, 1995 *in* Ismuranty, 2003) there exist 9 sea grass species, 26 mangrove species, 347 reef fish species, and various rare species such as the green turtle (*Chelonia mydas*), in the Berau ecosystem. The Berau coral biodiversity has 507 species of hard coral. It is considered as the second highest biodiversity area in Indonesia and the third in the world. Derawan Island and surrounding reefs and islands, which are located in the Berau estuary, have been classified as one of the top seven locations, among 120 potentials having outstanding universal value (UNESCO, 2002).

With the increasing impact of anthropogenic processes, such ecosystems however degrade. The seagrass for example, which is a food for the green turtle, decreased from 56% area coverage in 1994 to only approximately 37% in 2001. Several studies which have been done in the Berau waters show that the total fish catch has been declining in the last ten years (Ismuranty, 2003) due to the depletion of the coral reefs. Decreasing health of coral reef areas has affected the fish stock. The cause of coral depletion is well-known, coming from the anthropogenic processes on the land such as deforestation, illegal fishing practices, and also due to natural processes such as sea temperature change, e.g. related to El Niño.

2.2. The Indonesian Through-flow (ITF)

The Berau estuary is part of the East Kalimantan waters, which play an important role in the transfer of heat and fresh water in the region because it is located in the Indonesian Through-flow (ITF) as shown in Figure 2.2. The ITF is the region where warm waters from the western Pacific Ocean are transported to the Indian Ocean. These ocean currents flow through the Makassar strait, the Lombok strait, the Ombai strait and the Timor Passage (Murray & Arief, 1988; Meyer, 1996; Gordon *et al*., 1999; Hautala *et al*., 2001). The ITF transfers warm and lower salinity waters from the western Pacific into the Indian Ocean from where the Asian monsoon gathers strength. As an integral element of the global

ocean circulation, it is influential in regulating climate and rainfall across Indonesia, India and Australia.
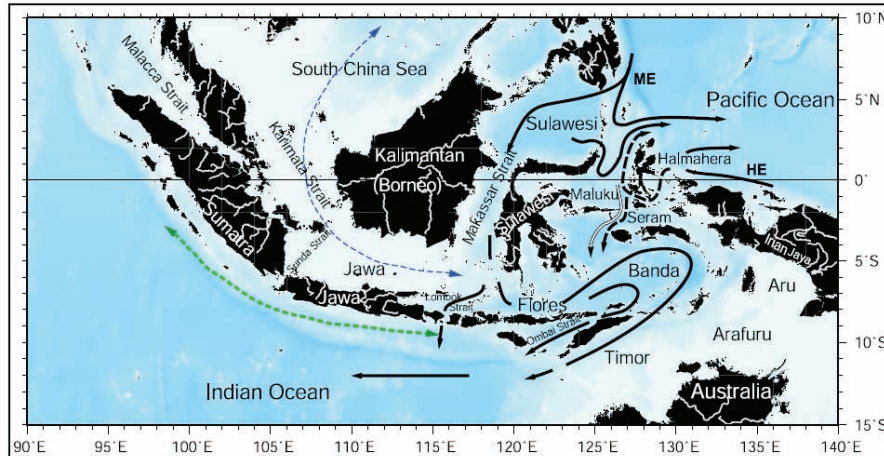
Figure 2.2 : Map of Indonesian Seas with major rivers and throughflow pathways (Susanto *et al.*, 2006). The solid arrows represent North Pacific thermocline water; the dashed arrows (black) are South Pacific lower thermocline water. The dashed arrows (green and blue) along the north and south Sumatra-Nusa Tenggara Island chain are seasonally reversed surface water flow due to the Asia-Australia monsoon. The Indonesian throughflow transport is estimated to be 9 Sv (1 Sv = 10^6 m^3/s).

Field & Gordon (1992) and Gordon *et al*. (1999) mentioned that the Makassar strait is the primary path of the ITF. The througflow is high during June–August (southeast monsoon) and low during December–February (northeast monsoon) (Wyrtki, 1987). Numerous authors have investigated the ITF phenomena in Indonesian waters based on *in situ* observations and model simulations (Wyrtki, 1987; Hautala *et al.*, 2001; Gordon *et al.*, 2003; Pandey, *et al.*, 2007). However, only limited research has been done on ocean color remote sensing in this region as well as in Indonesian seas. Susanto *et al.* (2006) and Hendiarti *et al.* (2004) have studied ocean color in the Indonesian Seas using SeaWiFS.

2.3. General condition

The Berau delta and the barrier reef system represent a complex coastal system with a variety of coastal landforms and associated ecosystems. These include the Berau river basin and delta with two major estuaries and surrounding mangrove swamps, an extensive lagoon system, a delta-front barrier reef system (coastal and shelf edge reefs) and the coastal part of Makassar strait with oceanic reefs. Geographically, the Berau estuary is situated between 01°45′ - 02°35′ North and 117°20′ - 118°45′ East (*see* Figure 2.3).
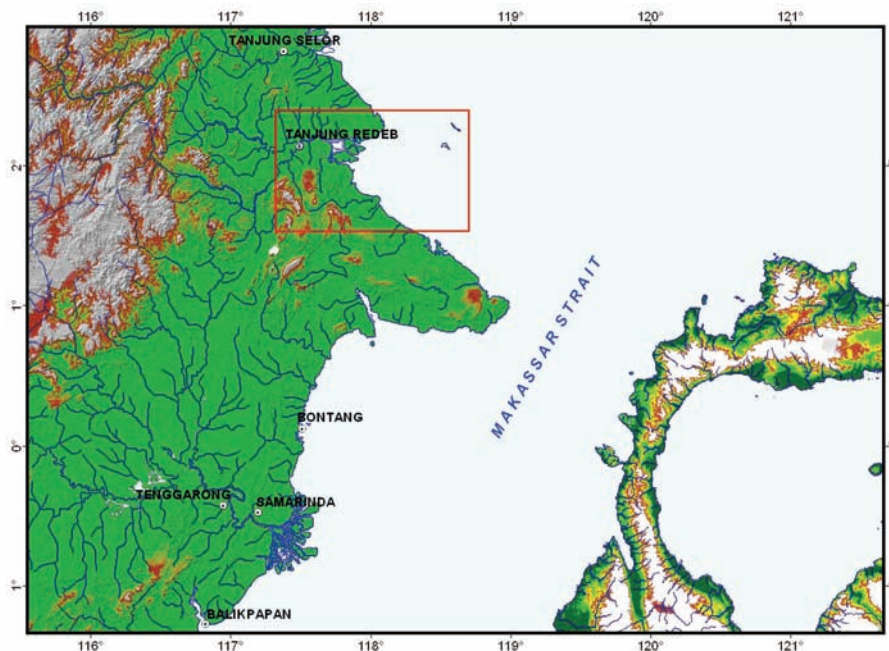
Figure 2.3 : The map of the Makassar strait (from SRTM); the study site is indicated by the red box.

The Berau river drainage basin has an area of 15,176 square kilometres (Timur Atlas). Four major rivers run through Kabupaten (district) Berau: The Berau river (292 km in length); Kelai river (254 km), Malinau river (58 km) and Segah river (152 km). The Berau islands, situated in front of Berau river mouth in the estuarium, consist of Derawan Island, Sangalaki, Kakaban, Maratua, Panjang

and Samama as well as several submerged reefs and small islets (Figure 2.4). The two inhabited islands are Derawan (3.5 km^2) and Maratua island (20 km^2)·
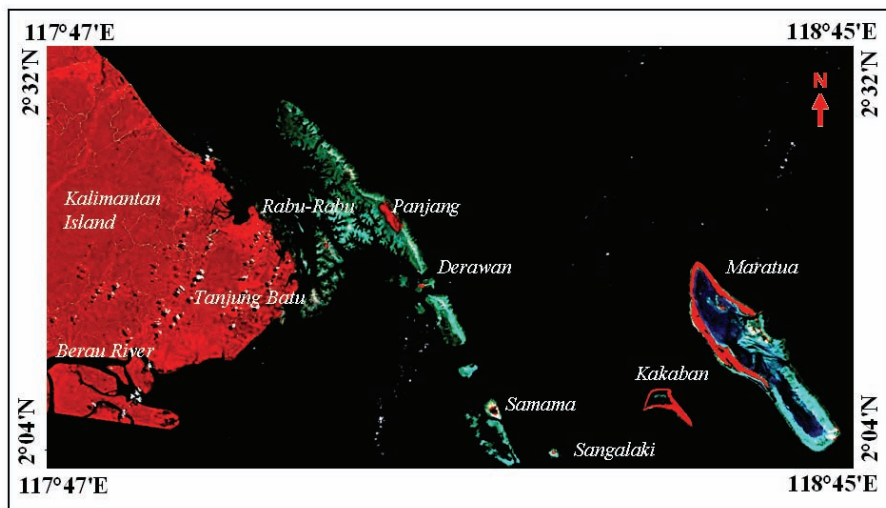
Figure 2.4 : Landsat image of the Berau estuary (Landsat ETM image from July 8, 2002)

2.4. Oceanography

The oceanographic condition of the Derawan Islands is influenced by the dynamics of Berau river and the Makassar straits. One of the major characteristics of an estuarine system is the variation in the spatial distribution of water salinity. Many processes, physical, chemical, or biological processes are related to salinity. Salinity is the main index of the mixture of seawater with water from the major rivers. According to a previous result (Ambarwulan *et al.*, 2005), the salinity of the Berau estuary, which was measured on August 2005, ranged between $10^0/_{00}$ and $15^0/_{00}$ in the Berau river and increased when going to the sea. Our observation indicated that the salinity of the Berau estuary varied between $5^0/_{00}$ and $39.50^0/_{00}$ during the field campaign of August 2006 and between $18^0/_{00}$ and $39.30^0/_{00}$ during the field campaign of August – September 2007. Wiryawan *et al.* (2004) found the salinity in East Kalimantan for open sea to be 33.5 $^0/_{00}$, while in the Berau river mouth it was around 32.5 – 33.0 $^0/_{00}$.

Water temperature is a measure of how cool or how warm the water is. It is expressed in degrees Celsius (C). Temperature is a critical water quality parameter, since it influences directly the amount of dissolved oxygen that is available to aquatic organisms. Water temperature affects the rates of all chemical and biological processes. According to the measurements made by Ambarwulan *et al.* (2005), the water temperature of the Berau estuary varied from 28.30 to 32°C. Our measurements at 123 field locations on August 2006 found that the temperature ranged from 27.9 to 32.9°C. The second field campaign which was conducted August – September 2007 with around 120 field measurements give a temperature measurement range between 27 and 31.70°C.

2.5. Climate

Like other parts of the Indonesian archipelago, Kalimantan and its coastal areas are affected by the Asia-Australia (AA) monsoon, a southeast monsoon from April to October and northwest monsoon from November to March. The southeast monsoon brings warm and dry air from Australia into the Kalimantan waters, whereas the northwest monsoon is associated with warm and moist air. The wet season starts in October and extends until May, with an average number of rainfall days of 15 to 20 per month. July until September is considered as the dry season, with the lowest rainfall in July. The annual rainfall average in the Berau catchment varies from 2400 to 3350 mm/year. Its maximum value ranges between 3800 and 4200 mm/year, while its minimum value ranges between 1620 and 1700 mm/year.

The yearly average rainfall in Berau recorded by Meteorological and Geophysical Agency (*Badan Meteorologi dan Geofisika - BMG*) station of Tanjung Redeb over the period of 1987 – 2007 was 2084 mm. The dry season occurred in the months of July-August-September, with the minimum rainfall in August, 117.4 mm. The wet season occurred from November to January, the maximum rainfall occurs in January (223 mm). The yearly rainfall average is displayed in Figure 2.5.
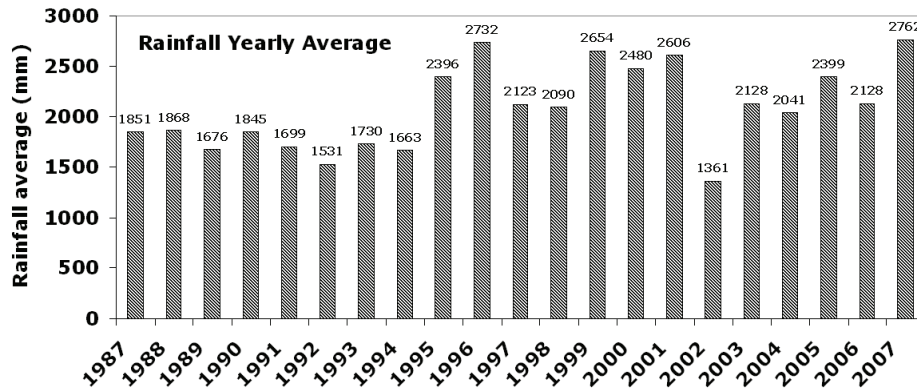
Figure 2.5 : Annual rainfall in Berau 1987- 2007 (Source: BMG data of Tanjung Redeb station).

2.6. Geological Formations

The geology of the Berau catchment is composed of 21 geological formations (Situmorang & Burhan, 1995) (Figure 2.6). In the lower part, one dominant geological formation is found, namely Alluvium (Qa) formation. This formation is composed of mud, silt, sand, gravel and peat; with gray to black in colour. The thickness of this formation reaches more than 40 m. The Domaring formation (Tmpd) is composed of reef limestone, chalky limestone; marl and recent coal intercalations. This formation is deposited in a littoral swamp area, its thickness can reach up to 1.000 m, and is probably developed in the late of Miocene to Paleocene age. The Tabalar formation (Teot) is arranged by gray marl, sandstone, shale, limestone intercalations and a basal conglomerate in the lower part, dolomite limestone, and calcarenite and marl intercalations in the upper part. This formation is deposited in the fluviatile-shallow marine area. The thickness is up to 1000 m. Looking in general over the Berau catchment, the Latih formation is the dominant formation, occupying 16% of the catchment area. In this research, the focus of the discussion will be the Alluvium formation (Qa) only. This formation has also a wide distribution, about 6% of the catchment area. This formation is the main geological constituent in the downstream area of the Berau catchment. This part constitutes the interface of the mainland and the ocean, which is the focus area of the research.
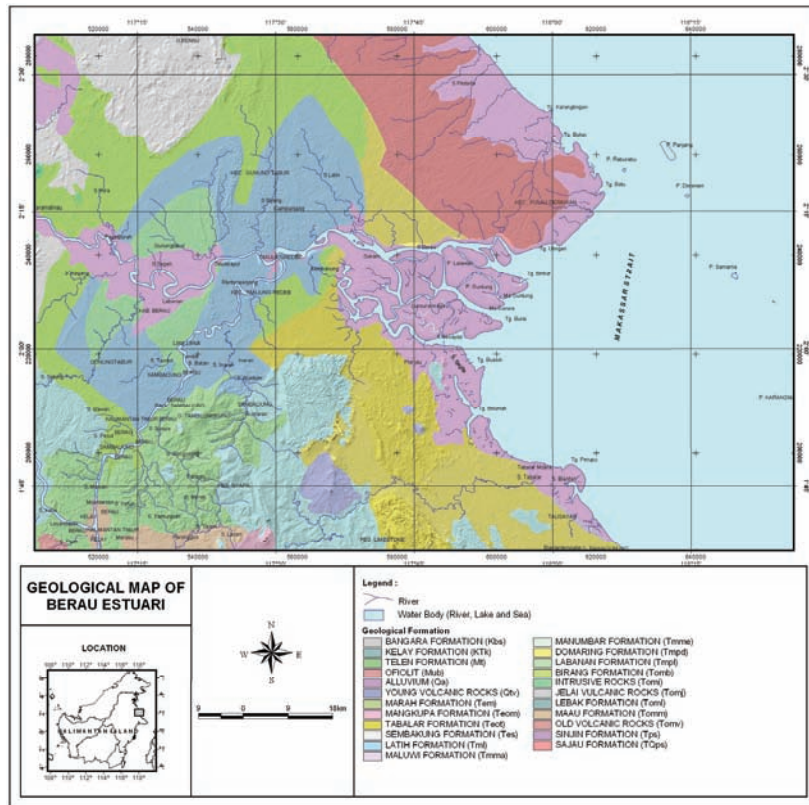
Figure 2.6 : Geological map of Berau District (Situmorang & Burhan, 1995)

2.7. Anthropogenic situation

The Berau river delta and estuary are located in Berau Regency ("Kabupaten"), East Kalimantan Province, Indonesia. It is one of the ten regencies in East Kalimantan. Its main historical and natural land cover is dense tropical rainforest. Due to human influences, a large area of the tropical rainforest is being converted into oil plantations, coal mining areas as well as fish ponds around the Berau delta in the last decades. As a result, more erosion is likely to occur and the major river, the Berau River, may supply more sediment to the estuary. This may become a major problem because the coral reefs in the nearshore and offshore coastal waters may be affected by increasing sediment supply. Eventually, if nothing is done, the coral reefs may irreversibly change and some species might even totally disappear.

21

CHAPTER 3

ESTIMATING THE SPECIFIC INHERENT OPTICAL PROPERTIES OF TROPICAL COASTAL WATER USING BIO-OPTICAL MODEL INVERSION

Abstract[*]

Specific inherent optical properties of the Berau coastal waters were derived from *in situ* measurements and inversion of an ocean colour model. Field measurements of water-leaving reflectance, total suspended matter (TSM) and chlorophyll-a (Chl-*a*) concentrations were carried out during the 2007 dry season. The highest values for specific inherent optical properties were found in the turbid waters, this decreased moving towards offshore waters. The specific backscattering coefficient of TSM varied by an order of magnitude and ranged from 0.003 m^2g^{-1} for clear open ocean waters to 0.020 m^2g^{-1} for turbid waters. On the other hand, the specific absorption coefficient of chlorophyll-a was relatively constant over the whole study area and ranged from 0.022 m^2 mg^{-1} for the turbid shallow estuary waters to 0.027 m^2 mg^{-1} for deeper continental shelf edge ocean waters. The spectral slope of coloured dissolved organic matter absorption was also derived with values ranging from 0.015 to 0.011 nm^{-1}. These derived values of specific inherent optical properties in the Berau estuary form a corner stone for future estimation of TSM and Chl-*a* concentration from remote sensing data.

3.1. Introduction

The Berau estuary is a complex inlet lying off the Makassar strait which consists of river deltas in the west and a barrier reef in the east. The area is a region of freshwater influence where the outflows of the Berau river and a number of smaller rivers (i.e., Sesayap and Lungsurannaga) mix with waters originating from the Pacific ocean through the Makassar strait. The dynamics of river discharges to the Berau estuary affect the spatial and temporal dynamics of water constituents causing small-scale patchiness in addition to the dynamic variability of the tidal currents. Berau estuary is located in the Indonesian Through-Flow (ITF) and ENSO regions, which affect this tropical area with centers of action around Indonesia - North Australia and the southern Pacific (Glantz *et al.*, 1991). The positions of these large weather systems affect also cloud coverage. Diurnal clouds that develop in the tropical area influence significantly the energy and radiation budget through diffusion and absorption in the solar spectrum (Sharkov, 1998).

Over the year, the Makassar Strait has been extensively surveyed and detailed descriptions have been published especially related to the ITF, in which a deep ocean current is also important in regional and global climate studies (Hautala *et al.*, 2001; Gordon, Susanto & Vranes, 2003; Susanto & Gordon, 2005). However, only limited research has been done in the field of water quality in the coastal shelf waters in this region as well as in general other parts of Indonesian waters (Dekker *et al.*, 1999; Van der Woerd & Pasterkamp, 2001; Hendiarti *et al.*, 2004).

Ocean colour applications utilize the spectral characteristics and variations of radiometric data to derive information about some of the constituents of the water. Techniques for water constituent retrieval have evolved from an empirical to the semi-analytical approach. The empirical algorithms (Gordon & Morel, 1983) often focus on a single constituent concentration. The semi-analytical method is capable in retrieving three water constituents simultaneously. This model has potential of providing accurate retrievals of several parameters because they attempt to model the physics of ocean colour

(Maritorena *et al.*, 2002). Semi-analytical models have been developed to derive waters constituents such as chlorophyll concentration (Chl-*a*), total suspended matter (TSM) concentration and colored dissolved organic matter (CDOM) absorption (Lee *et al.*, 2002, Maritorena *et al.*, 2002, Haltrin & Arnone, 2003, Maritorena & Siegel 2005, D'Sa *et al.*, 2006, Doerffer & Schiller, 2007, Van der Woerd & Pasterkamp, 2008, Salama *et al.*, 2009, Salama & Stein, 2009, Salama & Shen, 2010-a).

Understanding bio-optical properties of coastal waters is a key issue to improve the accuracy of derived water constituents from ocean colour data (e.g. Babin *et al.*, 2003; Hamre *et al.*, 2003). Various studies in coastal waters have demonstrated the need for regional algorithms in order to obtain better estimation of water constituents (Kahru & Mitchell, 2001; Reynolds *et al.*, 2001; D'Sa *et al.*, 2002). Inherent optical properties (IOP) are the optical properties of water that are independent of the ambient light field (Preisendorfer, 1976). IOP include light absorption and scattering coefficients. The Apparent optical properties (AOP), as measured by a spectroradiometer are additionally dependent on the ambient light field and its geometric structure. Various models have been developed to relate IOP to AOP (Gordon *et al.*, 1975; Morel & Prieur, 1977; Gordon & Morel, 1983; Kirk, 1984; Gordon, 1991; Carder *et al.*, 1999; Stramska *et al.*, 2000; IOCCG, 2006). Salama *et al.* (2009) developed an algorithm, modified from the GSM semi-analytical model, for deriving bio-optical properties such as inherent optical properties (IOPs) in inland waters. The model appears promising for these turbid coastal waters.

Subsurface irradiance reflectance, *R(0-)* is one of AOP parameters and is given by Gordon *et al.* (1975) as a function that relates the upwelling irradiance (E_u^-) to the downwelling sun irradiance (E_d^-) at null depth. The model that is of direct interest in this study is an inverted semi-analytical model transforming *R(0-)* data into IOP and specific inherent optical properties (SIOP). The SIOP can be estimated from derived values of inherent optical properties and measured concentrations of water constituents. Until recently, most of the IOP or SIOP data were collected from European coastal waters, mainly at mid-latitude, e.g. the North Sea and Baltic Sea. Limited research on the variability of

IOP and associated SIOP values has been carried out in the tropical equatorial region, especially in Indonesian waters. The objectives of this study are to estimate the SIOP of the Berau estuarine waters using ocean colour data, model inversion and *in situ* measurements and to estimate the TSM and Chl-*a* concentration from MERIS satellite sensor data by using a semi-analytical model.

3.2. Material

3.2.1 *In situ* measurements

In situ data were collected in the Berau estuary during the 2007 dry season, from 27 August to 18 September 2007, at representative locations (shown in Figure 2.3) ranging from more than 100 m depth waters near the shelf edge and open-ocean to less than 2 m depth in very turbid coastal waters. Under and above water radiometric measurements were carried out using the Ocean Optic Spectrometer USB4000 and REVAMP protocols (Tilstone *et al*., 2004). Spectra of subsurface irradiance were measured at three depths of 10, 30 and 50 cm. The subsurface irradiance reflectance *R(0-)*, was then calculated from the measured subsurface irradiance spectra at 10, 30 and 50 cm depth. Above water field observation consisted of measurements of sky irradiance and water leaving reflectance. Water quality variables were measured at the same location as the optical data. The water samples were collected at depth between 20 and 50 cm and were analyzed for their content of total suspended matter TSM and Chl-*a*. The REVAMP protocol was used in the analysis (Tilstone *et al*., 2004). Other water quality variables as Secchi disc depth, EC, temperature, pH, turbidity, dissolved oxygen and salinity were also measured.

In January 2009, a small additional field campaign was carried out in the Berau estuary. The main parameter collected then was coloured dissolved organic matter absorption (a_{CDOM}). The water samples were collected in the field and were filtered using Whatman 0.22 μm following REVAMP protocols (Tilstone *et al*., 2004). A statistical summary of *in situ* CDOM measured are given in Table 3.1.

Table 3.1: The statistical analysis of the Berau estuary water containing the CDOM absorption coefficient at 440 nm and the spectral slope of CDOM absorption (Slope *S*), resulting from field campaign of January 2009; n= 6

Parameters	Min	Max	Mean	SD
a$_{CDOM}$440 [m^{-1}]	0.140	1.666	0.672	0.583
Slope *S* [nm^{-1}]	-0.015	-0.011	-0.012	0.002

In the Table above, *S* (the spectral slope of CDOM) is the exponential parameter (nm^{-1}) is dependent on the composition of the CDOM present. We measured the slope *S* and the CDOM absorption coefficient at 440 nm (*a$_{CDOM440}$*) at 6 locations between lower left (2°11'05" N; 117°43'36" E) and upper right (2°14'50" N; 118°11'40" E) of the image. The *a$_{CDOM}$* was higher in the Berau river (mean = 1.35 m^{-1}) and logically decreased towards the open sea (mean = 0.19 m^{-1}). The *a$_{CDOM}$* around the Berau river mouth was 0.473 m^{-1}. The Slope S in the open sea waters was lower (-0.011 nm^{-1}) than in the Berau river mouth water (-0.013 nm^{-1}).

3.2.2 Ocean colour data

Medium Resolution Imaging Spectrometer (MERIS) Level 1b of Reduced Resolution (RR) and Full Resolution (FR) image data were used in this study. However, there was only one MERIS data which a full match-up in time with the *in situ* measurement, on 31 August 2007.

3.3. Methodology and data analysis

3.3.1. Hydro-optical model

A hydro-optical model relates the measured radiometric quantities above the water surface to the inherent optical properties of the water's upper layer, hence constituent concentrations. In the absence of IOP measurements, we chose a subsurface irradiance reflectance model (Gordon *et al.*, 1973) for

estimating IOP and associate SIOP using *in situ* measurement of AOP by inversion method as explained hereafter.

Sub surface irradiance reflectance, *R(0-)*, is the ratio of upward (E_u^-) and downward irradiance (E_d^-) just beneath the water surface, and was calculated as (Haan *et al.*, 1999):

$$R(\lambda, 0^-) = \frac{E_u^-}{\left(1 - r_\Theta(1 - F) - r_{dif}F\right)E_d^+ + 0.48E_u^-}$$ (3.1

where E_d^+ and E_u^- are the down-welling irradiance just above the water surface and the upwelling irradiance just beneath the water surface, respectively. These radiometric quantities (E_d^+ and E_u^-) were measured during the field campaign as has been explained in section (3.2). The Fresnel reflectance coefficient for sunlight, r_Θ, was calculated from viewing illumination geometry. *F* is the fraction diffuse light of E_d^+. The Fresnel reflectance coefficient of diffuse light (r_dif), in this study was set to 0.06 (Jerlov, 1976).

Subsurface irradiance reflectance in Eq. (3.1) can be related to the inherent optical properties (IOP) of the water using the Gordon *et al.* (1975) model:

$$R(0-) = f\frac{b_b(\lambda)}{a(\lambda) + b_b(\lambda)}$$ (3.2)

where *f* is a proportionality factor which can be treated as a constant with a default value of 0.33 (Gordon *et al.*, 1975); *a(λ)* and *b_b(λ)* are the bulk absorption and backscattering coefficients. We will use collective term IOP to refer to absorption and backscattering coefficients.

The absorption *a(λ)* and backscattering *b_b(λ)* coefficients (Eq. 3.2) are the sum of contributions by the various seawater constituents. These IOP are separated into components such as the dissolved and particulate fractions and water. The total absorption coefficient *a(λ)* (m⁻¹) is the sum of the contributions by pure water, *a_w*, phytoplankton, detritus or non algal particles and CDOM absorption. The total backscattering coefficient *b_b(λ)* can be separated into contribution of pure water and total suspended matter (TSM). IOP can be related to constituent concentrations and their SIOPs as follows (Gege, 2005):

$$a_{wc}(\lambda) = \sum_{i=0}^{5} C_i a_i^*(\lambda) + X.a_x^*(\lambda) + Y.a_y^*(\lambda) \qquad (3.3)$$

$$b_b(\lambda) = b_{b,w}(\lambda) + C_L.b_{b,L}^*(\lambda) + C_S.b_{b,S}^*(\lambda/\lambda_S)^n \qquad (3.4)$$

where, C_{chl}, X, Y, indicate the concentrations of chlorophyll-a, non-algae particles and gelbstoff respectively. SIOPs of these constituents are denoted as a_Chl^*, a_x^* and a_y^* respectively. Absorption and scattering of water molecules, $a_w(\lambda)$ and $b_{b,w}(\lambda)$, were taken from Pope & Fry (1997) and Morel (1974) respectively. $b_{b,TSM}^*(\lambda)$ is the specific backscattering coefficient of total suspended matter. Measured radiometric quantities in the field (Section 3.2) can now be related to the inherent optical properties of the water upper layer form Eq. (3.1) and (3.2). Equation (3.2) is then inverted to derive the IOP of the water upper layer. The specific inherent optical properties a^*_{Chl} and $b^*_{b,TSM}$ of the Berau estuary are estimated from the derived IOP and measured concentrations as:

$$b_{b,TSM}^*(\lambda) = b_{b,TSM}/C_{TSM} \qquad (3.5)$$

$$a_{Chl}^*(\lambda) = a_{chl}/C_{chl} \qquad (3.6)$$

where $b_{b,TSM}^*$ or $b_{b,L}^*$ is specific backscattering coefficient of large particles, $b_{b,TSM}$ is backscattering coefficient of particles and C_{TSM} is the concentration of TSM (mgl⁻¹). The C_{Chl} or C_i is the concentration of phytoplankton (µgl⁻¹). The a_{Chl}^* or a_i^* is the specific absorption spectra of phytoplankton. The a_Chl and $b_{b,TSM}$ are calculated by inverting Eq. (3.2). The C_{Chl} and C_{TSM} were measured in the field.

3.3.2. Processing of ocean colour data

The MERIS RR L1 of 31 August 2007 was used in this stage. Atmospheric correction was carried out using the method of Gordon & Wang (1994). The look-up table for atmospheric path radiances was generated using the 6S model (Vermote *et al.*, 1997). The distinctive signal of turbid waters was accounted for in the computations using the method of Salama & Shen (2010-b). IOPs were derived from MERIS water leaving reflectances using the model of Salama *et al.* (2009). The statistical evaluation of *R(0-)*, IOP and SIOPs as well as TSM and

Chl-*a* concentrations were done using the coefficient of determination (R^2), and Root Mean Square Error (RMSE). A logarithmic scale was used in the analysis of RMSE following standard practice (Eq.2.1, pp. 18, IOCCG, 2006).

3.3.3. Turbidity-based classification

Based on turbidity, we subdivided the *in situ* measurements into three groups to represents clear, moderately turbid and turbid waters. The grouping was based on applying K-means clustering on measured concentrations of Chl-*a* and TSM. Figure 3.1 shows the mean and standard deviation values of Chl-*a* and TSM concentrations as well as the Secchi disc depth for the three groups. According to the properties of *R(0-)*, waters in this research environment can be classified into three types: Type A, Type B and Type C. Here, it could be mentioned that the three water types, identified by unsupervised classification of the shape of *R(0-)*, differed noticeably in terms of their constituent concentrations. Water Types A, B and C correspond respectively to low, moderate and high concentration of chlorophyll and TSM. Instead of location, they correspond to offshore and shelf edge, transitional region and near shore coastal waters.
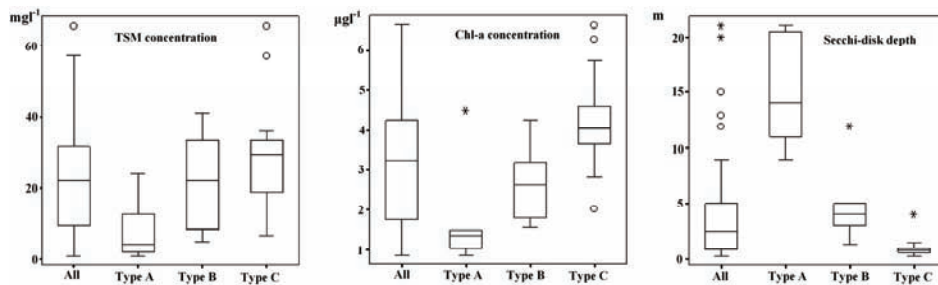
Figure 3.1 : Box plot of the TSM (left), Chl-*a* (middle) and Secchi disc depth (right) for all data and Type A, Type B and Type C waters, respectively. The boxes indicate the variation ranges defined by standard deviation; median is indicated as a horizontal line in the box; edge horizontal line of the box indicate quartile 1 and quartile 3 respectively; circle indicates outlier value; and star indicates extreme value.

3.4. Result

3.4.1. Subsurface irradiance reflectance of *in situ* measurement

The subsurface irradiance reflectance *R(0-)* is computed from the measured irradiances using Eq. (3.1), the resulting 36 spectra are presented in Figure 3.2a. Model (Eq.3.2) best-fits to the measured spectra are shown in Figure 3.2b. The means of measured *R(0-)* and the model best-fit are compared in Figure 3.2c. There is a good agreement between measured and model best-fit spectra with a R^2=0.74 and RMSE values of 0.113. Some mismatch is apparent in the short (blue) and long (NIR) wavelengths.
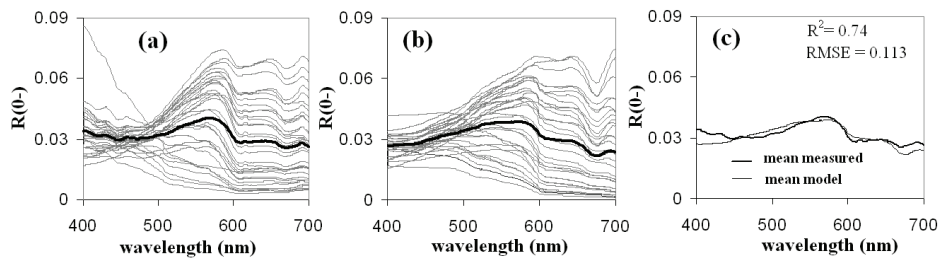
Figure 3.2 : The *R(0-)* field measurements (a); model-best-fit *R(0-)* (b); comparison of mean measured *R(0-)* and mean modelled *R(0-)* (c) of the Berau estuary (n=36). The thick lines indicate mean of the data.

The spectra of the three groups are shown in Figures 3.3a, 3.3b and 3.3c. Field measurement locations of each group are also displayed in Figure 3.3d. In Figure 3.3a, the *R(0-)* of Type A water shows an *R(0-)* curve shape which differs from that of the other two water types. In this water type, the highest value of the subsurface irradiance reflectance was obtained in the short wavelength (blue band), and continually decreases with increasing wavelength. A cross-check with the Secchi disc depth data indicates that this type of water corresponds mostly to clear blue water. Figure 3.3b shows the *R(0-)* of Type B water. The curves show a wide stable range between 400 and 580 nm. A moderate first peak is obtained at 550 to 580 nm. The second peak is found at

around 685 nm. A cross-check with the Secchi disc depth data indicates that this type of water corresponds mainly to the moderately turbid waters in the study area. Figure 3.3c shows the irradiance reflectance of Type C water. With the exception of the peak at 400 nm, this water type has generally the highest peak compared to the other water types. The first peak shifts towards 560-580 nm. The second peak occurs at 685 nm. Referring to the Secchi disc depth data, this type of water corresponds mainly to the most turbid water in the study area.
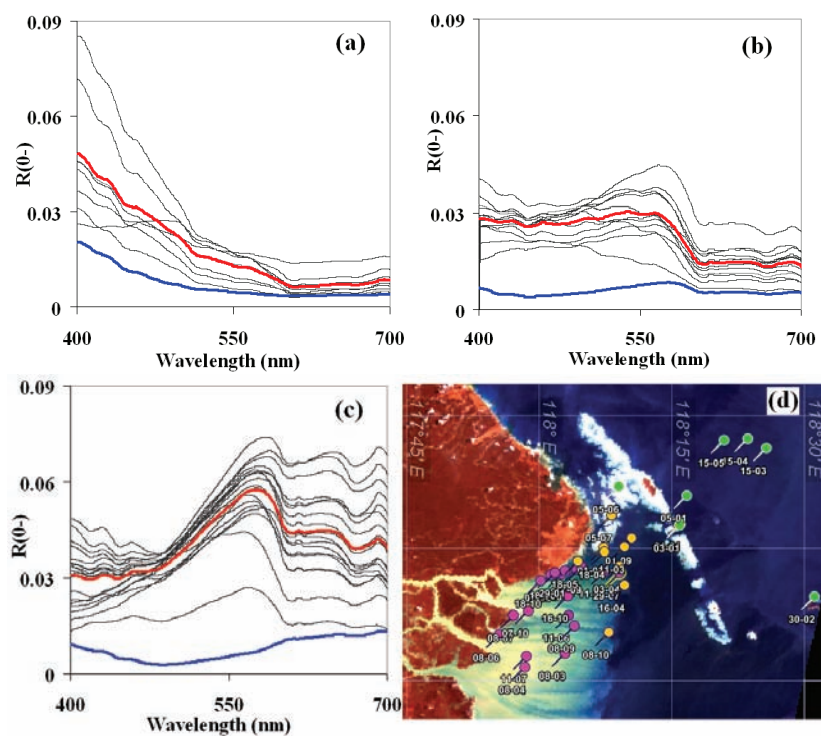
Figure 3.3 : The *R(0-)* spectra for the three water types: (a) Type A water (n=8), (b) Type B water (n=10), (c) Type C water (n=18) and (d) the locations of sampling. Grey lines are the individual spectra, red lines are the mean spectra of each class, and blue lines are the standard deviation spectra of each class.

A statistical analysis of *R(0-)* measured and *R(0-)* modelled of 36 measurement locations, is listed in Table 3.2. The R^2 for all wavelengths and the three types of water are high, especially for Type B and Type C waters. Based on the values of

R^2 (high) and RMSE (low), it can be concluded that at the wavelength of 489, 509, 559 nm and 619 nm, the best matches between measured and modelled *R(0-)* are achieved. After data classification, the R^2 improved significantly. However, the RMSE of the classified data sets was high, particularly for Type A water. A more detailed inspection of the statistical values indicates that the result of fitting between measured and modelled *R(0-)* in Type A waters (clear water) is generally less good than the results obtained for the other water types. The fitting of measured and modelled *R(0-)* in Type B and Type C waters gives sufficiently good results.

Table 3.2: Statistical summary of the measured *R(0-)* and modelled *R(0-)* at each wavelength (corresponding to the MERIS channels)

Wavelength (nm)	RMSE			R^2		
	Type A	Type B	Type C	Type A	Type B	Type C
412	0.175	0.057	0.057	0.83	0.87	0.93
442	0.083	0.013	0.018	0.92	0.96	0.98
489	0.064	0.028	0.036	0.97	0.95	0.92
509	0.133	0.019	0.027	0.85	0.99	0.96
559	0.155	0.017	0.027	0.77	1.00	0.99
619	0.136	0.075	0.028	0.56	0.99	1.00
664	0.284	0.138	0.032	0.57	0.99	1.00
680	0.362	0.187	0.066	0.56	0.99	0.99
708	0.531	0.248	0.070	0.47	0.96	0.96

3.4.2. Deriving Inherent Optical Properties from Model Inversion

The backscattering of the TSM coefficient at 550 nm ($b_{b,TSM}$) and the absorption of the Chl-*a* coefficient at 440 nm (*a_Chl*) are derived from *in situ* optical measurements using Eqs. (3.5 and 3.6) and presented in Table 3.3. The mean of $b_{b,TSM}$ data shows a higher value for Type C water (0.604 m^{-1}) than for Type A (0.019 m^{-1}) or Type B (0.196 m^{-1}) waters. The absorption of Chl-*a* shows a similar trend with backscattering TSM that was increased from Type A to Type C waters.

Table 3.3: Average $b_{b,TSM}$ (m^{-1}) at 550 nm and a_Chl (m^{-1}) at 440 nm for three types of Berau water during the dry season (August to September 2007)

	$b_{b,TSM}$ (m^{-1})			a_Chl (m^{-1})		
	Type A	Type B	Type C	Type A	Type B	Type C
Mean	0.019	0.196	0.604	0.037	0.057	0.108
Minimum	0.010	0.033	0.180	0.023	0.028	0.043
Maximum	0.036	0.527	0.995	0.061	0.110	0.484
St. Dev	0.009	0.174	0.247	0.011	0.028	0.098

3.4.3. Estimating Specific Inherent Optical Properties (SIOP)

The derived values of TSM specific backscattering coefficient are given in Table 3.4. The $b^*_{b,TSM}$ is 0.02 m^{2}g^{-1} in turbid water (Type C) and 0.003 m^{2}g^{-1} in open sea (Type A). The values are increasing form clear water to turbid water, corresponding to off shore to near shore sites.

Table 3.4: Specific backscattering coefficient of TSM, $b^*_{b,TSM}$ (m^{2}g^{-1}), at 550 nm for all water types

Water type	Known		Derived		RE
	Station	$b^*_{b,TSM}$	Station	$b^*_{b,TSM}$	(%)
Type A	30-2	0.005	5-6	0.008	36
	31-1	0.004	5-7	0.005	3
	3-1	0.003	15-3	0.002	19
	5-1	0.002	15-4	0.002	21
	Mean	0.003		0.004	20
Type B	1-8	0.004	11-3	0.003	44
	3-4	0.009	1-9	0.007	42
	8-10	0.008	18-6	0.009	11
	13-6	0.019	18-5	0.017	10
	15-7	0.015	16-3	0.012	30
	Mean	0.011		0.009	27
Type C	11-4	0.022	11-6	0.016	40
	11-7	0.021	8-3	0.023	8
	8-4	0.027	8-6	0.027	1

Water type	Known		Derived		RE
	Station	$b^*_{b,TSM}$	Station	$b^*_{b,TSM}$	(%)
	8-7	0.015	8-9	0.012	33
	1-6	0.019	7-10	0.018	4
	1-7	0.021	16-10	0.023	9
	17-9	0.012	18-10	0.016	23
	17-10	0.020	18-9	0.028	26
	29-1	0.027	29-7	0.021	25
	Mean	0.020		0.020	19

The specific absorption coefficients of Chl-*a* are given in Table 3.5. In the Berau estuary waters, the values of a^*_{Chl} were almost similar on those 3 types of waters. The values seem increasing from Type C (0.021 $m^2\,mg^{-1}$) to Type B (0.02 $m^2\,mg^{-1}$) to Type A (0.027 $m^2\,mg^{-1}$) waters. In the case of a^*_{Chl}, the relative error is 5% for Type A, 11% for Type B and 10% for Type C water.

Table 3.5: Specific Chl-*a* absorption, a^*_{Chl} ($m^2\,mg^{-1}$), at 440 nm for all water types.

Water Type	Known		Derived		RE
	Station	a^*_{Chl}	Station	a^*_{Chl}	(%)
Type A	30-02	0.031	5-1	0.031	1
	31-01	0.012	15-05	0.013	10
	3-1	0.026	15-04	0.027	2
	5-6	0.041	15-03	0.043	4
	Mean	0.027		0.028	5
Type B	1-8	0.032	11-3	0.028	14
	1-9	0.011	13-6	0.010	4
	3-4	0.026	8-10	0.027	5
	18-4	0.021	18-5	0.022	4
	5-7	0.010	16-4	0.009	11
	Mean	0.020		0.019	8
Type C	11-4	0.017	11-7	0.016	8
	11-6	0.038	17-09	0.041	8
	8-3	0.021	8-7	0.020	1
	8-4	0.035	8-6	0.031	10
	8-9	0.017	7-6	0.015	13

Water Type	Known		Derived		RE
	Station	a^*_{Chl}	Station	a^*_{Chl}	(%)
	7-10	0.020	18-06	0.023	16
	1-7	0.012	17-10	0.013	16
	16-10	0.016	18-10	0.017	5
	29-07	0.015	29-1	0.017	10
	Mean	0.021		0.022	10

The result of the simulations to assess the difference between derived and input $b^*_{b,TSM}$ and a^*_{Chl} is plotted in Figure 3.4. It shows the correlation between the derived and known values of SIOP for $b^*_{b,TSM}$ and a^*_{Chl}. The R^2 of $b^*_{b,TSM}$ is 0.87 and the R^2 of a^*_{Chl} is 0.89. From the performance of $b^*_{b,TSM}$, it can be concluded that a high correlation between the known data set and the derived data set can be observed. The RMSE was quite low on the $b^*_{b,TSM}$ than on the a^*_{Chl} .
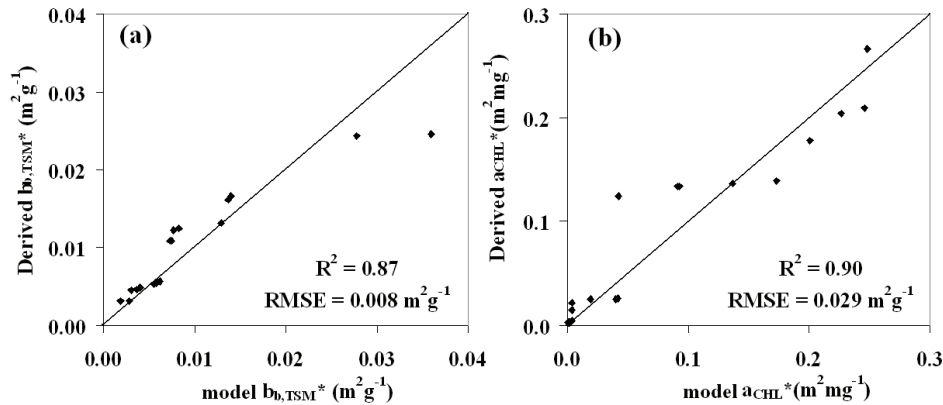
Figure 3.4 : Scatter plot of known/input and derived specific backscattering coefficient of TSM, $b^*_{b,TSM}$, at 550 nm (a) and specific absorption coefficient of Chl-*a*, a^*_{Chl}, at 440 nm (b).

3.4.4. Ocean colour imagery and *in situ* match up

A statistical analysis of the TSM and Chl-*a* concentration estimated from MERIS measurements and matching *in situ* measurements are given in Table 3.6. In general, there is a good agreement between TSM estimated from MERIS and

TSM measured in type A and B waters. The R^2 values are larger than 0.89 with RMSE between 0.060 and 0.079 mgl^{-1}. On the other hand, derived values of TSM were less reliable for type C water with R^2=0.66 and RMSE value up to 0.47 mgl^{-1}. In the case of Chl-*a* concentration, there is a moderately good correlation between the estimated and measured values for all types of waters. The R^2 values are between 0.62 and 0.7. The values of RMSE are however, in opposite to those obtained for TSM, i.e. larger errors are obtained in clear, type A, water with RSME value of 0.528 μg/l which is 3 folds larger than that of type C waters. For both variables, TSM and Chl-*a*, the best match-up results were obtained for type B waters. With large R^2 (≥0.7), a near to unity slope (~0.9) and small RMSE values of 0.06 mg/l and 0.21 μg/l for TSM and Chl-*a* respectively.

Table 3.6: Statistical summary of the relation between TSM measured and TSM estimated as well as Chl-*a* measured and Chl-*a* estimated from MERIS data in 3 types of waters.

	TSM Concentration [mg.l^{-1}]			Chl-*a* Concentration [μg.l^{-1}]		
	Type A	**Type B**	**Type C**	**Type A**	**Type B**	**Type C**
R^2	0.89	0.96	0.66	0.62	0.70	0.64
RMSE	0.079	0.060	0.465	0.528	0.206	0.177
Slope	0.630	0.856	0.386	1.806	0.875	0.488
Intercept	0.206	-1.106	-0.716	-1.379	-0.029	3.829
n	8	10	18	8	10	18

Figures 3.5a and 3.5b illustrate the estimated TSM and Chl-*a* concentrations for the Berau estuary waters from full resolution MERIS data on May 17, 2007. The 300 m resolution of MERIS data reveals the spatial distribution of TSM concentration throughout the study area. These concentration gradients are particularly evident in the middle portion of the image where the Berau river flows into the estuary. It shows clearly that TSM concentrations are higher around the coastal area and decrease when going to the sea. However, the Chl-*a* concentrations seem higher in some locations close to the Berau river mouth and decrease when going to the sea. The distribution of Chl-*a* was different and not entirely associated with TSM. The Chl-*a* concentration tended to be fairly uniform. The highest Chl-*a* levels were located in the region of fresh water

inflow. This region is located between Berau river mouth and the offshore reef and small island area.
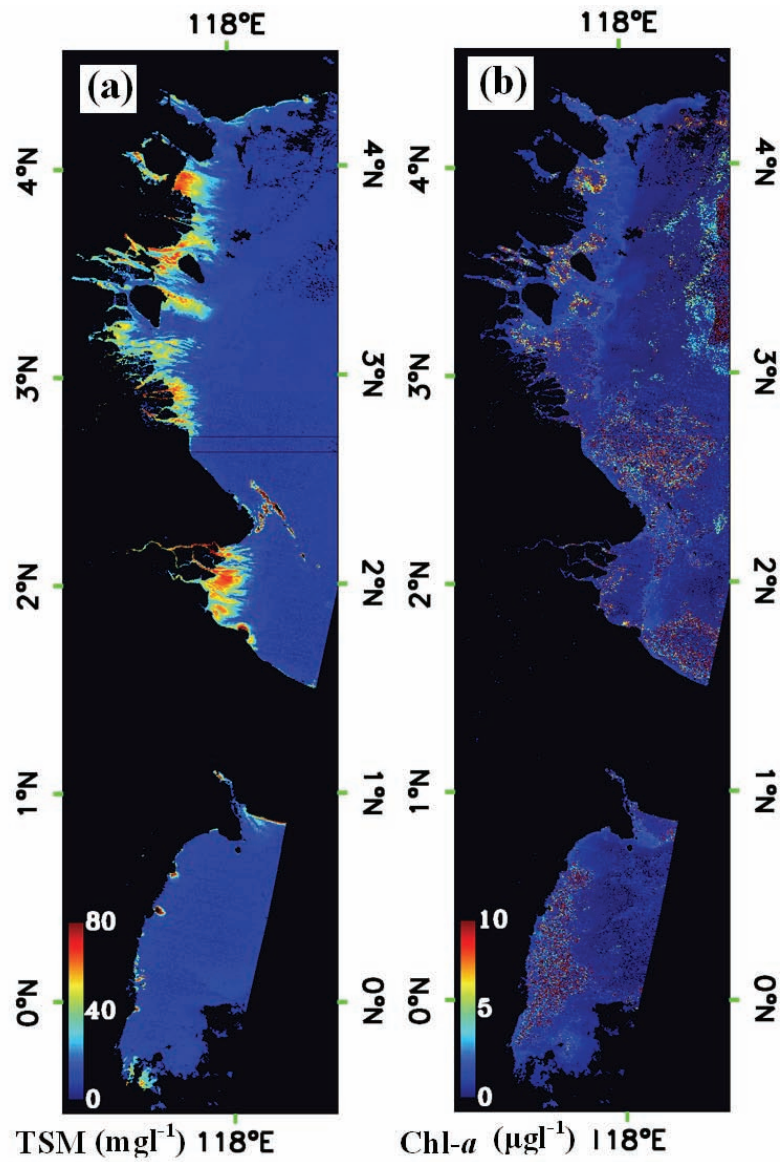
Figure 3.5 : TSM map (a) and Chl-*a* map (b) derived from MERIS FR Level 1b on May 17, 2007

3.5. Discussion

3.5.1. Classification

Type A water represents the clear water and close to the shelf edge and open ocean. This water type is characterized by low TSM concentration (mean = 8 mgl^{-1}), low Chl-*a* concentration (mean = 1.65 µgl^{-1}) and high Secchi disc depths (mean = 15 m). Type B water represents the region of fresh water influence where the fresh water mixes with saline ocean waters. This water type is characterized by TSM concentrations around 20.14 mgl^{-1}, Chl-*a* concentration 3.19 µgl^{-1} and Secchi disc depth around 4.5 m. Hundreds of typical in-water bamboo fishing houses are located in this Type B water. The last, Type C water is located around Berau river mouth with the TSM concentrations higher compared to others (mean = 28.9 mgl^{-1}) as well as high Chl-*a* concentration (mean = 4.43 µgl^{-1}) and very low Secchi disc depths (mean = 1 m).

The water close to the river mouth (Type C) is thus characterized by high values of TSM and Chl-*a* concentrations and low values of Secchi disc depth. Whereas, open waters (Type A) are relatively clear with low concentration of Chl-*a* and TSM. Hence, the IOPs of Type C water are higher than those of the other two water types. Similar results of decreasing IOP values moving off-shore were reported for the North Sea waters (Astoreca *et al*., 2006, Salama *et al.,* 2004),

3.5.2. Specific backscattering of TSM, $b^*_{b,TSM}$

The derived values of specific backscattering coefficient of total suspended matter (b^*_{TSM}, TSM) in the Berau estuary vary about an order of magnitude between Type A and Type C water, with the highest values being measured in turbid waters. In general, derived values of b^*_{TSM} water are in the range found by previous studies. For example, Dekker (1993) found a specific scattering coefficient (b^*_{TSM}) of 0.23 to 0.79 m^{2}g^{-1} for different trophic states in lakes, with a backscattering to scattering ratio varying from 0.011 to 0.020 m^{2}g^{-1}, and so a backscattering coefficient of TSM ($b^*_{b,TSM}$) of 0.003 to 0.016 m^{2}g^{-1}. Ibelings *et al*.

(2001) reported a specific scattering coefficient of 0.25 to 0.31 m²g⁻¹ for Lake IJssel in the Netherlands, with a backscattering to scattering ratio of 0.035 to 0.045, and so a backscattering coefficient of TSM ($b^*_{b,TSM}$) of 0.009 to 0.014 m²g⁻¹. However, our result seems to be higher than the results found by Heege (2000, in Albert & Mobley, 2003), who investigated the scattering of suspended matter in lake Constance. He found the specific scattering and backscattering coefficient of TSM to be b_{TSM}^* = 0.45 m²/g and $b^*_{b,TSM}$ = 0.009 m²g⁻¹, and thus a scattering ratio of 0.019. Table 4 shows that the relative error of $b^*_{b,TSM}$ at each station is relatively high, with an error average of 20% for Type A, 27% for Type B and 19% for Type C water. Although the individual errors between known data sets and derived data sets are high, the aggregate value of relative error for each type of water can be considered satisfactory.

This discrepancy between derived $b^*_{b,TSM}$ in the Berau water and reported values elsewhere can probably be explained by differences in sediment characteristics, i.e. particle size and composition. For example, Stramski *et al*. (2002) and Babin & Stramski (2004), showed that very fine particles are a more efficient scatterer and absorber of light than coarse particles.

3.5.3. CDOM

The CDOM absorption in the Berau estuary ranged from 1.67 m⁻¹ in the river to 0.091 m⁻¹ in clear open seawater. At the Berau river mouth, the CDOM absorption value was 0.5 m⁻¹. It is worth noting that the lowest measured values of CDOM absorption in the Berau are still higher than the threshold for Case-2 waters of ~ 0.03 m⁻¹ (Kratzer *et al*., 2008). The high values of CDOM absorption can also be noticed form the lower reflectance values of the type C waters in the Berau estuary as shown in Figure 3.3c. The spectral slope of the CDOM absorption was found to be spatially homogenous in the range, -0.011 to -0.015 nm⁻¹ with an average of -0.012±0.002 nm⁻¹.

3.5.4. Specific absorption of phytoplankton, a^*_{Chl}

Although the specific absorption coefficient of phytoplankton could vary for the same region (Mitchell & Kiefer, 1988), in the Berau estuary waters, it has a relative constant value. Its value (0.020 - 0.027 m2.mg^{-1}) is similar to what has been reported elsewhere. For example, Prieur & Sathyendranath (1981), Sathyendranath *et al*. (1987) and Gallegos *et al*. (1990) found that a^*_{Chl} for oceanic and coastal waters varies from 0.01 to 0.0473 m^2 mg^{-1}, whereas Smith & Baker (1978) found that a^*_{Chl} at 440 nm varied between 0.039 and 0.168 m^2 mg^{-1}. On the other hand Heege (2000, in Albert & Mobley, 2003) and Chengfeng *et al*. (2009) measured mean values of 0.034 m^2 mg^{-1} for Lake Constance and Lake Taihu, China, respectively.

Derived values of a_Chl indicate that the Berau estuary has lower content of green pigment when compared to other regions. For example, Astoreca *et al*. (2006) reported *a_Chl* values of the North Sea coastal waters to be between 0.48 ± 0.63 m^{-1} in May 2004 and 0.21 ± 0.14 m^{-1} in July 2004 which are four times larger than derived values in type C waters of the Berau estuary (*see* Table 3.3). On the other hand, offshore waters of the Berau and North Sea have comparable values of *a_Chl*. Astoreca *et al*. (2006) reported for offshore water of the North Sea, *a_Chl* values of 0.08 ± 0.04 m^{-1} in May 2004 and 0.05 ± 0.03 m^{-1} in July 2004, which is similar to type A and B waters of the Berau with mean values of 0.037 to 0.057 respectively, (*see* Table 3.3). These results indicate that the Berau estuarine waters have relatively low trophic state. This could also mean that the Phytoplankton average cell size in the Berau estuary is small, which is characteristic of oligotrophic waters (Mercado *et al*., 2007).

3.5.5. MERIS and *in situ* match-up

A good fit was found between MERIS-derived and measured variables of TSM and Chl-*a* concentrations. In the comparison we used statistical parameters of R^2, RMSE, slope and intercept. The best results were however, obtained for moderate turbid water of Type B. This could be explained by two reasons: (i) large error induced by atmospheric correction in cloud-shadowed (Matthew *et*

al., 2000) and hazy regions which prevailed off shore the Berau estuary; (ii) large error induced by model parameterization and inversion in turbid waters; and (iii) large error induced by model parameterization and inversion in clear area affected by bottom reflectance.

The relative contribution of these different error components to the total uncertainty in derived IOP was estimated for the same model as used in this study and MERIS sensor to be about 46-50% from atmosphere correction, 40-45 from model parameterization-inversion and 5-13% from sensor Noise (*see* table 3.4 *in* Salama & Stein, 2009).

3.5.6. Uncertainties

The specific inherent optical properties (SIOP) were derived from *in-situ* measurements and model inversion. However each step on the derivation procedure has an error component which will contribute to the total uncertainties of the derived SIOP. The total uncertainty of derived SIOP is a lumped effect of several error components, namely measurement, model parameterization and inversion, and atmospheric correction.

a. Field radiometric measurement

In situ data may contain significant errors caused by environmental factors, instrumental shortcomings and human errors (Hooker & Maritorena, 2000, Chang *et al*., 2003). In this study, we observed that the subsurface irradiance reflectance, *R(0-)* in the Berau estuary varied strongly from clear water to turbid waters due to the different water constituents. It can be seen that generally, the modeled *R(0-)* has good agreement with the *R(0-)* measurements. However, matching was poorer for some locations, particularly in clear water rather than turbid waters. This tendency of decreasing measurements reliability in clear water can be attributed to the reduced signal-to-noise ratio of the used Ocean-Optics device in very clear water under cloud cover: (i) the persistence of especially cirrus cloud cover during field measurements reduced the available

light; (ii) and reduced the signal of the water leaving reflectance for very clear ocean waters.

b. Model parameterization and inversion

The second major source of uncertainty is due to model parameterization. The used model (i) ignores the different phytoplankton species that may co-exist in inland water; (ii) ignores the great variability of Chl-*a* absorption as measured in nature, (iii) combines the absorption effect of detritus and CDOM in one spectral shape and magnitude. Inversion uncertainty is an inherent attribute to model optimization and it was estimated to be at least 17% for the absorption of Chl-*a* and 7% for the backscattering of TSM (*see* Table 1 *in* Salama & Stein, 2009).

3.6. Conclusion

In this paper we estimated and analyzed the variations of specific inherent optical properties (SIOP) in the Berau estuarine waters. The SIOP were derived from extensive *in situ* measurement of subsurface irradiance reflectance and water constituents and model inversion. The results were validated using *in situ* measurements and ocean colour satellite observations. The following points are concluded of this work:

1. Moving from turbid estuarine waters to clear off shore waters, we could spectrally distinguish three water types that differ in their composition, turbidity and hence optical signatures;
2. The specific absorption coefficient of Chl-*a* is relatively constant for the three types of waters with an average value of 0.024 m^2/mg;
3. The spectral slope of CDOM absorption was found to be spatially homogenous and in the range, -0.011 to -0.015 nm^{-1} with an average of -0.012±0.002.
4. The specific backscattering coefficient of TSM vary from 0.003 m^2/g for clear water to 0.020 m^2/g for turbid water;

Our reported values of specific inherent optical properties form a corner stone for future estimation of TSM and Chl-*a* concentration from remote sensing data in the Berau estuary.

CHAPTER 4

MERIS DATA FOR MONITORING TROPICAL COASTAL WATERS

Abstract[*]

This chapter investigates the performance of MERIS reduced resolution data to monitor water quality parameters in the Berau estuary waters, Indonesia. Total Suspended Matter (TSM), Chlorophyll-*a* (Chl-*a*) and diffuse attenuation coefficient (K_d) were derived from MERIS data using three different algorithms for coastal waters: MERIS L2 Standard Global processor, C2R and FUB. The outcomes were compared to *in situ* measurements, collected in 2007. MERIS data processed with C2R gave the best retrieval of Chl-*a*, while MERIS L2 performed the best for TSM retrieval. Large deviations from *in situ* data were however observed, pointing at inversion problems over these tropical waters for all standard processors. Despite of these deviations, MERIS can be of use for monitoring equatorial coastal waters like the Berau estuary and reef system with application of several precautions. Applying a $K_d(490)$ local algorithm to the MERIS RR data over the study area showed a sufficiently good correlation to the *in situ* measurements ($R^2 = 0.77$).

---

[*] Submitted as:

4.1. Introduction

The Berau estuary, East Kalimantan, is a high biodiversity site in Indonesia that has been declared as a Marine Protected Area (MPA) by the Indonesian government. Knowledge on the levels and spatial distributions of suspended sediment concentration, eutrophication and water transparency are essential for monitoring the health of the ecosystem and especially of coral reefs (Richmond *et al.*, 2007) in this site, located 40 to 100 km from the mouth of the Berau river. Water quality monitoring in this environment becomes increasingly important, because enhanced anthropogenic activities in the Berau catchment, such as coal mining and deforestation, have increased the load of suspended sediment, chemicals and nutrients into the estuary. Mapping of total suspended matter distribution as well as Chl-*a* concentration using an accurate methodology will help the coastal manager to arrange the plan of environmental protection in order to sustain such MPA. In addition, the study of coastal dynamics in the Berau estuary is getting increasingly important since it is located at the edge of Indonesian Through-flow (ITF) from the Pacific Ocean to the Indian Ocean through the Makassar strait, an ocean current that plays a key role in the global thermohaline circulation (Gordon, 2001).

Remote sensing of ocean color was initiated when the Coastal Zone Color Scanner (CZCS) was launched by NASA in 1978. This instrument demonstrated that satellite-based optical instruments have the capability to monitor oceans and coastal waters. Following the success of the CZCS, several sensors like SeaWIFS (Sea-viewing Wide Field-of-view Sensor) and MODIS (Moderate Resolution Imaging Spectroradiometer) were put into orbit to monitor global ocean color and coastal water quality (IGOS, 2006). The Medium Resolution Imaging Spectrometer (MERIS) was launched by European Space Agency (ESA) in 2002, mounted on the ENVISAT satellite platform. The MERIS sensor measures reflected solar radiation in the visible spectral domain at 15 wavelength bands with an average bandwidth of only 10 nm. The spatial resolution is 1.2 km at nadir in the Reduced Resolution (RR) mode and with a swath of 1200 km, the globe is fully covered every three days. This

configuration provides at present one of the best capabilities for observing the optically complex coastal or Case-2 waters (Rast *et al*., 1999).

The potential of the MERIS configuration has been investigated in pre-launch studies by Bricaud, *et al*. (1999) and Fischer & Fell (1999). Since its launch, several studies have been focussed on retrieval of water quality parameters in coastal marine waters, such as on TSM, Chl-*a* and Colour Dissolved Organic Matter (CDOM) retrievals (Alikas & Reinart, 2008; Aiken *et al*., 2007; Doerffer & Schiller, 2007; Schroeder *et al*., 2007; Ohde *et al.,* 2007; Folkestad *et al*., 2007; Krawczyk *et al*., 2007; Koponen *et al*., 2007, Sørensen & Høkedal, 2006). These studies confirmed that MERIS has large potential for water quality assessment in the coastal zone (Doerffer *et al*., 1999) as well as for freshwater basins (Koponen *et al*., 2002; Floricioiu *et al*., 2003).

A variety of techniques and algorithms to extract water inherent optical properties and water constituents from MERIS is available (IOCCG, 2006). Examples are the MERIS Neural Network Algorithm (Schiller & Doerffer, 1999; Doerffer & Schiller, 2007; Schroeder *et al.,* 2007), Linear Matrix Inversion Algorithm (Lyon & Hoge, 2004), the Quasi Analytical Algorithm (Lee *et al.,* 2002), the GSM (Garver-Siegel-Maritorena) Semi-Analytical Bio-optical Model (Maritorena & Siegel, 2005) and the HYDROPT Algorithm (Van der Woerd & Pasterkamp, 2008). Among these algorithms, the Case-2 Regional (C2R) Plug-In processor, developed by Doerffer & Schiller (2007) and the Free University Berlin (FUB) water Plug-In processor, developed by Schroeder & Schaale (2005) have been especially developed for coastal or Case-2 waters and those algorithms are a plug-in of the BEAM Visat software. These algorithms use artificial neural networks (ANN) that can be seen as an integrated approach of inverse modelling of radiative transfer within the coupled water-atmosphere system (Schroeder *et al.,* 2007).

Most of the algorithm development for estimating water quality parameters from MERIS data has been carried out in North European coastal waters, mainly at mid-latitude, for example the North Sea and Baltic Sea. Limited research has been carried out in the tropical equatorial region, especially in

Indonesian waters. The aim of this study is therefore to analyze the performance of MERIS Case-2 water products and their applicability for monitoring the Berau tropical coastal waters. In particular, we investigated the reliability of water quality parameters along a transect from the river mouth to the coral reef that might be used to establish the influence of the river system on these reefs. If successful, MERIS data could be one of the key elements in the protection of coral reef life in this area.

In this research, we compare the TSM and Chl-*a* concentration derived from MERIS RR data using global and regional Case-2 algorithm processors and analyze the water leaving remote sensing reflectance (R_{rs}) and the diffuse attenuation coefficient, $K_d(490)$, for understanding the water column spectral response of the Berau estuary waters. These products are then compared to data collected during an extensive field campaign in August and September 2007.

4.2. Data set

In order to verify and test MERIS data over coastal waters, a field campaign was carried out in the dry season of August and September 2007. A handheld GPS (GARMIN) was used to establish the geographical position of each station. The field stations cover the full range of water conditions of the Berau estuary, from turbid river water to clear oceanic waters. A field laboratory was set up at Derawan Island for analysis of the waters samples. In total, 18 transects were measured in 30 days, consisting of 171 field stations, with 80 field stations where optical spectrometer *in situ* measurements were conducted. The distribution of the stations is shown in Figure 4.1.

Timing of the MERIS overpass in this study area is typically within 15 minutes from 02:00 UTC or 10:00 local time. Field measurements were carried out preferably within -1 to + 5 hours difference with the MERIS overpass. Table 4.1 shows the dates, stations and types of data measured. From all the stations, only one day of the field campaign (9 stations) gave a full match-up with cloud-free MERIS products having little sun glint. The field campaign of August 31,

2007 was used for validating the TSM and Chl-*a* concentration, K_d *(490)* and water leaving remote sensing reflectance (R_{rs}) derived from MERIS data.
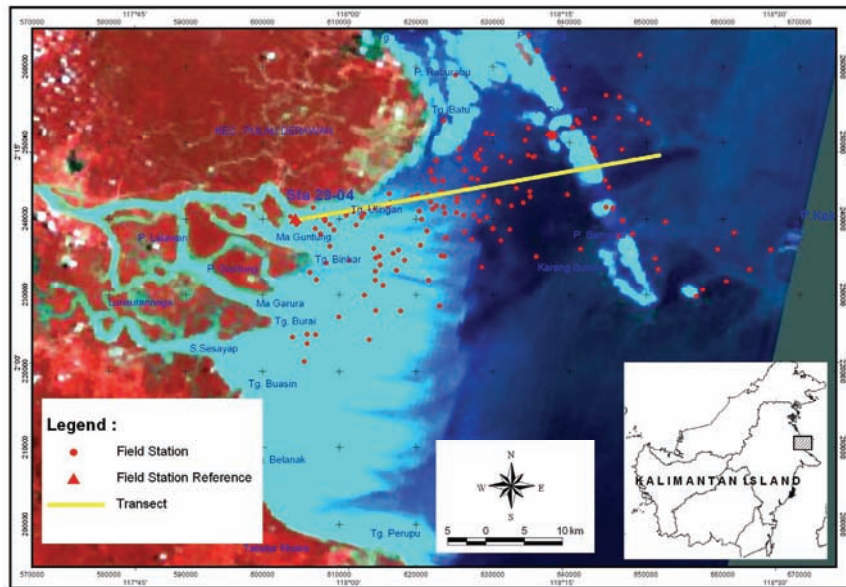
Figure 4.1:   The location of field stations in the Berau estuary, plotted on the MERIS FR L1 image, false colour composite (RGB:14-8-4), taken at May 17, 2007.

Table 4.1:   Dates of measurements, number of stations and measurements obtained.

Date	Stations	Water Quality	Optical Parameters	MERIS Image quality
27/08/2007 to 30/08/2007	35	TSM, Chl-*a*	Secchi disk, R_{rs}	Poor due to Clouds or Sun glint
31/08/2007	9	TSM, Chl-*a*	Secchi disk, R_{rs}	Good RR at 01.55 UTC
01/09/2007 to 18/09/2007	127	TSM, Chl-*a*	Secchi disk, R_{rs}	Poor due to Clouds or Sun glint

An Ocean Optic spectrometer (USB4000) was used to collect *in situ* spectral measurements. The water leaving radiance, the downward skylight irradiance and subsurface upwelling irradiances were scanned in each station at different depths (10, 30 and 50 cm), providing a more robust R_{rs} spectrum than only above-water spectra (Bhatti *et al.*, 2009).

50

Bio-geophysical variables such as TSM, Chl-*a* concentrations, Secchi disc depth and other generic water quality variables (EC, temperature, pH, turbidity, dissolved oxygen, salinity) were also collected and have been described in Chapter 3 (*see* subsection 3.2.2).

4.3. Models and algorithms

The MERIS RR L1b and L2 images of August 31, 2007 were analyzed. L2 is processed by the ESA ground segment processor. The Basic ENVISAT Toolbox for MERIS BEAM version 4.5.1 was used for processing the MERIS L1 data. BEAM is open-source software for visualizing, analyzing and processing the Envisat MERIS, AATSR, ASAR, ERS ATSR and MODIS and AVHRR data (Brockmann, 2009, http://www.brockmann-consult.de/cms/web/beam).

The MERIS RR L1b TOA radiances were processed into L2 with two regional Case-2 water processors, C2R and the FUB processor, both ANN algorithms and provided as plug-in for the BEAM VISAT software. A description of the C2R algorithm can be found in Doerffer & Schiller (2007). From the C2R water products, the water leaving reflectance, TSM concentration and Chl-*a* concentration were used in this study. In order to have the same units of Apparent Optical Properties (AOPs) variables, the water leaving radiance reflectance was converted into remote sensing reflectance. Schroeder & Schaale (2005) describe in detail the FUB water processor. The FUB processor uses MERIS Level-1b TOA radiances of bands 1–7, 9–10 and 12–14. Three variables derived by the FUB water processor were used in this study: water leaving remote sensing reflectance (8 bands), TSM concentration and Chl-*a* concentration.

From *in situ* optical measurements obtained with the Ocean Optic spectrometer, the subsurface irradiance reflectance $R(\lambda,0^-)$ at each wavelength (λ) was calculated. The $R(\lambda,0^-)$ is given by Mobley (1994) as the ratio of upward (E_u) and downward (E_d) irradiance ($\mu W\ cm^{-2}\ nm^{-1}$) just beneath the water surface:

$$R(\lambda, 0^-) = \frac{E_u(\lambda, 0^-)}{E_d(\lambda, 0^-)} \qquad (4.1)$$

The subsurface remote sensing reflectance was calculated using:

$$R_{rs}(0^-) = \frac{R(0^-)}{Q} \qquad (4.2)$$

where *Q* stands for the geometric anisotropy factor of the under water light field, usually taken as $Q = 5$ sr (Albert & Mobley, 2003; Gege, 2005). From the subsurface remote sensing reflectance, the above surface remote sensing reflectance was calculated using (*see* e.g. Bhatti *et al.*, 2009):

$$R_{rs}(0^+) = 0.544 * R_{rs}(0^-) \qquad (4.3)$$

The diffuse attenuation coefficient, K_d (m^{-1}) is an important environmental variable determining the light conditions for phytoplankton and coral reef life. It has been shown that K_d can be estimated reliably from remote sensing data in the Baltic Sea (Darecki & Stramski, 2004; Kratzer *et al.*, 2008). K_d is a function of the downward irradiance (E_d) at different depths, it can be defined by the equation (Mobley, 1994):

$$K_d(\lambda) = -\frac{1}{\Delta z} \ln \frac{E_d(z_2, \lambda)}{E_d(z_1, \lambda)} \qquad (4.4)$$

where, Z_2 and Z_1 are depths (m) and $\Delta z(m) = Z_2 - Z_1$. $K_d(490)$ is the diffuse attenuation at a wavelength of 490 nm, which can be derived from normalized water leaving radiance, L_{wN} (µW cm^{-2} nm^{-1} sr^{-1}) by using a band ratio algorithm (Mueller, 2000) as:

$$K_d(490) = K_w(490) + A \left[L_{wN}(\lambda_1)/L_{wN}(\lambda_2) \right]^B \qquad (4.5)$$

where $K_w(490)$ is the diffuse attenuation coefficient for pure water at 490 nm, taken here as 0.022 m^{-1} (Smith & Baker, 1981). The bands are taken at wavelengths of (λ_1, λ_2). The *A* and *B* coefficients are determined from empirical fits to *in situ* data. Kratzer *et al*. (2008) modified the algorithm for deriving $K_d(490)$ from MERIS reflectance (ρ_w) data as follows:

$$\ln\left[K_d(490) - K_{dw}\right] = -1.03 * \ln\left[(\rho_{490}/\rho_{620})\right] - 0.43 \qquad (4.6)$$

where, K_{dw} is diffuse attenuation coefficient of water molecules.

In this study, K_d *in situ* was estimated by converting the Secchi disc depth (Z_{SD}) that was described by Kirk (1994), from a linear relationship:

$$K_d(\lambda) = 1.44/Z_{SD} \qquad (4.7)$$

Following the work of Kratzer *et al*. (2008), the algorithm for estimating K_d from MERIS data in the Berau estuary was developed by using the natural logarithm of remote sensing reflectance (R_{rs}) ratio at wavelengths of 490, 560 and 620 nm against [$K_d(490)$– K_{dw}]. The combination of band reflectance ratios from *in situ* R_{rs} data that scored the highest coefficient of determination was chosen for the final algorithm. This algorithm was subsequently applied to the three remote sensing reflectances (R_{rs}) derived from the MERIS data (C2R, FUB and MERIS L2).

4.4. Results

4.4.1. Water quality dynamic of *in situ* observation

The Berau estuary belongs to the category of Case-2 waters that are characterized by the presence of relatively high quantities of suspended particulate matter (TSM) and coloured dissolved organic matter (CDOM). The CDOM absorption at 440 nm (g_{440}) was measured in a small additional field campaign, done in January 2009. The CDOM absorption in the Berau estuary ranged from 1.67 m^{-1} in the river to 0.091 m^{-1} in clear waters. Around the Berau river mouth, CDOM absorption value was 0.5 m^{-1}. We note that the lowest CDOM measured was still higher than the threshold for Case-2 waters (Kratzer *et al*., 2008).

The TSM concentration measured in the field campaign of August - September 2007 varied from 0.2 mgl^{-1} (in clear waters, close to the open ocean) to 81.2 mgl^{-1} (in the Berau river mouth) with an average value of 21.4 mgl^{-1}. In order to understand better the spatial and temporal distribution of TSM concentration in

the Berau estuary, the TSM concentration measured *in situ* is plotted against the distance to the Berau river mouth (Latitude-Longitude of 117º 56' 15.9 E 02º ; 10' 16.8 N, indicated with station 29-4 in Figure 4.1) as a starting point (Figure 4.2a). The result shows that there is a large temporal variability of TSM in this period and that no clear relation exists between TSM concentration measured *in situ* and distance.
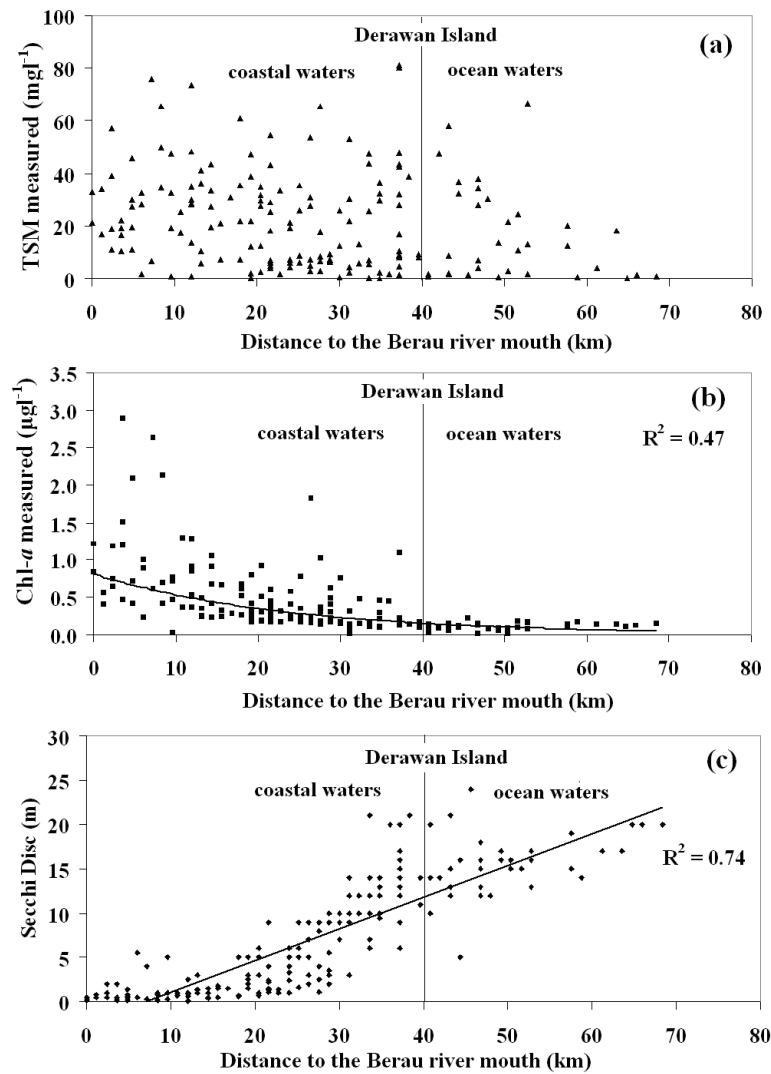
Figure 4.2 : The water quality parameters TSM concentration (a), Chl-*a* concentration (b) and Secchi disc depth (c), plotted as a function of the radial distance from the Berau river mouth.

The pattern of Chl-*a* concentration measured *in situ* seems more correlated with the distance (Figure 4.2b). Concentrations of Chl-*a* found in the location close to the river mouth decrease offshore. The distribution trend of Chl-*a* against the distance favors an exponential model with R^2 = 0.47 (n = 171). For the Secchi-disc depth (SD), low SD values (1-2 m) were found close to the river mouth and increased to 15 m or more in offshore direction (Figure 4.2c). A simple linear regression model gave a best fit, with R^2 = 0.74 with n = 171.

4.4.2. MERIS water quality maps

The distribution of TSM concentration and Chl-*a* concentration derived from MERIS RR data of August 31, 2007 using the C2R, FUB processor algorithms and MERIS L2 are displayed in Figure 4.3. All images show high TSM concentrations in the location close to river discharge and tend to decrease when going to offshore. The TSM concentration derived with the C2R processor algorithm (Figure 4.3a) was higher than ones derived with FUB and MERIS L2 (Figure 4.3b and Figure 4.3c). For Chl-*a*, the concentration derived with FUB (Figure 4.3d) was higher than with C2R and MERIS L2 (Figure 4.3e and Figure 4.3f). These patterns appear more clearly when they are plotted along the same transect, as is shown in Figure 4.4. The greatest difference between the three algorithms occurred in the most turbid waters, located at distances between 0 km and 20 km.

Figure 4.4b and Figure 4.4d present the transect analysis of the TSM and Chl-*a* concentration collected from i*n situ* stations that were located between 28 km and 40 km from the river mouth. Those 9 stations were collected at the same day as the MERIS data August 31, 2007. Figure 4.4b and Figure 4.4d show that the values of TSM as well as Chl-*a* concentration retrieved from MERIS are lower than the values of the *in situ* measurements. The correlation analysis of TSM and Chl-*a* concentration for those 9 stations is presented in Table 4.2.
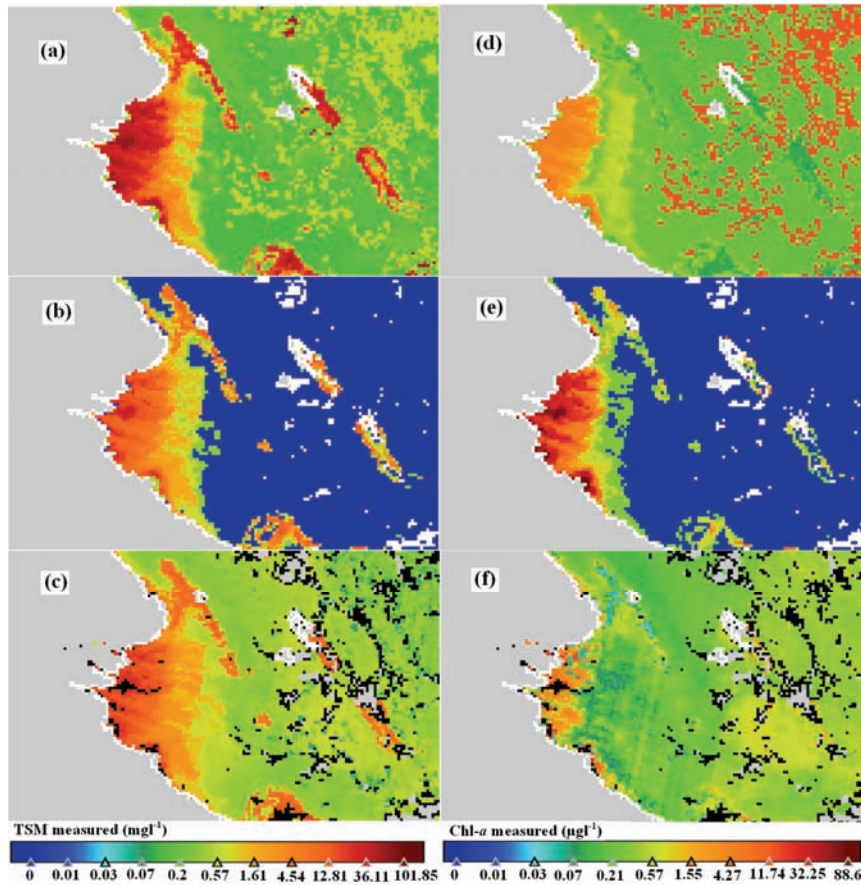
Figure 4.3 : Concentration maps of TSM (a,b,c) and Chlorophyll-*a* (d,e,f) derived from MERIS RR image of August 31, 2007. The processing from L1 to L2 was carried out with C2R (a,d), FUB (b,e) and standard ESA processors (c,f).

Table 4.2: Summary of the correlation between TSM concentration and Chl-*a* concentration estimation from MERIS data and field data on August 31, 2007.

TSM Concentration (mgl^{-1})			
	RMSE	% Difference	R^2
C2R	2.88	-44	0.03
FUB	3.13	-64	0.05
L2	2.76	-36	0.05
Chl-*a* Concentration (µg l^{-1})			
	RMSE	% Difference	R^2
C2R	0.33	47	0.75
FUB	0.54	-65	0.85
L2	0.63	-17	0.53
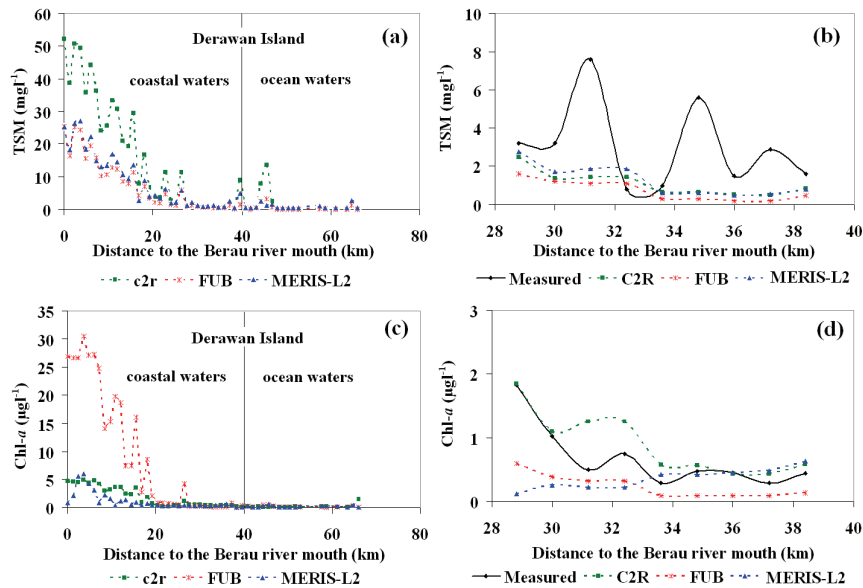
Figure 4.4 : Concentration transects of TSM (a,b) and Chl-*a* (c,d) derived from the MERIS RR image and *in situ* measurements (b and d only) taken on August 31, 2007.

Table 4.2 shows that in terms of the RMSE and R^2, the TSM of MERIS L2 was closest to the *in situ* data, but no relation could be established. The lowest RMSE of Chl-*a* was obtained with C2R.

4.4.3. Remote sensing reflectance (R_{rs})

The magnitude and the spectral variation of remote sensing reflectance (R_{rs}) depend on the IOPs, i.e. the absorption and backscattering properties of seawater itself, phytoplankton, Colour Dissolved Organic Matter (CDOM) and detritus. There were 9 stations with remote sensing reflectance data measured by the Ocean Optic USB4000 which matched up with MERIS L1 of August 31, 2007. The spectra retrieved by applying different algorithms on the MERIS L1 image data showed different shapes and magnitudes of water leaving remote sensing reflectance, R_{rs}. Consequently, the inter-comparison between *in situ* reflectance data and R_{rs} retrieved from MERIS L1 as well as MERIS L2 satellite data showed also different degrees of correlation and RMSE.
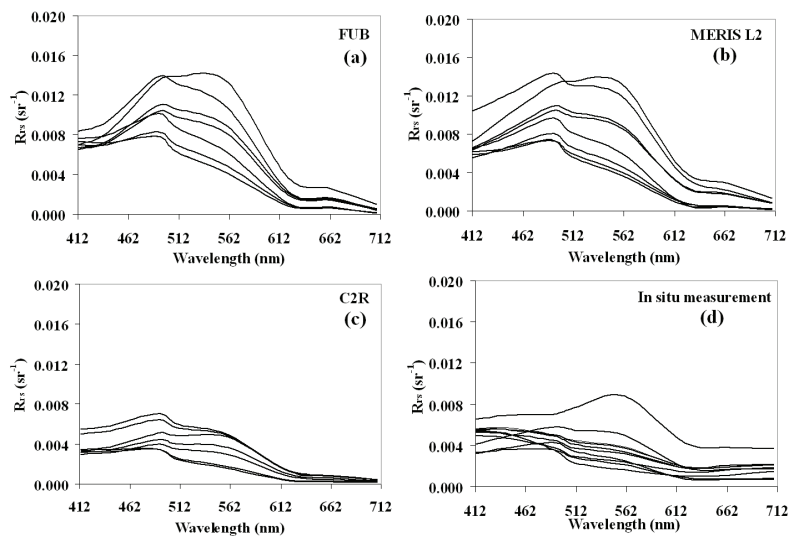
Figure 4.5 : The remote sensing reflectance (R_{rs}) derived from MERIS data using different processors (a, b, c) compared to *in situ* data (d) taken at the match-up stations on August 31, 2007.

For this study, the R_{rs} of *in situ* measurements have been calculated using Eq. (4.1) to Eq. (4.3), whereas, the R_{rs} from MERIS data were derived by applying the global algorithm of MERIS L2, as well as the C2R and FUB algorithms using the BEAM software. The MERIS L2 and C2R water leaving radiance reflectances

58

(R_w) were converted to R_{rs}. The three R_{rs} outputs obtained from three different algorithms for the 9 stations (data set of August 31, 2007) are plotted in Figure 4.5.

The R_{rs} spectra from FUB and MERIS L2 data sets are characterized by a strong slope at short wavelengths and have a maximum value at 490 nm (band 3). The maximum R_{rs} of the FUB data set at 490 nm varies from 0.008 to 0.014 sr^{-1}, while for the MERIS L2 data set, the values vary between 0.007 and 0.014 sr^{-1}. The R_{rs} of C2R showed also similar characteristics to the R_{rs} of FUB and MERIS-L2, where the peak is visible at 490 nm, but with smaller magnitude (0.004 - 0.007 sr^{-1}). In contrast, the R_{rs} of *in situ* data sets shows different characteristics, and the peak varies from 0.004 to 0.009 sr^{-1}. The R_{rs} was relatively high in the blue wavelengths and decreases with increasing wavelength. Moreover, some stations have a maximum R_{rs} at 412 nm (band 1) and a minimum R_{rs} at 490 nm (band 3). The RMSE was used to express the differences between R_{rs} measured and R_{rs} derived from MERIS data and is displayed in Figure 4.6. The R_{rs} derived from MERIS with FUB and MERIS L2 and R_{rs} measured were relatively similar at all wavelengths and RMSE decreased towards longer wavelengths. The RMSE between R_{rs} derived from MERIS with C2R and R_{rs} measured was higher than with FUB and MERIS L2 at short wavelengths. Moreover, the RMSE of R_{rs} with C2R at wavelengths of 490 nm, 510 and 560 nm were lower than with FUB and MERIS L2.

The coefficients of determination of the relation at each MERIS wavelength between R_{rs} measured and R_{rs} retrieved by using different algorithms are displayed in Figure 4.7. It seems that the R^2 between R_{rs} measured and R_{rs} derived from MERIS with different algorithm processor was very low at short wavelength (412 nm) and increased with increasing wavelength. The highest correlations were obtained at wavelength of 490, 510 and 560 nm.
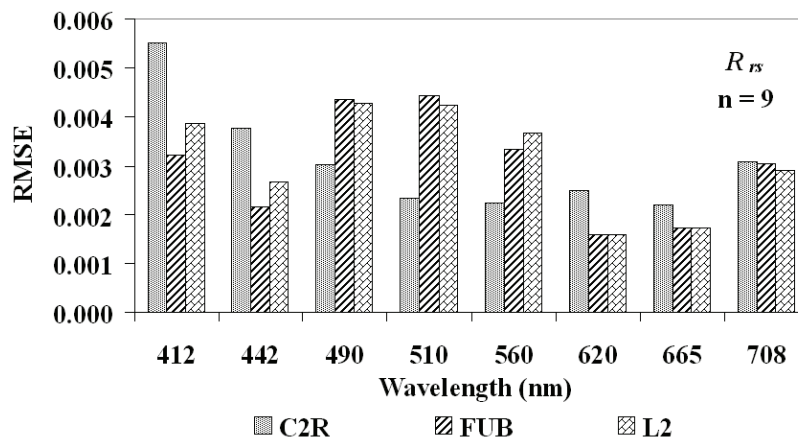
Figure 4.6 : The RMSE between R_{rs} measured and R_{rs} derived from MERIS data with the C2R algorithm, FUB and MERIS L2, n=9
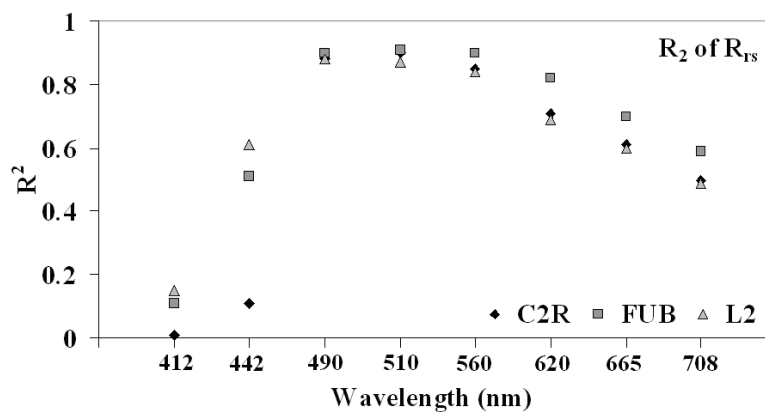
Figure 4.7 : The coefficient of determination (R^2) of the relation between *in situ* R_{rs} and MERIS R_{rs} using different processors, based on 9 stations.

4.4.4. The diffuse attenuation coefficient

The diffuse attenuation coefficient from *in situ* measurements in the Berau estuary waters was derived by using Eq. (4.7). The K_d varied from 0.07 to 2.88 m⁻¹ with an average of 0.86 m⁻¹ (n = 63). The K_d measured and R_{rs} measured in the field on August 31, 2007 (9 locations) were used to establish the relationship between K_d and R_{rs} measured. The best fit between R_{rs} measured and K_d measured, that was achieved with the ratio of R_{rs} at 490 and 620 nm ($R^2 = 0.76$) for the Berau estuary waters, is:

$$\ln\left[K_d(490) - K_dW\right] = 0.49 * \ln\left[(\rho_{490}/\rho_{620})\right] + 0.028 \qquad (4.8)$$

In order to estimate $K_d(490)$ from MERIS, Eq. (4.8) was applied to the three sets of R_{rs} MERIS data. Figure 4.8a shows the $K_d(490)$ derived from MERIS data by using different R_{rs} data set versus distance. The $K_d(490)$ model seems to have a similar pattern: it is high at locations close to the Berau river mouth and decreases towards the open sea. The best model between $K_d(490)$ and distance was exponential, with R^2 values of 0.61, 0.67 and 0.77 for C2R, MERIS L2 and FUB, respectively. The $K_d(490)$ derived from MERIS data was underestimated for the stations close to the river mouth, at the distance of < 20 km and was overestimated in the ocean water (> 20 km).
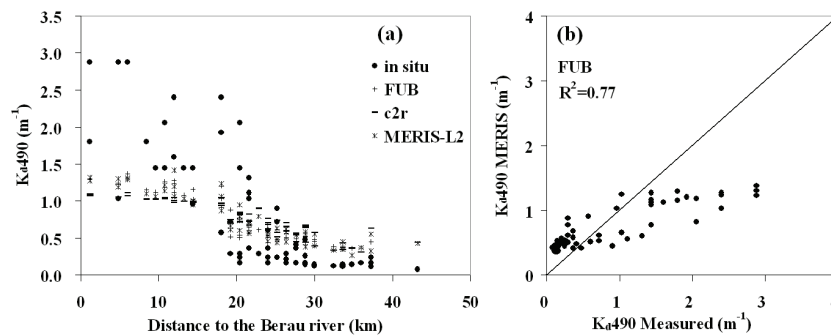
Figure 4.8 : Transect of $K_d(490)$ derived from *in situ* data and MERIS data at 63 stations (a) and the scatter plot of $K_d(490)$ measured versus the MERIS results (b).

Figure 4.8b shows the scatter plot between the $K_d(490)$ measured and $K_d(490)$ modeled from R_{rs} MERIS data derived using the FUB algorithm. A statistical analysis between $K_d(490)$ measured and modeled is displayed in Table 4.3. It shows that the C2R algorithm resulted the highest discrepancy between $K_d(490)$ measured and $K_d(490)$ derived, as evidenced by the highest RMSE, higher percentage difference and lower R^2.

Table 4.3:   Statistical summaries of $K_d(490)$ estimation resulting from different R_{rs} data
sets, based on the R^2, percentage difference and RMSE of August 31, 2007;
n = 63 stations

	RMSE (m^{-1})	R^2	% Difference
C2R	0.72	0.61	90
FUB	0.62	0.77	65
L2	0.65	0.67	71

4.5. Discussion

This study demonstrates that the MERIS reduced resolution L1 and L2 data can
successfully be used to obtain a first estimation of suspended particulate matter
(TSM) and Chl-*a* concentration*s*, and also permit to derive water leaving remote
sensing reflectance and diffuse attenuation coefficient in equatorial coastal
waters like the Berau estuary in East Kalimantan. Efforts to obtain MERIS FR
and RR data L1 and L2 for the Berau estuary encounter however major
problems of cloud cover. MERIS cloud free image data during the wet season
are almost impossible to be obtained, and there were only few images with little
cloud cover in the dry season during the period of 2003 - 2007. Studying ocean
colour remote sensing with optical VIS and NIR sensors presents therefore a
major challenge in these equatorial coastal regions.

The objective of this study was to estimate and validate TSM and Chl-*a*
concentrations from MERIS RR data in tropical coastal waters using different
standard processor algorithms. The results indicate that the correlation between
TSM retrievals from MERIS satellite and *in situ* measured data was low,
indicated by a very low R^2 (Table 4.2). This can be explained by the fact that the
Berau estuary waters are affected by the Berau river outflows, tidal currents
with resuspension and the presence of CDOM absorption. As has been
mentioned by Fischer & Fell (1999), the presence of TSM is highly depending on
river outflow, biological products, depth of the ocean bottom and the
circulation of the ocean itself. The reference point was located in the river
mouth. A number of points at a relatively large offshore distance, however, still

indicate high values of TSM, which cause the low correlation between TSM distribution and offshore distance. This may be related to the fact that some sampling points, although far from the Berau river mouth, were still relatively close to the coast line or reefs, and so they were still influenced by the coastal and shallow water processes. The *in situ* observations were collected during 18 days, thus the dynamics of the coastal input from the Berau river as well as the ocean, tidal and weather influences were significant. As an example of such dynamics, the measurements at the station at 38 km from the river mouth (light house station, 02°16' 06.5 North; 118°14'26.6 East) varied considerably during the field campaign, from 1.2 mgl^{-1} to 48 mgl^{-1} with a standard deviation of 16.6 mgl^{-1} and a mean value of 23.5 mgl^{-1}.

Another cause of this unsatisfactory result may be due to the high local and dynamic atmospheric variability in haze and cloud cover. This spatial and temporal variability hampers the atmospheric correction in the C2R and FUB algorithms. The bio-optical models included in the Case-2 regional algorithm represent a standard case only, based on the specifics training data. Therefore, for other locations with different spectral characteristics, for example in shallow water with sea bottom reflectance, or when there are an insufficient accurate atmospheric correction (Doerffer & Schiller, 2007), the result may turn out to be unsatisfactory.

The C2R and FUB algorithms as well as MERIS L2 can be used to derive the water reflectances or R_{rs} from the Berau waters. The spectra derived from the three algorithms showed similar spectral characteristics. Among them, the spectra obtained by the C2R algorithm corresponded better to the *in situ* spectra. This is indicated by a higher correlation squared (R^2) and a low RMSE found between the R_{rs} derived by the C2R algorithm with *in situ* data. This result can be explained by the fact that the C2R and the FUB algorithms were developed for coastal waters, based on radiative transfer model simulations and their parameterization by a neural network. The slight difference in the results for the C2R and FUB algorithms in terms of magnitude of R_{rs} parameters can be explained by the fact that C2R algorithm takes into account the effect of cirrus clouds, sun glint and water leaving radiance reflectance, caused by the different

sorts of water constituents (Doerffer & Schiller, 2007), phenomena which were not initially taken into account in the conception of the FUB algorithm.

This study investigated also the R_{rs} retrievals at different wavelengths. The results shows a large discrepancy between spectra of satellite and measured R_{rs} in the blue wavelength (412 nm), indicated by a very low correlation squared (R^2) between MERIS data and *in situ* data. The insufficient atmospheric correction achieved in the blue wavelength domain may be responsible for this. Therefore, further improvements should be made by using aerosol spectral and other atmospheric properties at this study location. Low correlation was also found at long wavelengths (708 nm), which could be due to the relatively weak signal at this wavelength. The best accuracies of MERIS data in tropical turbid coastal water of the Berau estuary were reached in bands 3 to 6 (490, 510, 560 and 620 nm), with higher discrepancies in the other bands. This phenomenon was also found in the study done by Ohde *et al*. (2007).

The $K_d(490)$ algorithm based on the R_{rs} ratio of 490:620 gave the best fit for the study area compared to the R_{rs} ratio of 490:560. This can be explained by the variation in CDOM absorption. The wavelength of 560 nm is still influenced by CDOM absorption (Kratzer, 2000). The diffuse attenuation coefficient derived from MERIS data with different R_{rs} data sets shows almost similar results. However, $K_d(490)$ from R_{rs} MERIS with the FUB algorithm shows slightly better result compared to ones resulting from the C2R and MERIS L2 algorithm (*see* Table 4.3).

The discrepancies between measured and satellite-derived water quality constituents TSM, CHL-*a*, and the optical properties such as reflectance (R_{rs}) and light attenuation or $K_d(490)$ in this study seem mostly due to spatial haze variability, pixel heterogeneity and possible measurement errors. The local haze and atmosphere variability in these equatorial land-sea boundary areas is quite high, so that the standard atmosphere pre-processing algorithms used in the MERIS L2 and Case-2 regional algorithms (C2R and FUB) did not work optimally.

64

The difference between *in situ* measurement and MERIS data can also be due to the within-pixel heterogeneity. The *in situ* measurements were obtained at point locations that represent a very small homogenous water footprint, while the MERIS sensor records the signal over a much larger 1.44 km^2 water surface area (1.2 km resolution RR data).

The study area is located in an equatorial tropical region, where clouds and atmospheric haze are present at almost all times. As has been mentioned by Matthew *et al*. (2000), clouds and cloud shadows pose several problems for atmospheric correction. Not only because cloud contaminated pixels give an incorrect reflectance, but they can also degrade the reflectance accuracy in other parts of the scene. Clouds have an impact on the spatially averaged radiance. The haze in this study area has a very high and dynamic variability. This can be proved by the fact that applying MERIS L2, C2R and FUB gave almost similar result on derived R_{rs}, $K_d(490)$, Chl-*a* concentration and TSM concentration. This can be explained maybe by the fact that the three algorithm processors are based on the same atmospheric correction concept, which assumes zero reflectance in the NIR.

4.6. Conclusions

From the results obtained, it can be concluded that in this equatorial coastal zone, the MERIS RR data permit to derive optical water properties such as water reflectance, R_{rs} and light attenuation, $K_{d(490)}$ with a reasonable accuracy. The standard water quality algorithms (MERIS L2, C2R, FUB) available to derive TSM and Chl-*a* concentrations from MERIS data however permit only a first approximation of the order of magnitude of constituent concentrations. The C2R algorithm proved more robust for estimating Chl-*a* and water leaving remote sensing reflectance, R_{rs}. On the other hand, the FUB algorithm was more robust for estimating the diffuse attenuation or $K_d(490)$ coefficient. The relatively poor accuracy is due to the fact that all three ANN algorithms were originally developed and calibrated for coastal waters in temperate regions at higher latitudes, e.g. from 30° to 60° North. The highly variable atmospheric conditions, especially at the land - sea boundary in these equatorial regions,

seem to hamper accurate retrievals of water quality constituents. In order to get a better accuracy in estimating water quality concentrations, a more adequate atmospheric correction, taking into account the strong dynamics of the tropical atmosphere, can be recommended. Also, more quantitative information of optical water properties and water constituents in these regions as documented and analyzed in this paper, remains essential in order to allow a remote sensing based assessment of the behavior of coastal ecosystems in these regions.

CHAPTER 5

ESTIMATING TOTAL SUSPENDED MATTER CONCENTRATION IN TROPICAL COASTAL WATERS

Abstract[*]

This study presents the application of a semi-empirical approach, based on the Kubelka-Munk (K-M) model, to retrieve the total suspended matters (TSM) concentration of water bodies from ocean colour remote sensing. This approach is validated with *in situ* data sets compiled from the tropical waters of Berau estuary, Indonesia. Compared to a purely empirical approach, the K-M model provides better results in the retrieval of TSM concentration on both data sets used (*in situ* and MERIS). In this study, the K-M model was calibrated with *in situ* measurements of remote sensing reflectance (R_{rs}) and TSM concentration. Next, the inverse K-M model was successfully applied to images taken by the MERIS instrument by generating regional maps of TSM concentration. MERIS top-of-atmosphere radiances were atmospherically corrected using the MODTRAN radiative transfer model. The best correlation between R_{rs} measured *in situ* and R_{rs} MERIS was at the wavelength of 620 nm. The TSM concentrations retrieved using this K-M model showed a lower RMSE, a higher coefficient of determination and a smaller relative error than those retrieved by the purely empirical approach.

5.1. Introduction

The goal of ocean colour remote sensing is to derive quantitative information present in the water column, based on variations in the spectral shape and the magnitude of the ocean colour signal. The Coastal Zone Colour Scanner (CZCS), launched on board of the Nimbus-7 satellite in 1978 was the first sensor specifically designed to monitor ocean colour. Inspired by the success of CZCS, the Medium Resolution Imaging Spectrometer (MERIS), mounted on the European Environmental Satellite (ENVISAT) was launched in March 2002 by the European Space Agency (ESA). MERIS is applicable for water related studies in the open sea (Bricaud *et al.*, 1999; Fischer & Fell, 1999) and water quality in the coastal zone (Doerffer *et al.*, 1999) or in freshwater basins (Hoogenboom & Dekker, 1997; Koponen *et al.*, 2002).

Mapping of TSM concentration, Chl-*a* concentration and CDOM from MERIS data has been studied by many investigators. In particular, Koponen *et al.* (2006) studied the concentrations of Chl-*a* and TSM as well as the absorption coefficient of CDOM in Case-2 water from MERIS data using empirical band-ratio algorithms together with an extensive set of *in situ* observations. Artificial Neural Network (ANN) based semi-analytical models have been applied to MERIS data of Case-2 waters (Doerffer & Schiller, 2007; Schroeder *et al.*, 2007). These models give generally unsatisfactory results for extremely turbid waters (Shen *et al.*, *submitted*). For that reason, it is necessary to investigate alternative algorithms for these complex coastal waters.

When light enters the water, four processes associated with the interaction of water with the light flux can be distinguished: (1) specular transmission, (2) specular reflection, (3) absorption, and (4) scattering. The methods of calculus can be used to derive the theoretical relations of diffuse light fluxes into and out of a turbid and light-scattering medium. The Kubelka-Munk (K-M) theory is one of the most frequently used theories to predict colour matches, because it provides a reflectance model for translucent materials placed on backings of different colours. The K-M model applies a two-stream radiative transfer approach which deals with the combined effect of absorption and scattering

processes (Yang & Kruse, 2004). In general, the K-M model characterizes colourants according to two coefficients, *a* and b_b, the absorption and (back) scattering coefficients respectively (Westland *et al.*, 2002). A study on ocean colour by applying the K-M model in the Yangtze river estuary using MERIS data by Shen *et al.* (*submitted*) found that the K-M model appears promising for these extremely turbid waters.

The goal of ocean colour remote sensing is to retrieve quantitative information exclusively from the water column; thus the contributions from the atmosphere and from specular reflection at the sea surface have to be corrected. Small errors in estimating the atmospheric contribution can cause significant biases in the estimation of water constituents. At satellite level, more than 80% of the light reaching the detector is of atmospheric origin (Morel, 1980). Several radiative transfer models for atmospheric simulation and correction have been developed such as MODerate spectral resolution atmospheric TRANsmittance (MODTRAN) (Berk *et al.*, 2000), Second Simulation of the Satellite Signal in the Solar Spectrum (6S) (Vermote, 1997), and the Simplified Method for Atmospheric Correction (SMAC) (Rahman & Dedieu, 1994). The Case-2 Regional algorithm processor (C2R) (Doerffer & Schiller, 2007) and the Free University of Berlin algorithm processor (FUB) (Schroeder & Schaale 2005) are Case-2 plug-in algorithms in BEAM Visat, and they are based on an Artificial Neural Network trained on the basis of radiative transfer model calculations. The main task of these algorithms is to retrieve the Top-of-water (TOW) reflectance from the Top-of-atmosphere (TOA) reflectance that is derived from the radiance measured by the sensor. For this reason, information about the sensor spectral profile and the atmospheric properties at acquisition time is required to estimate atmospheric scattering and absorption effects.

Investigations on ocean colour remote sensing, especially those based on the use of MERIS data, were mostly carried out in high latitude regions such as Europe and North America. Few investigations have been done in tropical regions, especially in Indonesian coastal waters. In order to fill this gap, this research was focused on retrieval of TSM concentration in tropical waters in order to find the best model suitable for this region.

70

The purpose of this study was to retrieve TSM concentration from MERIS data by using a semi-empirical approach, based on the K-M model, applied to tropical coastal waters. To this end, different methods for atmospheric correction and for TSM retrieval from water reflectance were tested.

In this study, *in situ* data such as optical data, TSM concentrations, Chl-*a* concentrations as well as MERIS L1b data of the Berau estuary were collected. The data covered the period of August and September 2007. The TSM concentrations estimated from MERIS data were then processed with empirical and semi-empirical models and then statistically analysed.

5.2. Field data set

The optical spectral data and bio-geophysical variables measurements in the field were described in Chapter 3 (*see* sub-section 3.2.2). During the field campaign, the optical data set was obtained from 80 stations in the Berau coastal waters and nearby regions; however, only 33 stations were used in this study due to data validity. The number of MERIS data that could be matched-up with *in situ* data was also limited: of the 33 stations, only 9 could be applied for validation of the R_{rs} reflectances derived by atmospheric correction with MODTRAN in this study. The field stations distribution around the Berau estuary is displayed in Figure 5.1.
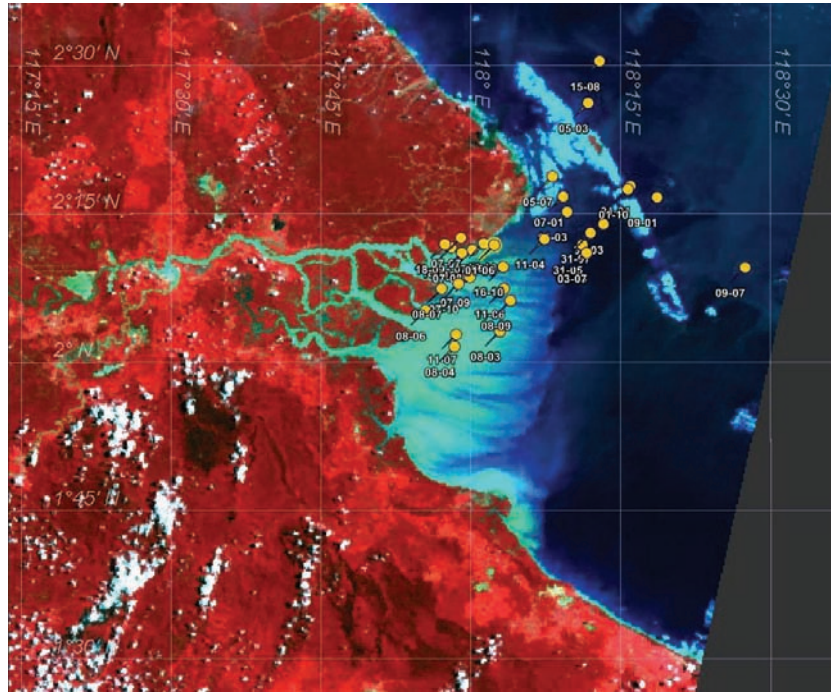
Figure 5.1 : The field station locations, collected in the field campaign of August 2007 and plotted on the subset of MERIS L1b, FR, RGB:14-8-4 (date of acquisition: May 17, 2007).

5.3. The MERIS data

For the present study, the MERIS imagery data of Level 1b (L1b) and Level 2 (L2) provided by the European Space Agency (ESA) were used. Of 20 MERIS L1b and L2 data sets at Reduced Resolution (RR) and Full Resolution (FR) available for this study area from 2003 until 2007, only four images were coincident with *in situ* measurements: August 21, 28 and 31, 2007 and September 15, 2007. Among these four images, there were only two images (August 31 and September 15, 2007) which were coincident with sufficiently complete *in situ* (optical and water quality) measurements. Due to the bad quality of MERIS data on September 15, 2007 (bright pixel flag), only the MERIS RR of L1 data mode taken on August 31, 2007 was used for validating the R_{rs} results retrieved by the atmospheric correction. Moreover, MERIS L1b on

August 28 and 31, 2007 were used for deriving TSM concentration and were validated with the match-up *in situ* measurements.

5.4. Methods

Three main processing steps have been carried out in this study in order to estimate the TSM concentration from MERIS data: (1) the estimation of TSM concentration from the *in situ* data set, (2) the retrieval of TSM concentration from MERIS data, and (3) data analysis.

5.4.1. Estimation of TSM concentration from the *in situ* data set

a. An empirical approach

In order to find a simple and robust method for estimating the TSM concentration, an empirical approach was applied in this study. In a practical perspective, the relationship between the R_{rs} measured and TSM concentration measured can be directly established. However, the dynamics of the *in situ* data set related to the geographical location and seasonal variation influence the result. As has been described in IOCCG Report No. 3 (IOCCG, 2000) and MERIS ATBD 2.7 (Antoine & Morel, 2005), empirical algorithms establish a relationship between the optical measurements and the concentration of constituents based on experimental data sets, i.e. measurements of above or below-surface reflectance (or radiance) spectra and coincident measurements of *in situ* concentrations. Advantages of empirical algorithms are that they are simple, easy to derive, and easy to implement and test. Nevertheless, empirical models always need *in situ* data because the water quality parameters may change between different remote sensing acquisitions. In this study, we used a linear regression to correlate the remote sensing reflectance measured in the field with the logarithm of TSM concentration from *in situ* measurements.

b. A semi-empirical approach, K-M model: algorithm development

A semi-empirical model which is based on two-stream Kubelka-Munk (K-M) theory for radiative transfer in the water body was applied in this study as well. The K-M model was originally developed to describe scattering and absorption of upward and downward diffuse light in turbid media. It has been applied to describe mixing of paint colours, the optical properties of ink in paper, the reflectance and transmittance of plant leaves, et cetera. For a semi-infinite medium like optically deep water, it has only one effective parameter, the ratio of backscattering (b_b) to absorption (a). In water, this ratio changes as a function of the sediment concentration. Because of the effects of the air-water interface, the influence of the solar zenith angle, and other complicating factors, in this particular study the K-M model was applied only in a semi-empirical way, namely to model the dependence of remote sensing reflectance on sediment concentration TSM. Two free constants are used to fit the model to measurements. This makes it just as economic as the fully empirical linear-logarithmic 2-parameter regression model, while it retains the property of producing only physically possible reflectance values. For low turbidity, the widely-used Gordon *et al*. (1975) model $R_{rs} = f * b_b / (b_b + a)$ and the K-M model behave similarly, but K-M is expected to function also for high turbidities. This is why it was applied to the coastal waters of this study. Another advantage of the K-M model, compared to more complicated models, is that it is still analytically invertible.

According to the K-M model, a turbid medium of infinite optical thickness has a bi-hemispherical reflectance equal to:

$$r = \frac{x}{1 + x + \sqrt{1 + 2x}} \qquad (5.1)$$

where x is equal to the ratio of the coefficients of backscattering and absorption, b_b/a. We assume here that this ratio is proportional to the sediment concentration, and that the calculated reflectance is scaled to take into account the air-water interface. This leads to a semi-empirical model with two free parameters that have to be found by fitting the model to measurements. The

74

forward model predicts the remote sensing reflectance R_{rs} from TSM concentration C_{TSM}, by:

$$R_{rs} = \frac{\alpha\beta C_{TSM}}{1 + \beta C_{TSM} + \sqrt{1 + 2\beta C_{TSM}}} \tag{5.2}$$

where C_{TSM} is the TSM concentration in arbitrary units, and α and β are the fitting coefficients. The coefficient α represents the saturation level of the reflectance. If βC_{TSM} equals 4, R_{rs} equals $\alpha/2$, so the constant $4/\beta$ is equal to the TSM concentration for which the water-leaving reflectance is at half of the saturation level.

The empirical constants α and β were determined for each MERIS wavelength band by numerical optimization of the inverse model, which is given by:

$$C_{TSM} = \frac{2\left(\dfrac{R_{rs}}{\alpha}\right)}{\beta\left(1 - \dfrac{R_{rs}}{\alpha}\right)^2} \tag{5.3}$$

In this study, the K-M model was calibrated by using the *in situ* measured R_{rs} and TSM data. The coefficients α and β for each MERIS band were found by minimising the sum of squared errors in log TSM. The most sensitive MERIS band was selected on the basis of the highest coefficient of determination and the lowest RMSE. The next step was applying the inverse K-M algorithm to the R_{rs} of MERIS data that was atmospherically corrected by using MODTRAN and the BEAM plug-in methods.

5.4.2. Retrieval of TSM concentration from MERIS data

This study focused on the determination of TSM concentration from radiances measured by the MERIS sensor. However, the radiance in the satellite data does not only come from the target, but also from atmospheric scattering. Thus, firstly, an atmospheric correction is performed, and this is followed by estimating TSM using the empirical and the K-M inverse model. In this study, two main atmospheric correction methods were applied: (1) by using

MODTRAN and (2) by using standard atmospheric corrections that are available in the BEAM Visat software.

a.   Atmospheric correction

Atmospheric correction is a very critical step for the correct interpretation of the ocean colour signal. The process of atmospheric correction is described in IOCCG (2000). The authors mentioned that the performance of retrieval algorithms and the quality and accuracy of the derived quantities are strongly influenced by atmospheric corrections. For the atmospheric correction over ocean waters one often assumes that the water-leaving radiance is zero in the near-infrared part of the spectrum (Gordon & Wang, 1994). However, this assumption is not valid for very turbid waters (IOCCG, 2000). Therefore, it was decided not to rely on this assumption and to perform an independent atmospheric correction based on MODTRAN (Berk *et al.,* 2000).

The MODTRAN model is based on a set of user input parameters and a physical description of optical processes in the atmosphere. The MODTRAN program was run with surface albedos of 0%, 50% and 100%, respectively, for deriving the correction parameters for a given atmospheric state and angular geometry (Verhoef & Bach, 2003). In this study, we tested 7 levels of visibility (5, 10, 20, 40, 45, 50 and 60 km). Visibility is related to surface aerosol extinction at 550 nm (Berk *et al.*, 2000). By varying the visibility, we were able to produce a series of corresponding atmospheric parameters (e.g. atmospheric path radiance, transmittance, etc.) at all wavelengths. Next, these parameters were used to calculate the remote sensing reflectance from the MERIS data. Aerosol extinction models applied in this study were the maritime and rural models. We assumed a Lambertian surface reflectance of the waters, no adjacency effects and a laterally homogeneous atmosphere. The tropical atmospheric profile of the atmosphere was applied in this study and the spectral Full Width at Half Maximum (FWHM) used in the calculations was 10 nm.

The TOA total radiance of MERIS data in the MODTRAN output file, L_{TOA} (W m^{-2} sr^{-1} μm^{-1}), can be expressed in surface reflectance r by the equation:

$$L_{TOA} = L_0 + \frac{Gr}{1-rA} \tag{5.4}$$

The water leaving reflectance was calculated by the inverse equation:

$$r = \frac{L_{TOA} - L_0}{G + (L_{TOA} - L_0)A} \tag{5.5}$$

where r is the water surface reflectance, and L_0 is the total radiance for zero surface albedo (W m^{-2} sr^{-1} μm^{-1}), A is the spherical albedo of the atmosphere, and G is the gain factor. The constants L_0, A and G were determined using the outputs of the three MODTRAN runs (Verhoef & Bach, 2003) by applying the following equations, in which the subscripts indicate the respective surface albedo percentages:

$$L_0 = LTOT_0 \tag{5.6}$$

$$A = \frac{\Delta_{100} - 2 \times \Delta_{50}}{\Delta_{100} - \Delta_{50}} \tag{5.7}$$

$$\Delta_{100} = LTOT_{100} - LTOT_0 \tag{5.8}$$

$$\Delta_{50} = LTOT_{50} - LTOT_0 \tag{5.9}$$

$$G = \Delta_{100} \times (1 - A) \tag{5.10}$$

The last step was the calculation of the water leaving remote sensing reflectance $R_{rs} = r/\pi$ of MERIS L1b data by using the surface reflectance resulting from Eq. (5.5). The selection of the appropriate aerosol model and visibility for this study was based on the minimum RMSE criterion. The validation was done for the MERIS L1b image recorded on August 31, 2007 and match-up field measurements (9 stations) from the same date.

b. TSM concentration retrieval

The MERIS L1b RR scene from August 28 and 31, 2007 and MERIS L1b FR on August 21, 2007 were processed into TSM concentration maps by using the empirical and the K-M model. The first step was converting the TOA radiance of MERIS band 6 into surface reflectance. Lastly, the inverse K-M model was applied to the corrected images. All of the image processing was performed

using the BEAM software toolbox, developed by Brockmann Consult on behalf of ESA (Brockmann, 2009).

In this study, the TSM concentration was also calculated from R_{rs} of MERIS data that was derived with different atmospheric correction methods. Those algorithms are the ones that are plugged-in on BEAM Visat: the C2R algorithm, FUB and SMAC. These deliver various output products. However, in this study focus will be on the water leaving reflectance products from C2R, SMAC and MERIS L2, and the remote sensing reflectance (product from FUB) as well as the TSM concentration that was derived directly from these algorithm processors (C2R, FUB and MERIS L2). In total, there were 8 sets of TSM concentrations derived in this study by using different atmospheric correction models as well as TSM models. Table 5.1 gives the description of each TSM concentration product.

Table 5.1: Description of different TSM concentration name

Name of TSM	Atmospheric correction (R_{rs} MERIS)	TSM model
KM-MODTRAN	MODTRAN	K-M model
KM-C2R	C2R plug-in	K-M model
KM-FUB	FUB plug-in	K-M model
KM-L2	Standard global algorithm - ESA	K-M model
KM-SMAC	Standard on BEAM Visat	K-M model
C2R	C2R plug-in	C2R
FUB	FUB plug-in	FUB
L2	Standard global algorithm - ESA	ESA

5.4.3. Data analysis

In order to evaluate the performance of the TSM concentration retrieval using the empirical and the semi-empirical approaches, the regression parameters, the Root Mean Square Error (RMSE) and the Relative Error (RE) were used. The RMSE was calculated based on:

$$\text{RMSE} = \sqrt{\frac{\sum (\text{R}_{\text{rs}}\text{model} - \text{R}_{\text{rs}}\text{measured})^2}{\text{n}}} \qquad (5.11)$$

where R_{rs} *model* stands for the remote sensing reflectance derived from MERIS data after atmospheric correction and R_{rs} *measured* stands for the remote sensing reflectance from *in situ* measurements. The squared differences were summed over the bands and the locations. Eq. (5.11) was also used for calculating the RMSE of the logarithm of TSM concentration. Next, the Relative Error (RE) was estimated from the RMSE of the logarithm of TSM by:

$$RE\ (\%) = RMSE\ (\log \text{TSM}) * \ln(10) * 100 \qquad (5.12)$$

This equation can be derived from the derivative of a natural logarithm as follows:

$$\frac{\text{dlnx}}{\text{dx}} = \frac{1}{\text{x}} \text{ , or } \Delta\text{lnx} \approx \frac{\Delta\text{x}}{\text{x}} \text{ , which can be identified as the relative error.}$$

Since $\Delta\text{lnx} = \ln10 \times \Delta\text{logx}$, the relative difference is given by $\frac{\Delta\text{x}}{\text{x}} = \ln10 \times \Delta\text{logx}$.

5.5. Results

5.5.1. TSM concentration retrieval from *in situ* data set by using the empirical approach

The correlation between the R_{rs} measured versus log TSM concentration measured was established by linear regression. Six wavelengths (corresponding to MERIS wavelengths of 490, 510, 560, 620, 665 and 708 nm) from 33 field stations have been selected to present the empirical model, and the data are plotted in Figure 5.2. A relatively good correlation was found between R_{rs}

measured and log TSM measured, especially at the wavelength of 620 nm ($R^2 =$ 0.75).
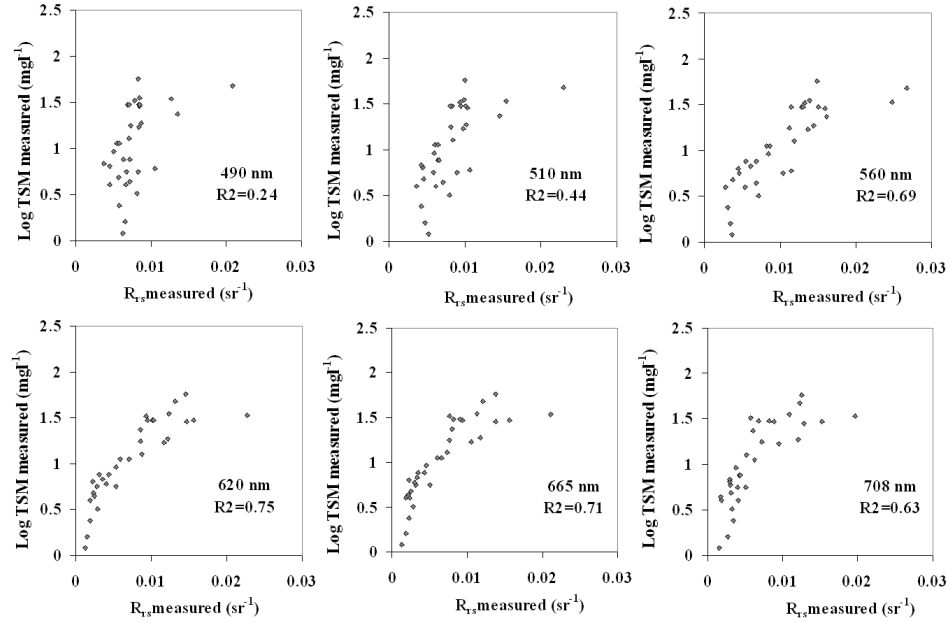
Figure 5.2 :   Scatter plots between R_{rs} measured (sr^{-1}) and log TSM (mgm^{-3}) at selected wavelengths and n = 33.

5.5.2.   TSM concentration retrieval from *in situ* data set by using the semi-empirical approach (K-M model)

The TSM concentration has been derived by using the semi-empirical relationship based on the K-M model, applying Eq. (5.1) to (5.3). The R_{rs} measured and the logarithm of the measured TSM concentration were used to calibrate the K-M model. The fitting coefficients, α and β, were derived from the criterion of a least sum of squared errors in log TSM using the inverse model of Eq. (5.3). Plots of the R_{rs} measured on the *X*-axis and log TSM concentration on the *Y*-axis for several MERIS bands are displayed in Figure 5.3. The empirical linear regression lines (previous section) are also included here. Note, that the curved K-M lines follow the data better than the straight lines of the empirical model can. This is especially true for low sediment concentrations, where the

empirical model tends to give negative reflectances, whereas the K-M model gently approaches to a zero reflectance.
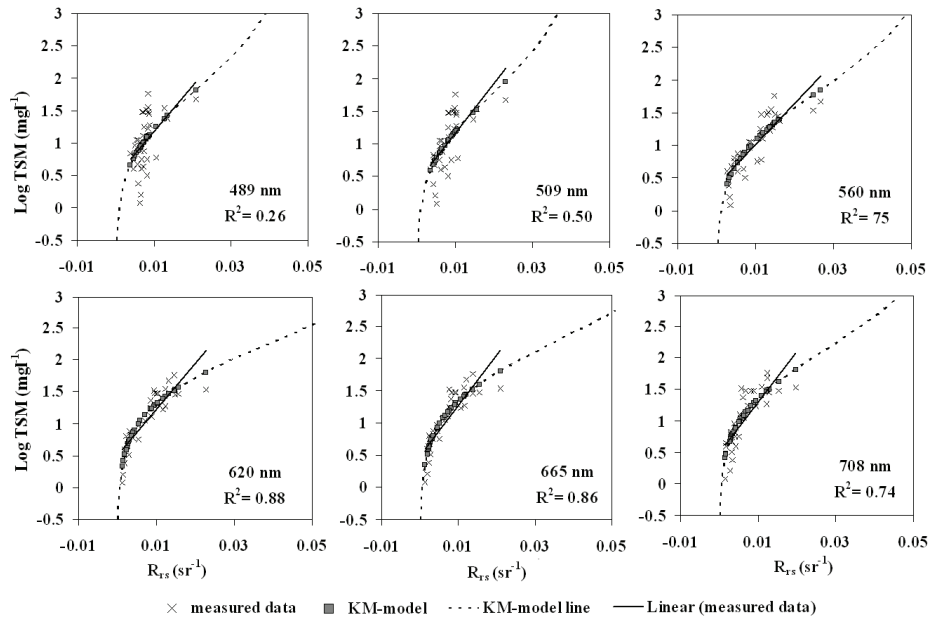
Figure 5.3 :   The relation between R_{rs} measured versus log TSM measured and log TSM retrieved with the K-M model at selected wavelengths, n = 33. The empirical model is given by the solid lines.

The results (Figure 5.3) show that the best fit between R_{rs} measured and TSM measured was obtained for the wavelength of 620 nm (corresponding to the MERIS channel 6), as appears from the highest R^2 and the lowest RMSE (Table 2). The fitting coefficients, α and β, resulting from the numerical optimization in this case were 0.097 and 0.012, respectively.

During algorithm development, the K-M model was calibrated with R_{rs} measured for all MERIS wavelength bands. A statistical summary of log TSM measured versus log TSM predicted from R_{rs} measured by using the empirical approach and the K-M model is listed in Table 5.2. The K-M model shows better results compared to the empirical approach, as appears from the RMSE of log TSM for the K-M model which was lower than for the empirical model, especially at the wavelength of 620 nm. In addition, the correlation coefficient

81

between log TSM measured and log TSM predicted with the K-M model was higher than for the empirical approach. The RE of TSM derived with the K-M model at each wavelength was lower than for the empirical model. Moreover, at the wavelength of 620 nm, the RE of the K-M model was 15% lower than for the empirical approach. In general, the wavelength of 620 nm gave better results for both approaches.

Table 5.2:   Statistical summary of the relation between log TSM measured and log TSM predicted by using the empirical approach and the semi-empirical approach with R_{rs} measured in 33 locations.

Wavelength	RMSE (mgm^{-3})		Relative Error (%)		R^2	
(nm)	Empirical	K-M	Empirical	K-M	Empirical	K-M
412	3.03	2.90	111	106	0.01	0.00
443	2.69	2.66	99	98	0.08	0.06
490	2.40	2.36	88	86	0.24	0.26
510	2.11	2.04	74	71	0.44	0.50
560	1.75	1.65	56	50	0.69	0.75
620	1.66	1.42	50	35	0.75	0.88
665	1.71	1.46	53	38	0.71	0.86
681	1.72	1.49	54	40	0.70	0.85
708	1.84	1.67	61	51	0.63	0.74

5.5.3. Atmospheric correction: retrieving remote sensing reflectance (*Rrs*)

The final objective of this study was to estimate TSM concentration from MERIS L1b data. Here, the atmospheric correction is very important and this has been done by using the MODTRAN radiative transfer model. The R_{rs} of MERIS data was calculated by using Eqs. (5.4) to (5.10) at nine match-up locations for different atmospheric inputs (visibilities and aerosol types). The RMSE of the R_{rs} derived from MERIS data versus the R_{rs} measured for both aerosol types and at 7 different visibilities are displayed in Figure 5.4.
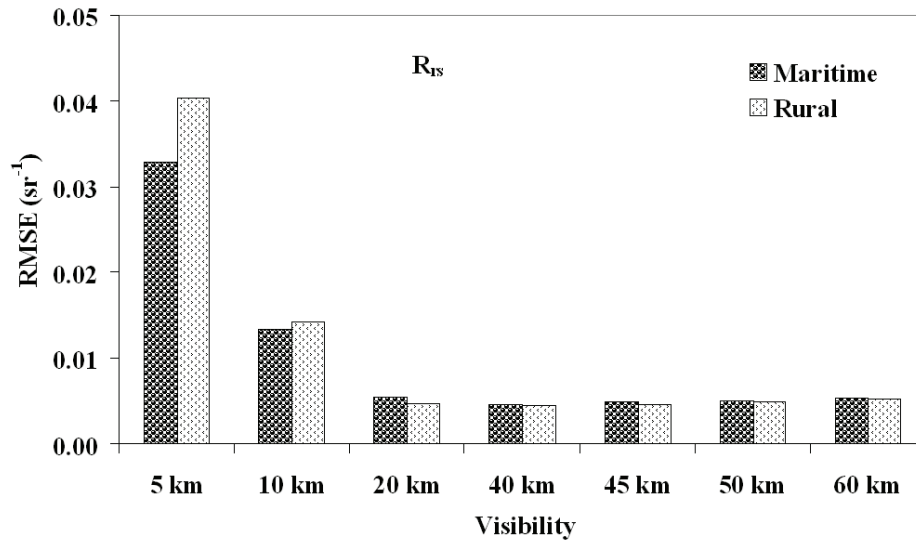
Figure 5.4 : The RMSE of R_{rs} of the MERIS data and R_{rs} measured on August 31, 2007 at 9 match-up locations with both aerosol types (maritime and rural) and 7 different visibilities.

From the results it appeared that the R_{rs} from MERIS at visibilities of 5 and 10 km got a negative value at all wavelengths. However, at a visibility of 20 km, a negative value of R_{rs} was found only from 560 nm onwards. Figure 5.4 shows that the RMSE of R_{rs} with rural and maritime aerosol models decreased with increasing visibility. At visibilities of 5, 10 and 20 km, the RMSE were very high for both types of aerosol model. The RMSE at visibilities of 40, 45, 50 and 60 km were almost similar (0.005 sr^{-1}). Based on this result, it was decided to use the R_{rs} at a visibility of 50 km with the maritime aerosol model for retrieving the TSM concentration, since at this visibility only few stations give a negative value. These might be related to cloud shadows. In this case, negative values were only found occasionally from 660 nm onwards. Since the results for the maritime and rural aerosol model were quite similar, the maritime model was used because the location is situated in a coastal area.

The analysis of the relation between Rrs MERIS and Rrs measured was carried out at 9 match-up locations on August 31, 2007. The scatter plot between Rrs MERIS and Rrs measured at selected wavelengths is displayed in Figure 5.5.

The Rrs MERIS seem to be overestimated at short wavelengths and underestimated at long wavelengths. The best fit was found at the wavelength of 620 nm as appears from the highest R2 (0.73) and the lowest RMSE (0.002 sr-1).
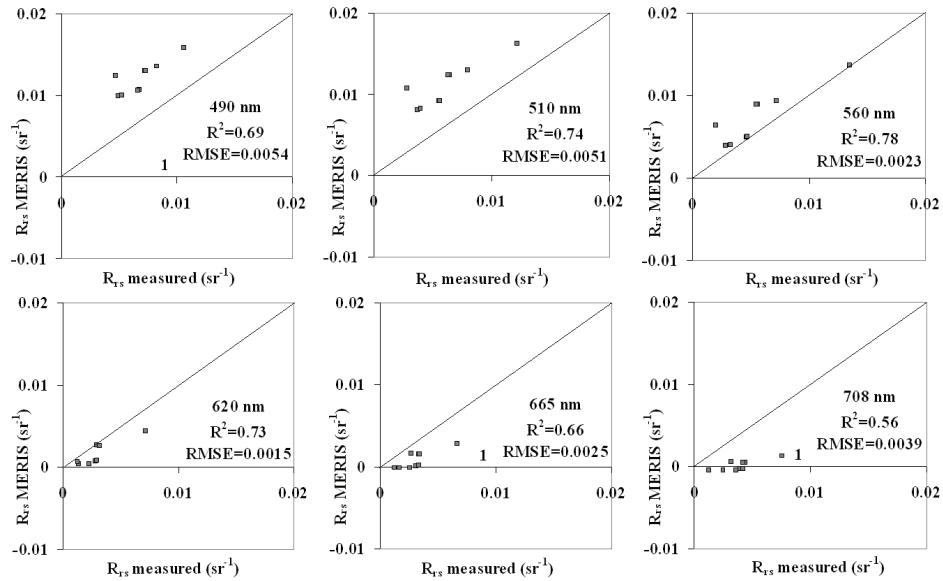
Figure 5.5: Scatter plot of R_{rs} measured versus R_{rs} derived from MERIS using MODTRAN (maritime aerosol type and at visibility of 50 km) in 9 match-up locations (August 31, 2007).

5.5.4. The TSM concentration derived from MERIS data

The TSM was derived with the empirical and the K-M model from corrected MERIS data. The correlation between log TSM measured and log TSM derived with the empirical and K-M model using two data sets are presented in Figure 5.6. A strong correlation can be observed between log TSM measured versus log TSM model that was based on the R_{rs} measured data set (n = 33) (Figure 5.6*a*).

As a validity check, the TSM derived from MERIS RR data recorded on August 28 and 31, 2007 were also compared numerically to the TSM measured in the field. Eight and nine field locations matching up with MERIS RR of August 28,

2007 and MERIS of August 31, 2007 were respectively used for inter-comparison. The statistical summary of TSM measured and TSM MERIS is listed in Table 5.3. When the K-M model was applied to the R_{rs} MERIS data set, low correlations were found (Figure 5.6*b* and Figure 5.6*c*).
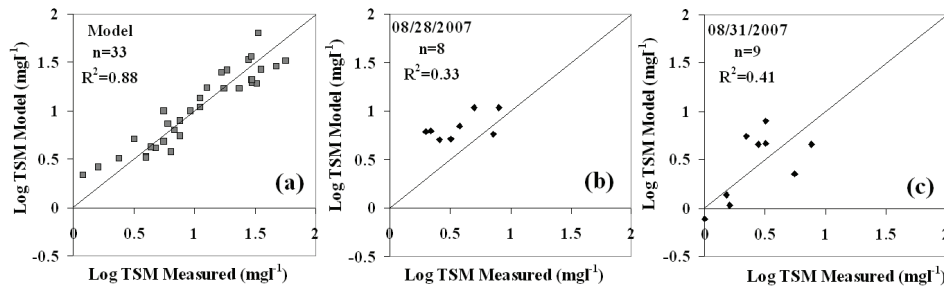
Figure 5.6 : Scatter plot: (*a*) between log TSM measured and log TSM model (R_{rs} measured) n = 33, (*b*) between log TSM measured (August 28, 2007) and log TSM MERIS (R_{rs} MERIS August 28, 2007) n = 8 and (*c*) between log TSM measured (August 31, 2007) and log TSM MERIS (R_{rs} MERIS August 31, 2007) n = 9.

As a validity check, the TSM derived from MERIS RR data recorded on August 28 and 31, 2007 was compared to the TSM measured in the field. Eight and nine field locations matching up with MERIS RR of August 28, 2007 and MERIS of August 31, 2007 were used for inter-comparison. The statistical summary of TSM measured and TSM derived from MERIS is listed in Table 5.3.

The TSM concentrations appear low on both dates. This is because the match-up field stations were located in relatively clear waters, also implying little variation. TSM derived from MERIS data was overestimated. This explains the high relative error between TSM measured and TSM MERIS. The K-M model improves the accuracy more than the purely empirical approach does. This can be confirmed by the RMSE as well as the RE for the K-M model on both data sets, which were lower than for the empirical model.

Table 5.3: Inter-comparison between TSM derived from MERIS with the empirical approach and the K-M model with the match-up TSM measured on August 28 and 31, 2007.

Parameters	August 28, 2007 (n = 8)			August 31, 2007 (n = 9)		
	TSM Measured	TSM MERIS Empiric	K-M	TSM Measured	TSM MERIS Empiric	K-M
Min (mgl^{-1}	2.00	6.06	5.04	1.00	3.40	0.77
Max (mgl^{-1})	8.00	9.71	10.88	7.60	6.56	7.97
Mean	4.25	7.32	7.13	3.19	4.51	3.64
RMSE (mgl^{-1})		2.16	2.05		2.12	1.84
Relative Error (%)		77	72		75	61
R^2		0.35	0.33		0.18	0.41

MERIS band 6 (620 nm) was used for deriving TSM concentration. The TSM map derived from MERIS by using the K-M model is presented in Figure 5.7. It clearly shows that the study area, which is located in a tropical region, was usually covered by clouds. It was difficult to find MERIS data with low cloud cover, as shown clearly in Figures 5.7a, 5.7c, and 5.7e. High TSM concentrations were found at the location close to the river mouth and they decrease when going into the outer shelve. The TSM concentration distribution on August 21, 2007 looks sharper because it was derived from FR MERIS data which has 300 by 300 meter ground resolution. It is different with the image of August 28 and 31, 2007, which was derived from RR data with 1200 by 1200 meter ground resolution.
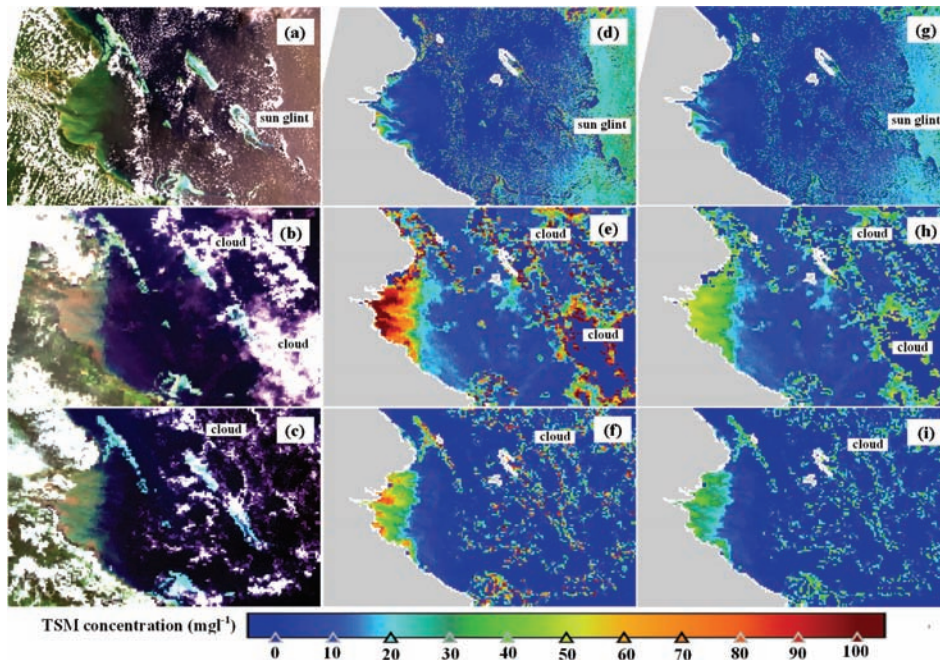
Figure 5.7 : Temporal variation of TSM concentration (mgl^{-1}) in the Berau waters estimated from MERIS data with K-M model. Upper: MERIS RR of August 31, 2007, (a) Colour composite, and (b) TSM map; Middle: MERIS RR of August 28, 2007, (c) Colour composite, and (d) TSM map; Lower: MERIS FR of August 21, 2007 (e) Colour composite, and (f) TSM map

The TSM concentrations were also derived by using the K-M model with R_{rs} MERIS obtained after applying different atmospheric correction procedures. Moreover, we also derived TSM concentration by using existing semi-empirical models such as C2R and FUB and MERIS L2. The inter-comparison among those TSM MERIS derived with TSM measured was calculated based on the RMSE (mgl^{-1}) and RE (%) and is displayed in Figure 5.8. The result shows clearly that the K-M model applied to five types of R_{rs} MERIS (MODTRAN, C2R, FUB, SMAC and L2) gave better results than the TSM produced by the standard C2R, FUB and L2 algorithms, as shown by the lower RMSE and RE. Nevertheless, if the inter-comparison among the TSM measured and TSM MERIS derived is based only on the K-M model (in combination with various atmospheric corrections), then the results are more interesting. The RMSE and RE of KM-FUB on both dates are lower than those of KM-MODTRAN. In this

case, we may conclude that the atmospheric correction is responsible for the different results. The fact that in the case of KM-MODTRAN a laterally homogeneous atmosphere was assumed explains why sometimes other results were better. The FUB algorithm uses the assumption of a zero water radiance in the NIR, and therefore it can correct the spatial haze variations. Also, relatively clear water pixels were used in the match-up, so that possible failures of the FUB algorithm due to high sediment concentrations were not likely to occur for this data set.
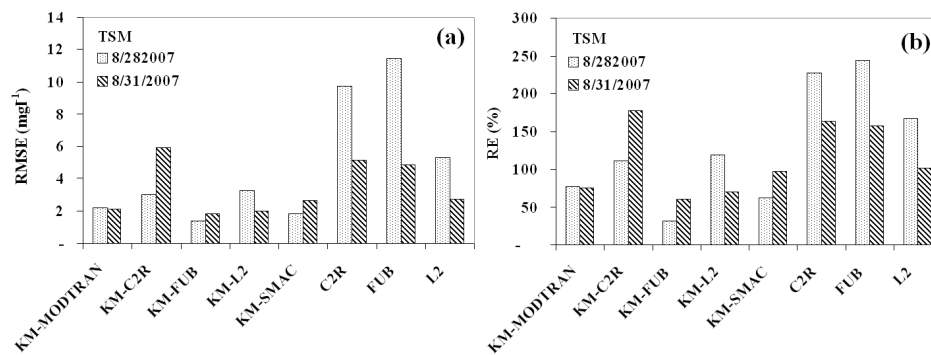
Figure 5.8 : Statistical analysis between TSM measured and TSM modelled derived with different atmospheric correction methods; (*a*) the RMSE (mgl^{-1}) and (*b*) the RE (%). The MERIS RR of August 28, 2007 and August 31, 2007

In order to understand the spatial and temporal dynamics of TSM concentration in the Berau estuary, 3 samples or pin points representing different water turbidity levels were selected. These pin points spread out from shallow and turbid water close to the Berau river mouth into the inner shelve and lastly in the outer shelve. The analysis of TSM concentration dynamics at the 3 pin points is displayed in Figure 5.9. Similar patterns of TSM concentration occurred for turbid, medium turbid and clear water with Secchi disk depths of 0.5, 4 and 10 meter respectively. The TSM concentration was low on August 21; it increased on August 28 as well as on August 31, 2007. The ENVISAT satellite recorded the study area at 10:00 hours local time or 02:00 hours UTC. The tide prediction at the moment of satellite overpass is displayed in Figures 4.9c, 4.9d and 4.9e. The tide prediction is based on the tide at Tawau Station, recorded by the Service Hydrographique et Océanographique de la Marine

(http://www.shom.fr/). The highest TSM concentration was found on August 28, 2007, coinciding with a tide height of 1.1 m. It is followed by the TSM concentration of August 31, 2007, which coincides with a 2.7 m tide. The lowest TSM concentration was obtained on August 21, 2007, which coincides with a tide height of 1.1 m. So, the tide height does not seem to have a large impact on the TSM distribution in this study.
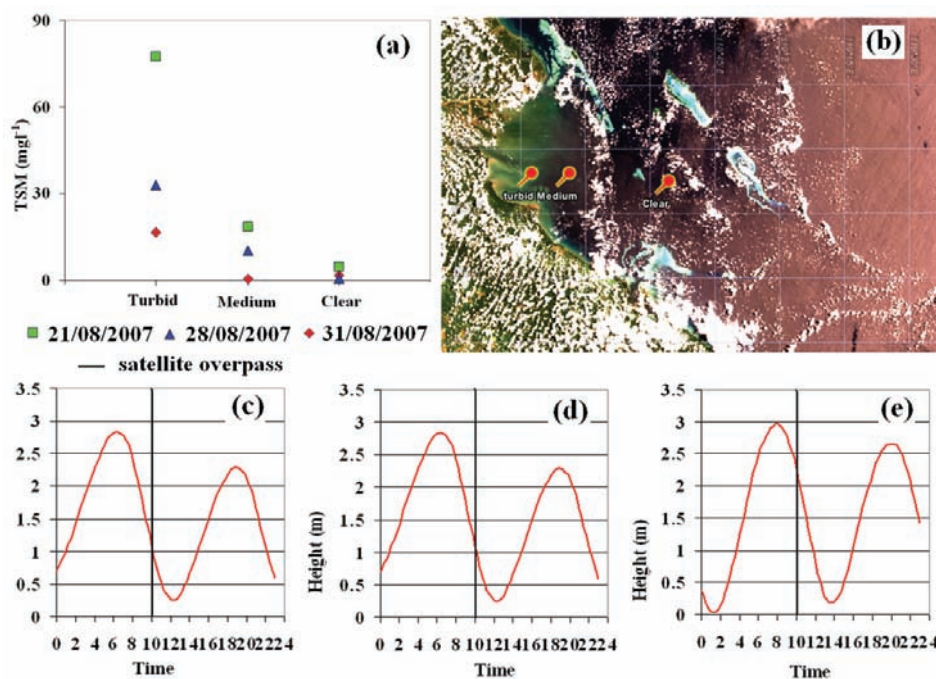
Figure 5.9 : (*a*) Spatial and temporal dynamics of TSM concentration in the Berau estuary waters; (*b*) the locations of 3 pin points at the sub image of MERIS FR August 21, 2007; (*c*) the tide at August 21, 2007; (*d*) the tide at August 28, 2007; and (*e*) the tide at August 31, 2007

5.6. Discussion

This paper studied the application of a semi-empirical approach based on the K-M model for estimating the TSM concentration in the Berau estuary. The proposed model seemed to work reasonably well in this study area, especially at the wavelength of 620 nm (*see* Table 5.2). However, atmospheric conditions

are seldom ideal in this tropical region, and developing water reflectance models for tropical coastal areas and better methods for atmospheric correction over very turbid waters could be of great help in this respect.

TSM concentrations predicted from R_{rs} measured *in situ* show a good agreement with TSM measured *in situ*. This can be explained by the fact that they come from the same or nearby geographic locations, with similar atmospheric conditions. Furthermore, the semi-empirical approach based on the K-M model was more robust than the empirical approach. This can be explained by the fact that the K-M model describes the physical processes of light scattering and absorption in water.

The application of the K-M model established from *in situ* measurements to MERIS L1 data seems less robust, as shown by the less agreement between TSM model from MERIS data and TSM measured *in situ*. This discrepancy can be explained by the spatial variation of atmospheric haze and by within-pixel heterogeneity.

The TSM concentrations derived from MERIS data by using the K-M model were more accurate than those derived with other TSM algorithms applied in this study. This can be explained by fact that the K-M model was calibrated on *in situ* measurements. In contrast, the algorithms of C2R and FUB were based on a radiative transfer model plug-in of BEAM Visat, which was not based on local measurements but on the bio-optical parameters for European waters.

The study area is located in a tropical equatorial region, where clouds and atmospheric haze are always present. Thus, the atmospheric correction in this study area should be done with great care. As has been mentioned by Matthew *et al*. (2000), clouds and cloud shadows pose several problems for atmospheric correction. Not only because cloud-contaminated pixels give an incorrect reflectance, but also because they can degrade the reflectance accuracy in other parts of the scene. In this study, the atmospheric visibility was assumed to be constant over the entire image while on the other hand it is known that the haze in this area has a very high variability. This is illustrated by the fact that

applying MODTRAN with the maritime aerosol type and a visibility of 50 km gives improper results at some locations where negative reflectance values were obtained. In future research, this problem could be solved by applying different visibilities in the MODTRAN simulations, depending on the local haze conditions.

The rural and maritime aerosol types give almost similar results in this study area. This can be explained by the fact that the study area is located in a coastal region, so the influence of both land and maritime air masses are mixed in this region. As mentioned by Fischer & Fell (1999), the aerosol properties over the open ocean are usually dominated by maritime aerosol, while the coastal area is usually influenced by continental aerosol. Doerffer & Schiller (2008) explained that the mean aerosol climate depends on the area type (industrial coast, volcanoes, and deserts) and the main wind direction.

5.7. Conclusion

For a range of TSM concentrations, the relationship between the logarithm of TSM and remote sensing reflectance is approximately linear, and a simple linear regression model can be applied to predict log TSM from remote sensing reflectance. This two-parameter model gave a minimum relative error of 50% at 620 nm. For a semi-empirical relationship derived from the two-stream Kubelka-Munk model, we found that for the same wavelength the relative error reduced to 35%. The semi-empirical K-M model has two parameters with a clear physical meaning and, unlike the regression-based model, it can only predict physically possible reflectance values.

Atmospheric correction methods over water often assume a zero water reflectance in the near infrared. This allows taking into account the spatial variation of haze (aerosols) over the scene. However, for high TSM values (> 50 mgl^{-1}) this assumption becomes invalid. Therefore, for the study area this assumption was not relied upon, and the radiative transfer model MODTRAN was applied to estimate the atmospheric parameters, assuming a spatially constant atmosphere. It is recommended to investigate alternative methods of

atmospheric correction over sediment-rich waters under conditions of spatially variable haze.

Applying the inverse K-M model to atmospherically corrected MERIS data from two dates resulted into less accurate estimations of TSM than the ones obtained from the *in situ* R_{rs} measurements. Several atmospheric correction methods were tested, and the best results were obtained for the FUB BEAM plug-in algorithm. Since the match-up pixels had relatively clear water (~1 mgl^{-1} TSM maximum), the zero water NIR reflectance assumption is correct, so the atmospheric correction of FUB performed better than the MODTRAN-based one, which assumed a laterally homogeneous atmosphere.

CHAPTER 6

SPECTRAL UNMIXING APPLIED TO MERIS IMAGES OF EAST KALIMANTAN COASTAL WATERS TO SEPARATE ATMOSPHERIC HAZE FROM WATER SEDIMENT EFFECTS

Abstract[*]

This study presents the application of a spectral unmixing approach combined with coupled water-atmosphere radiative transfer modelling to derive Total Suspended Matter (TSM) concentrations of water bodies from ocean colour remote sensing data. This approach is applied to MERIS data of the equatorial tropical waters of Berau estuary, East Kalimantan, Indonesia. The MERIS data were processed to suppress local haze variations and to preserve sediment variations in the image. Next, after the applied spectral unmixing, the MERIS data were corrected from atmospheric distortion, based on the MODTRAN radiative transfer model. The inverse of a semi-empirical water turbidity model, based on Kubelka-Munk theory, was successfully applied to the corrected MERIS data for generating a regional map of TSM concentration. Retrieval of TSM concentrations in relatively clear waters using this approach resulted in overestimated values. In turbid waters however, a lower RMSE and a higher coefficient of determination than those retrieved for clear waters were obtained. This study found that the spectral unmixing combined with radiative transfer modelling improved significantly the TSM concentration retrieval, in terms of the RMSE, from 7.57 mgl^{-1} (for MERIS L2) to 4.60 mgl^{-1} for this proposed model.

6.1. Introduction

Ocean colour remote sensing is becoming a powerful tool for quantifying and monitoring coastal and marine waters on regional and global scales. This tool is widely used to map optical water quality (suspended sediment concentration, chlorophyll concentration and yellow substrate absorption) in coastal and marine waters. The advantage of remote sensing data is its higher spatial coverage compared to *in situ* measurements. Satellites have a fixed repetition rate, so that time series can be obtained and changes of environmental conditions can be detected.

Several investigators (e.g., Doerffer & Schiller, 2007; Van der Woerd & Pasterkamp, 2008; Salama *et al*., 2009) have developed semi-analytical models for evaluation of water quality parameters for coastal waters. Characterizing the heterogeneity and temporal change of water quality across coastal water is difficult. An area represented by a single pixel of a remote sensing image usually contains several different materials. These materials are mixed together and the pixel reflectance observed by sensors is a combination of reflectances of individual materials. Spectral unmixing techniques can be used for resolving this problem.

Spectral unmixing is a method in which the measured spectrum of a mixed pixel is decomposed into endmembers and abundances (Kashava and Mustrad, 2002). This method has been successfully employed in terrestrial applications (Lunetta, 1998; Lu *et al*., 2003; Souza *et al*., 2003; Parente, 2007; Kärdi, 2007; Arroyo-Mora, *et al*., 2009). Following the success of spectral unmixing technique in terrestrial applications, Novo and Shimabukuro (1994) proposed a spectral mixture analysis of optically active substances for inland waters. Many investigations have used the spectral unmixing approach for estimating the Chlorophyll-*a* (Chl-*a*) concentration distribution in lake waters. Thiemann (2000) successfully mapped the Chl-*a* concentration distribution in Mecklenburg Lake by linear spectral unmixing using IRS-1C satellite data. Seasonal changes in chlorophyll distributions in the Amazon floodplain lakes have been studied by Novo *et al*. (2006) using a linear mixing model from

MODIS. A linear mixture modelling approach was applied to derive accurate estimates of Chl-*a* from Landsat Thematic Mapper imagery in Lake Balaton (Tyler *et al*., 2006). Oyama *et al*. (2007) estimated Chl-*a* concentrations from Landsat TM in Case-2 waters by a spectral decomposition algorithm (SDA). The estimation accuracy of Chl-*a* concentrations with the SDA method was found to be superior to that of conventional methods. Alcántara *et al*. (2009) evaluated the suitability of the spectral unmixing algorithm to map the turbidity of the Curuai floodplain lake from MODIS data.

Contrary to many successful investigations for Case-1 waters, some studies on ocean colour for Case-2 waters failed due to the optical complexity of these waters. These conditions become even more difficult in equatorial tropical regions due to spatial variations of atmospheric haze. Finding good quality remote sensing data in these regions is hard due to the frequent cloud coverage. In addition, satellite images of tropical regions are frequently contaminated with spatially variable amounts of atmospheric haze, making atmospheric correction methods based on the assumption of a homogeneous atmosphere of limited use. Based on the successful application of spectral unmixing for the land part and a few studies for the water part in subtropical regions, this study is focused on testing the spectral unmixing technique for tropical coastal waters. The objective of this study is to estimate total suspended matter concentration by using a spectral unmixing technique based on a coupled water-atmosphere radiative transfer model from MERIS data of the Berau estuary waters of East Kalimantan, Indonesia.

6.2. Data set

The *in situ* data used in this study was described in Chapter 3. The TSM measured *in situ* on August 29 and 31, 2007 were used for validating TSM retrieval. MERIS Reduced Resolution (RR) data of Level 1b (L1b) and Level 2 (L2) on August 31, 2007 was used in this study.

6.3. Method

Spatial variations of the top-of-atmosphere radiance (L_{TOA}) signal of ocean scenes in coastal areas can often be decomposed in variations due to two major constituents, atmospheric haze and sediment in the water. Both have a different spectral colour, so in principle it is possible to apply spectral unmixing of the spectrum to separate the signal variations into two components, haze and sediment. Thus, this study uses spectral unmixing to decompose the TOA radiance into suspended sediment and haze in the coastal waters. The general methodology of the presented algorithm can be regarded as an integrated approach based on inverse modelling of radiative transfer within the coupled ocean-atmosphere system by applying a spectral unmixing technique. In this particular case, a water optical model was coupled to the MODTRAN atmospheric model in order to determine endmembers in a controlled way. An alternative is selecting endmember spectra from the image, but this is much more subjective. The generation of a concentration map includes three major steps: (i) generating a look-up table (LUT) of spectral TOA radiances by using the coupled forward model, (ii) selecting endmembers, and (iii) applying the spectral unmixing algorithm to MERIS data.

6.3.1. Generating a look up table (LUT) of TOA radiance simulations

In this stage, a look-up table of TOA radiance data (L_{TOA}) was developed by simulating 36 combinations of haze level (visibility) and concentration of TSM. The visibilities used in this study were 10, 20, 40 and 50 km, while the concentration of TSM was varied quasi-exponentially over the steps of 1, 5, 8, 10, 30, 50, 60, 80 and 100 mgl^{-1}. Firstly, the forward model predicts remote sensing reflectance R_{rs} from TSM concentration. For this, we applied a semi-empirical model based on Kubelka-Munk (K-M) radiative transfer theory. According to this model, the relationship between TSM concentration and remote sensing reflectance is given by Shen *et al.* (*submitted*) as:

$$R_{rs} = \frac{\alpha\beta C_{TSM}}{1 + \beta C_{TSM} + \sqrt{1 + 2\beta\, C_{TSM}}} \qquad (6.1)$$

where C_{TSM} is the TSM concentration in arbitrary units, and α and β are fitting coefficients. In this paper, the α and β were estimated by fitting the model to *in situ* measurements. The α and β obtained for the Berau estuary are displayed in Table 6.1. Secondly, the R_{rs} was converted into reflectance, r, by using the relationship $r = \pi\, R_{rs}$. Lastly, the TOA total radiance in the MERIS channels, L_{TOA} (W m^{-2} sr^{-1} μm^{-1}), can be expressed by the equation:

$$L_{TOA} = L_0 + \frac{G * r}{1 - r * A} \qquad (6.2)$$

where L_0 is TOA radiance (the atmospheric path radiance) for zero surface albedo (W m^{-2} sr^{-1} μm^{-1}), A is the spherical albedo of the atmosphere for diffuse illumination from below, and G is the gain factor, which includes the gain factors for the target and the background. The constants L_0, A and G were determined for various cases from the outputs of MODTRAN. The MODTRAN program was run with surface albedos of 0%, 50% and 100%, respectively, for deriving the correction parameters for a given atmospheric state and angular geometry (Verhoef & Bach, 2003). In this particular study, the rural aerosol model, and the assumption of a Lambertian surface reflectance of the waters, no adjacency effects (large target assumption) and a laterally homogeneous atmosphere were used as inputs for MODTRAN. The parameters produced by MODTRAN for August 31, 2007 are listed in Table 6.1, together with the parameters of the semi-empirical water turbidity model.

Table 6.1: L_0, G and A in all bands and at different visibilities (10, 20, 40 and 50 km) resulting from MODTRAN and α and β, which are fitting coefficients.

	Vis	490 nm	510 nm	560 nm	620 nm	660 nm	680 nm	710 nm
L0	10	62.2	54.3	40.5	28.7	23.1	21.6	17.2
	20	49.1	42.1	29.8	20.1	15.8	14.5	11.5
	40	41.9	35.4	24.1	15.6	11.9	10.8	8.5
	50	40.4	34.1	23.0	14.7	11.1	10.0	7.9
A	10	0.230	0.216	0.192	0.168	0.152	0.150	0.130
	20	0.191	0.175	0.150	0.126	0.110	0.109	0.090
	40	0.164	0.147	0.120	0.096	0.081	0.080	0.063

	Vis	490 nm	510 nm	560 nm	620 nm	660 nm	680 nm	710 nm
	50	0.157	0.140	0.113	0.090	0.075	0.073	0.057
G	10	321	319	320	306	288	293	250
	20	369	365	362	342	320	325	277
	40	398	392	387	363	339	344	293
	50	404	398	392	367	343	348	296
α		0.049	0.045	0.061	0.097	0.084	0.071	0.064
β		0.040	0.048	0.039	0.012	0.014	0.018	0.019

[*] Vis = MODTRAN Visibility (km)

6.3.2. Selection of endmembers

The selection of endmembers is a very important step in the spectral unmixing technique. In this study, we proposed two methods for selection of endmembers: (1) visual selection of endmembers by the user from the image and (2) selection of endmembers from a LUT based on radiative transfer model calculations.

a.   Selection of endmembers by the user from the image

This method has the advantage that it is simple and straightforward. However, it depends on the way the user selects the spectral endmembers, and therefore it is more subjective. In order to demonstrate this method, the L_{TOA} of MERIS data on August 31, 2007 was used for the selection of endmember spectra, which correspond to:

1)   a pixel with minimal haze and sediment, *r*
2)   a pixel with minimal sediment and much haze, *h*
3)   a pixel with minimal haze and much sediment, *s*

The main difficulty with this method is finding pixels in the image which really have the same minimum haze and sediment levels, i.e. the difference between pixels 1 and 2 should only be caused by a difference in haze level, and that between pixels 1 and 3 only by a difference in sediment level.

b. Selection of endmembers from a LUT and transforming LTOA data into standard haze level

This method uses model-calculated spectra of L_{TOA} as a basis for selecting the endmembers. The spectrum corresponding to the minimum haze and sediment levels can be taken close to the one of the darkest pixel in the ocean part of the scene. The other endmembers have to be chosen in accordance with the actual haze and sediment variations in the image.

Regardless of the method of endmember selection, one may assume that the L_{TOA} images of ocean scenes in coastal areas can be decomposed in two major constituents, atmospheric haze and sediment in the water. The linear unmixing model to be applied for the combination haze-sediment can be formulated as follows.

Suppose that the TOA spectral radiance vector of a pixel is approximated by:

$$\hat{p} = r + a_1 h + a_2 s \qquad (6.3)$$

Then the real TOA radiance spectrum of the pixel is supposed to be given by:

$$p = \hat{p} + \varepsilon \qquad (6.4)$$

where:

r = the reference spectrum for standard haze level and zero sediment

h = spectrum for increased haze level and zero sediment, relative to r

s = spectrum for standard haze level and increased sediment, relative to r

$\hat{p}$ = modelled TOA radiance spectrum

a_1 = amount of haze above the standard in arbitrary units

a_2 = amount of sediment in arbitrary units

ε = the residual error radiance spectrum.

Suppression of haze variations is possible by transforming the TOA radiance spectrum into one which corresponds to the standard haze level. This spectrum

is called p' and it is created by setting a_1 equal to zero, which is equivalent to subtracting the contribution $a_1 h$, so we have:

$$p' = p - a_1 h \tag{6.5}$$

The operation to go from p to p' is called a projection. By setting a_1 equal to zero, the data are projected onto the p vector along the direction of the h vector.

In order to enable this transformation, the actual haze amount in arbitrary spectra p, given by the coefficient a_1, has to be estimated. For this, in equation (6.3) $\hat{p}$ is replaced by p, and multiplied by the transposed vectors of h and s, which yields:

$$
\begin{aligned}
h^{\mathrm{T}}(p-r) &= a_1 h^{\mathrm{T}} h + a_2 h^{\mathrm{T}} s \\
s^{\mathrm{T}}(p-r) &= a_1 s^{\mathrm{T}} h + a_2 s^{\mathrm{T}} s
\end{aligned}
\tag{6.6}
$$

From this, one finds both coefficients from:

$$
\begin{pmatrix} a_1 \\ a_2 \end{pmatrix} = \begin{pmatrix} h^{\mathrm{T}} h & h^{\mathrm{T}} s \\ s^{\mathrm{T}} h & s^{\mathrm{T}} s \end{pmatrix}^{-1} \begin{pmatrix} h^{\mathrm{T}}(p-r) \\ s^{\mathrm{T}}(p-r) \end{pmatrix} = \begin{pmatrix} m_{11} & m_{12} \\ m_{21} & m_{22} \end{pmatrix} \begin{pmatrix} h^{\mathrm{T}}(p-r) \\ s^{\mathrm{T}}(p-r) \end{pmatrix}
\tag{6.7}
$$

One can write:

$$a_1 = (m_{11} h^{\mathrm{T}} + m_{12} s^{\mathrm{T}})(p-r) = u^{\mathrm{T}}(p-r) \tag{6.8}$$

$$p' = p - a_1 h = p - u^{\mathrm{T}}(p-r)h \tag{6.9}$$

Since :

$$(u^{\mathrm{T}} p)h = h(u^{\mathrm{T}} p) = (h u^{\mathrm{T}})p \tag{6.10}$$

one can finally write:

$$p' = (I - h u^{\mathrm{T}})p + u^{\mathrm{T}} r h \tag{6.11}$$

where I is the identity matrix. This equation represents a linear transformation of the input vector. However, in practice it is simpler to subtract directly the haze contribution $a_1 h$ from the original spectrum p, since in that case no matrix multiplication is needed.

6.3.3. Applying the spectral unmixing algorithm to the MERIS data

The spectral unmixing technique was applied to MERIS data. In general, the MERIS data was processed as follows: (1) generating a MERIS image with a constant haze level (visibility) over the image by applying the spectral unmixing and projection approach, (2) applying atmospheric correction to the MERIS data with a constant haze level, resulting in the remote sensing reflectance for each pixel, and (3) deriving TSM concentration from remote sensing reflectance by applying the inverse K-M model. The Basic ENVISAT Toolbox for MERIS BEAM, version 4.5.1, was used for processing the MERIS L1 data. BEAM is an open-source software package for visualizing, analyzing and processing the Envisat MERIS, AATSR, ASAR, ERS, and ATSR data (Brockmann, 2009, http://www.brockmann-consult.de/cms/web/beam).

6.4. Results

6.4.1. Sediment image derived from MERIS data using spectral unmixing based on user-selected endmembers

The separation of haze from suspended sediment for the water pixels has been done successfully by using linear spectral unmixing. In this study, we used raw data of MERIS L1 on August 31, 2007 as an input. We selected three pixels, representing low sediment and low haze, low sediment and high haze and high sediment and low haze, respectively. These three endmember spectra (*r*, *h* and *s*) selected by the user from the MERIS data are displayed in Figure 6.1a. The positions of the three endmembers, and of six other spectra from field locations, representing the wavelengths of 490 nm on the X-axis and 620 nm on the Y-axis, are also displayed in the scatter plot of Figure 6.1b. This figure shows that the radiances from the field locations are slightly higher in the 490 nm band.
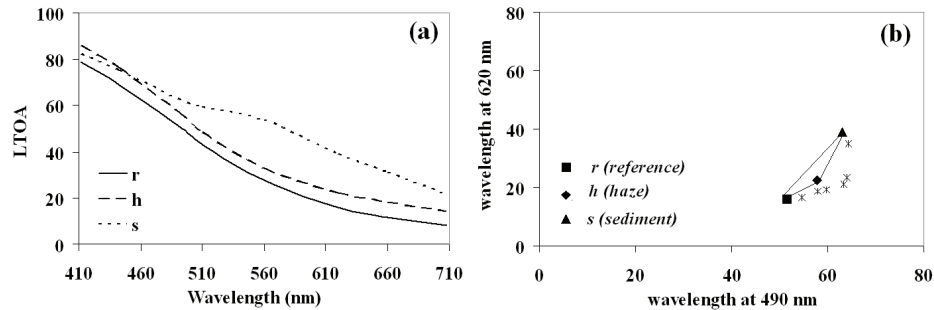
Figure 6.1 : The endmembers visually selected by the user from the image MERIS RR L1, August 31, 2007, (a) the three endmembers, and (b) Scatterplot of the three endmembers and 6 spectra from field locations.
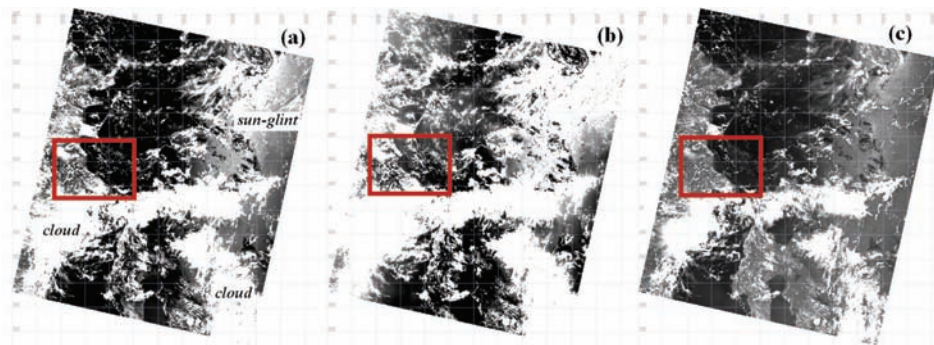
Figure 6.2 : The MERIS RR of August 31, 2007: (a) original radiance at a wavelength of 620 nm, (b) haze level in arbitrary units, and (c) sediment level in arbitrary units. The red boxes indicate the sub-image where the study area is located

Figure 6.2 displays the full scene of MERIS data RR, L1 at August 31, 2007 at a wavelength of 620 nm (band 6). The MERIS data was dominated by clouds and sun glint (Figure 6.2a). The haze and sediment images were derived by using Eq. (6.7). Although much of the image was cloudy and hazy (Figure 6.2b), the Berau river mouth looks reasonably good. The sediment level in this image is high in the mainland and for coastal waters, and decreases when going to the sea (Figure 6.2c). The correlation between TSM concentration measured *in situ* on August 29, 2007 and sediment level was very high ($R^2 = 0.92$ and n = 6).

6.4.2. Suppression of haze variations on spectra of TOA radiance simulations

Spectra of TOA radiances of the combined water turbidity – atmosphere model were generated by using Eq. (6.1) and Eq. (6.2) for 36 combinations of atmospheric visibility and total suspended sediment concentration. The atmospheric visibilities were 10, 20, 40 and 50 km, while the TSM levels were varied quasi-exponentially over the steps of 1, 5, 8, 10, 30, 50, 60, 80 and 100 mgl^{-1}. In order to illustrate the mixing between sediment and haze influence, a "fishing net" plot was created. Figure 6.3 illustrates quite well that the mixing of 3 levels of haze (10, 20 and 50 km) and 5 levels of sediment influences (10, 30, 60, 80 and 100 mgl^{-1}) is approximately linear for the spectral bands of 490 nm and 620 nm. It also illustrates that increasing the TSM concentration has a different spectral effect than increasing the amount of atmospheric haze (decreasing visibility), so in principle both effects should be separable.
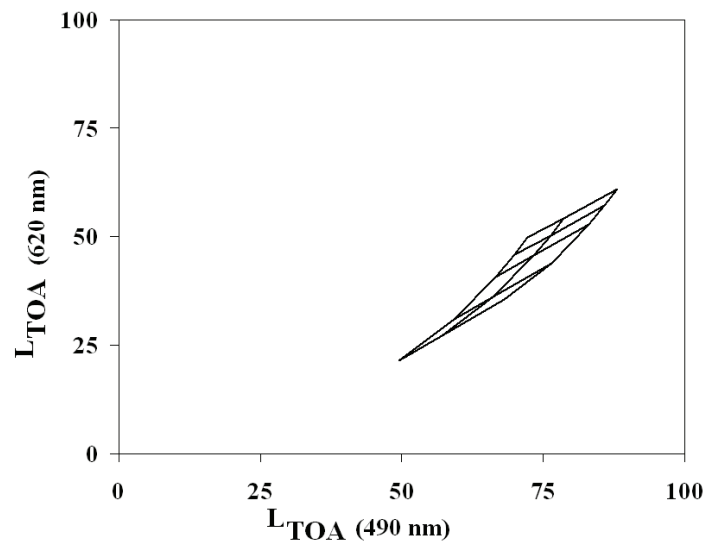
Figure 6.3 : A fishing net plot of the effects of haze and sediment variation for the wavelengths 490 nm and 620 nm, using 15 combinations of haze and sediment.

104

Corresponding spectra of L_{TOA} for all 36 combinations of haze and sediment are given in Figure 6.4. This displays the L_{TOA} spectra at 4 levels of visibility for each TSM concentration. By increasing the TSM concentration, the spectral shapes of L_{TOA} change. For low TSM concentrations, the spectral shapes resemble those of clear water, and by increasing the TSM concentration, the spectra change to those of turbid waters, which are higher especially at longer wavelengths. An increasing haze influence (lower visibility) has a different effect since this produces a spectral increase, especially at shorter wavelengths.
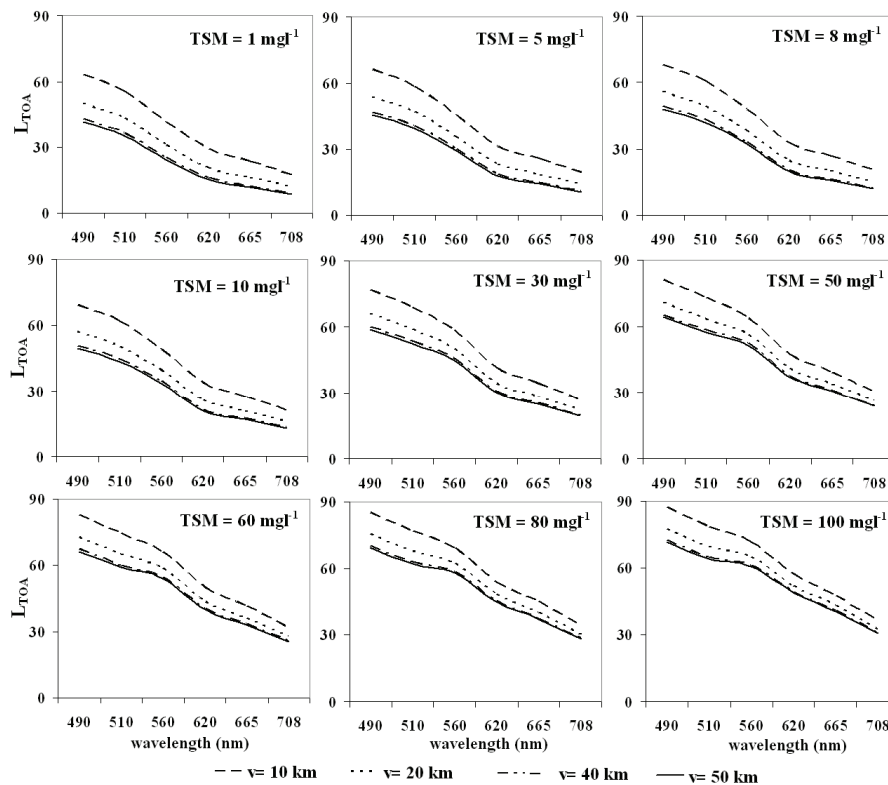
Figure 6.4 :   Simulated TOA radiance spectra for 36 combinations of haze and sediment at each TSM concentrations before projected

The original L_{TOA} spectra for a visibility of 50 km with 9 levels of TSM concentration are plotted in Figure 6.5a. The L_{TOA} spectra start from a high value at a wavelength of 490 nm (corresponding to MERIS band 3) and decrease with

increasing wavelength, due to decreasing atmospheric scattering. In this study, the reference endmember was taken to be the spectrum corresponding to the combination of 50 km visibility and a TSM concentration of 1 mgl^{-1}. The increased haze endmember spectrum was taken from 10 km visibility, while the increased sediment spectrum was taken from the TSM concentration of 100 mgl^{-1}. These three basis spectra are shown in Figure 6.5b, where the solid line is the reference spectrum (*r*), the dotted line is the L_{TOA} for 50 km visibility and a TSM concentration of 100 mgl^{-1} (*r* + *s*), while the dashed line is the L_{TOA} for a visibility of 10 km and a TSM concentration of 1 mgl^{-1} (*r* + *h*).
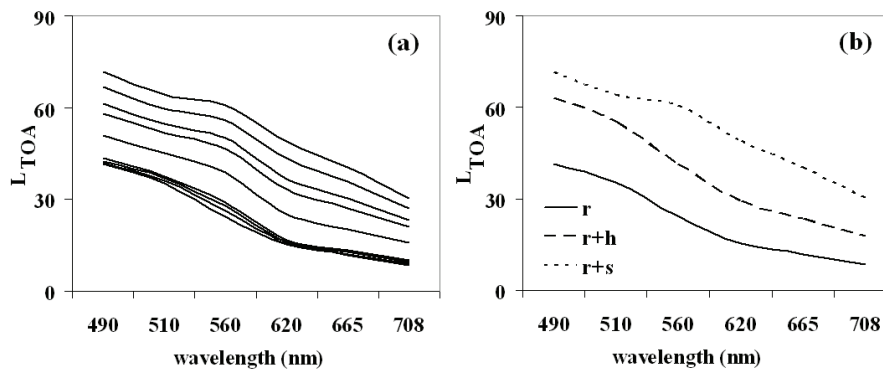
Figure 6.5 :   The LTOA spectra for 9 levels of TSM concentrations for a visibility of 50 km (a), and the LTOA endmember spectra selected for the linear unmixing (b)

Transforming all 36 spectra by the projection method of Eqs. (6.3 to 6.11) gives the results as displayed in Figure 6.6. Haze variations have been largely removed while sediment effects are preserved. At low TSM concentration, all haze levels now produce virtually identical spectra, while for the highest TSM concentrations some haze effects are still visible.

106
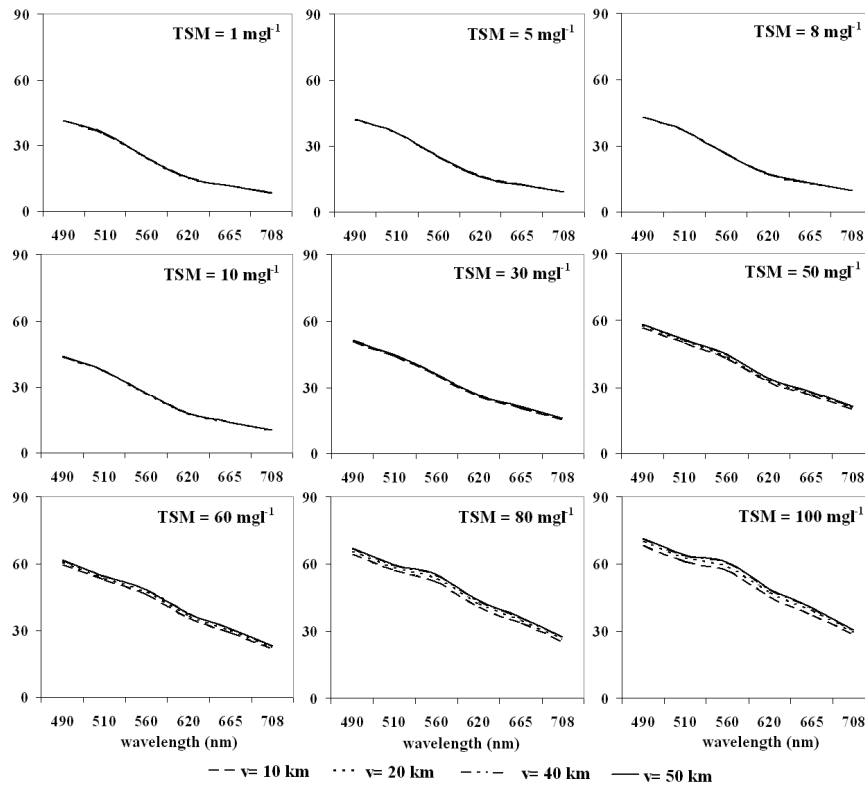
Figure 6.6 : The LTOA simulation of the projection method for all 36 combinations given by 4 levels of visibility and 9 levels of TSM concentrations after spectral projection.

6.4.3. Suppression of haze variations in MERIS TOA radiance images

As shown in Figure 6.2 of section 6.4.1, the full image of MERIS of August 31, 2007 has heavy haze variations over the Berau estuary water and the adjacent coasts. Haze and sediment components are clearly mixed there. The haze component was suppressed by the projection method for MERIS images in all bands by applying Eq. (6.5).

In order to better focus on this area, a sub-image of MERIS RR of August 31, 2007 was created. Figure 6.7a displays the sub-image of band 6 before projection, while Figure 6.7b displays the sub-image of the same band after

projection. It is clear that the projection method has removed some haze variations, while sediment variation is preserved. The area inside the red box in Figure 6.7b shows that the sediment area is clearly larger compared to the same location presented in Figure 6.7a.
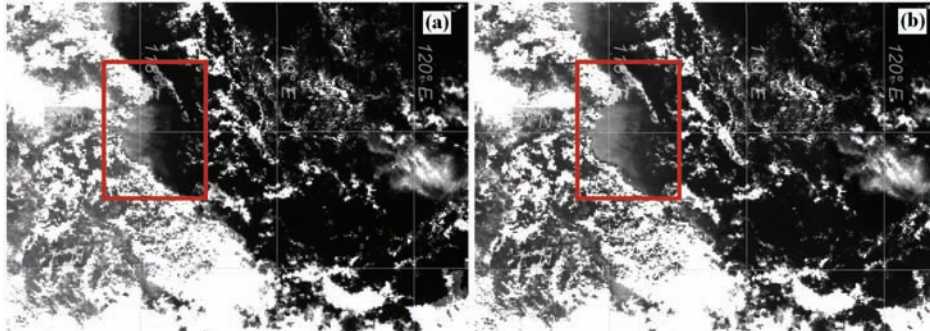
Figure 6.7 : Sub-image of MERIS RR of August 31, 2007 at wavelength of 620 nm: (a) before projection, and (b) after projection.

The TSM was retrieved from MERIS surface reflectance data using the semi-empirical K-M model. Results from Chapter 5 indicated that the most appropriate band for retrieval TSM concentration from MERIS data for the turbid water of the Berau estuary was band 6 (620 nm). The TSM concentration map on August 31, 2007 of the Berau estuary waters is displayed in Figure 6.8. Visual analysis of the TSM concentration image shows that the spatial distribution pattern of TSM concentration corresponds well with the reflectance data. Difficulties arise where sun glint and clouds are not masked out and so, these could cause be mistaken for high TSM concentrations. Figure 6.8 clearly shows that high TSM concentrations are found near the coast and decrease when moving eastward to the sea.
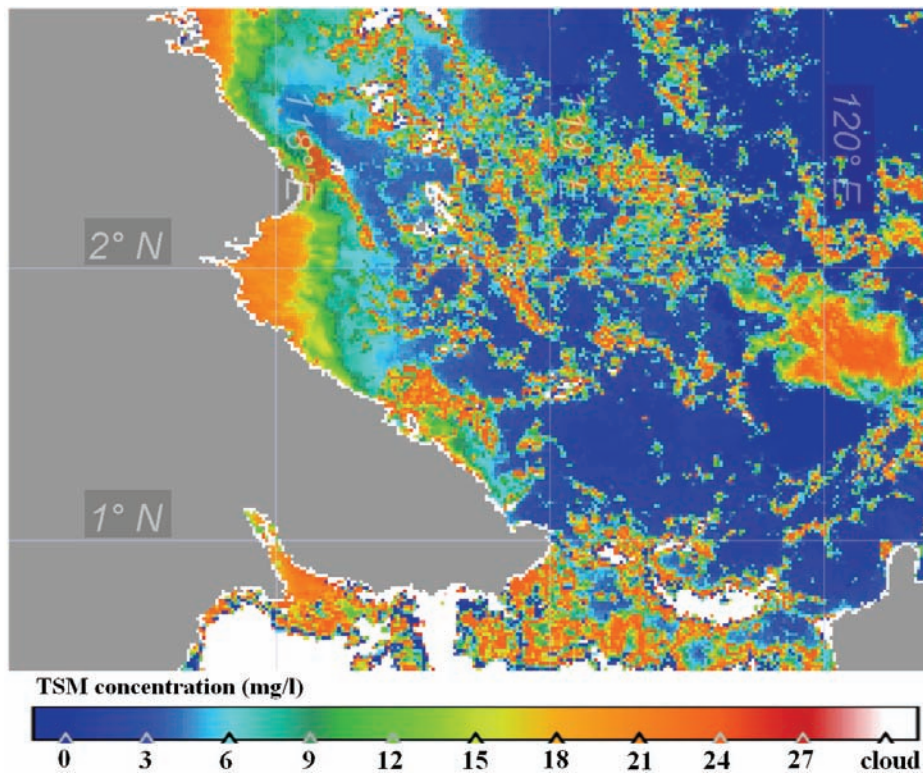
Figure 6.8 :   The TSM concentration map derived from MERIS data on August 31, 2007 with the coupled spectral unmixing and the inverse K-M model

Figure 6.9 displays a scatter plot between TSM concentrations measured *in situ* versus TSM derived from MERIS RR data. In this validation test, we used two sets of TSM concentration data measured in the field. One was the TSM concentration set collected on 31 August 2007. This data set matches with the MERIS data, with only a few hours difference. The 9 field stations of this data were located in clear water; not any of them represents turbid water. Due to the weather conditions during the field campaign, the area close to the Berau river mouth and near the coast had high cloud cover. The second data set, which is composed of 6 field stations, is used in order to examine the TSM concentration distribution in the relatively turbid water. It was the data set collected on August 31, 2007 when the weather conditions were more favourable.
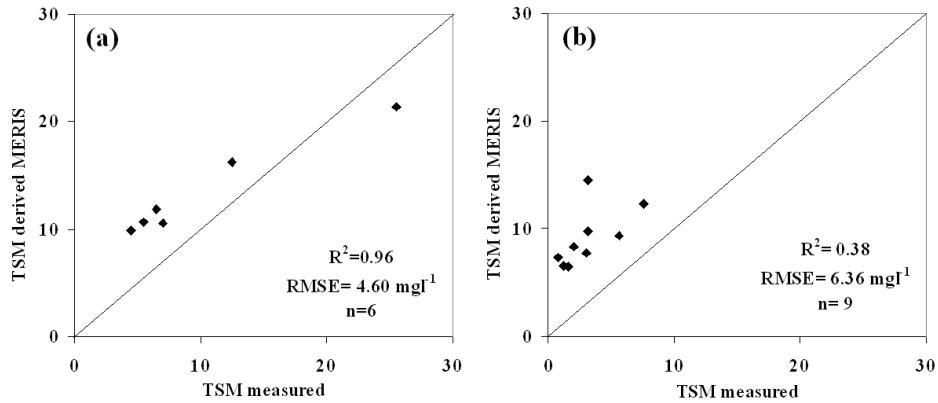
Figure 6.9 : Scatter plot between TSM concentration derived from MERIS data and TSM concentration measured *in situ*, for relatively turbid water on August 29, 2007 (a) and TSM concentrations measured *in situ* in clear water on August 31, 2007 (b).

The statistical analysis of the relation between TSM concentration measured and TSM concentration derived from MERIS was done by calculating the coefficient of determination (R^2) and the Root Mean Square Error (RMSE). Figure 6.9a reveals that TSM concentration derived from MERIS data has a higher correlation with the TSM concentration measured *in situ* on August 29, 2007. This is evident from the higher coefficient of determination ($R^2 = 0.96$). The distribution of the TSM derived from MERIS data in relatively turbid water looks promising and the values are not too far from the 1:1 line. Nevertheless, the TSM concentrations derived for the clear water (Figure 6.9b) seem to be overestimated.

6.4.4. TSM concentrations derived with different algorithms and their inter-comparison

The MERIS RR L1 was processed with BEAM Visat version 4.5.1 in order to retrieve TSM concentration using the C2R and FUB algorithm processors as well as the MERIS L2 algorithm. In this inter-comparison, we used TSM concentrations measured *in situ* on August 29, 2007 because on that date the field stations ranged from relatively turbid water to clear waters (Figure 6.10).

TSM concentration derived from MERIS with the global algorithm, MERIS L2 (*see* Figure 6.10a), with the C2R algorithm (Figure 6.10b) and with FUB (Figure 6.10c) all are well correlated with measured TSM, but there is a large underestimation of TSM levels, especially at high concentrations.
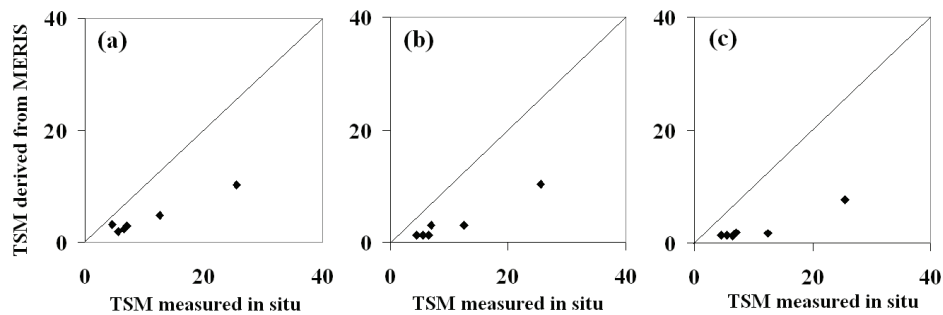
Figure 6.10 : Scatter plot between TSM measured *in situ* on August 29, 2007 versus TSM concentration derived from MERIS August 31, 2007: (a) using L2, (b) C2R and (c) FUB.

The results of the statistical analysis between TSM concentration measured *in situ* and TSM concentration derived from MERIS data using various algorithms used in this study are summarised in Figure 6.11. The coupled spectral unmixing with the coupled radiative transfer model and inverse K-M model (indicated by SUKM) proposed in this study produces a very good correlation between TSM concentration measured *in situ* and TSM concentration derived from MERIS data (R^2 = 0.96), but this holds for other algorithms as well (*see* Figure 6.11a). However, the new approach improved also the accuracy of estimation, expressed by the decreasing RMSE compared to L2, C2R and FUB (*see* Figure 6.11b). This is mainly because the underestimations of TSM by L2, C2R and FUB do not occur for SUKM. This, in turn, can be explained by the fact that the SUKM method included a semi-empirical calibration of the water turbidity model.
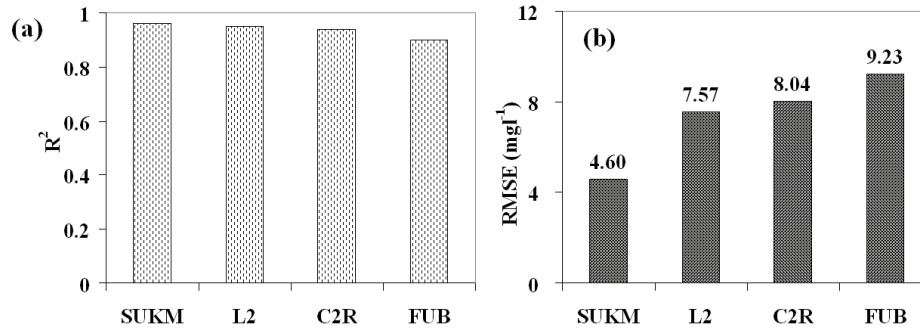
Figure 6.11 : Statistical summary between TSM concentration measured and TSM concentration derived from MERIS data: (a) R^2, and (b) RMSE in mgl^{-1}

6.5. Discussion

The top-of-atmosphere (TOA) radiance signal recorded by earth observation sensors like MERIS is a mixture of signals coming from the surface and from the atmosphere. Many atmospheric correction methods are based on the assumption that the atmosphere is laterally homogeneous. In most cases however, the amount of atmospheric haze varies spatially. Atmospheric correction methods that are applied to water areas often exploit the low reflectance of water in the near infrared in order to get an estimate of the variable atmospheric influence from the TOA signal in that spectral region. In waters with high sediment loads, this does not work however, since in that case water reflects also radiation at near infrared wavelengths. Therefore, this study demonstrated a novel approach of using a coupled application of spectral unmixing and radiative transfer modelling to derive TSM concentrations in the Case-2 water of the Berau estuary, Indonesia.

The main purpose of the proposed spectral unmixing technique is separating spatial variations of haze from sediment variations in the water. In this research this was done by selecting endmembers in a controlled way from a look-up table of simulation results obtained from a coupled water turbidity – atmosphere model in which visibility and TSM concentration were varied. In this study, we also tested the visual selection of endmembers from the image by the user. This approach is simple and straightforward. However, it is very

subjective. The other limitations of this method are: (1) we do not know the TSM concentration of the endmember pixels we selected from the image, (2) the haze levels for these pixels are also unknown. Therefore, the model-based selection of endmembers is preferred.

The accuracy of TSM concentration derived from MERIS by applying the inverse K-M model to atmospherically corrected data, after spectral projection to reduce haze variations, increased compared to the MERSI L2 and C2R as well as the FUB algorithm processors (*see* Figure 6.11). The RMSE decreased to around 40%, 43% and 50% with respect to L2, C2R and FUB respectively. The spectral unmixing worked well in this study by spectrally projecting the MERIS image to a similar haze level (visibility 50 km).

Discrepancies between TSM concentrations measured and TSM concentrations derived from MERIS data in this study can be explained by the presence of clouds and sun-glint on the MERIS image of August 31, 2007. The study area is located in a tropical equatorial region, where clouds and atmospheric haze variations are very frequent. As has been mentioned by Doerffer & Schiller (2006), the right side of a MERIS image is always contaminated by sun glint. This is due to the orbit parameters of ENVISAT and sea state conditions expressed by waves and wind speed.

As has been mentioned by Matthew *et al*. (2000), clouds and cloud shadows pose several problems for atmospheric correction, not only because cloud-contaminated pixels give an incorrect reflectance, but also because clouds can degrade the reflectance accuracy in other parts of the scene, for instance due to cloud shadows.

In this study, we used the wavelength of 620 nm (MERIS band 6) for deriving the TSM concentration image. This is because the wavelength of 620 nm reflects most strongly the influence of suspended matter (Fischer and Fell, 1999). We found that the area of the coastal sediment region on the MERIS RR L1 image at a wavelength of 620 nm became larger after spectral projection compared to the image at the same wavelength before projection (Figure 6.7). In the clear water

close to open sea, the TSM concentration derived was overestimated compared to TSM concentration measured *in situ*.

In situ measurements are frequently used as a reference compared to satellite data (IOCCG, 2006). Nevertheless, *in situ* data may contain significant errors caused by environmental factors, instrumental shortcomings and human errors. The uncertainties associated with *in situ* measurements have various sources, such as the deployment protocols used in the field, the environmental conditions and the processing scheme.

The large difference between *in situ* measurements and MERIS data is also due to within-pixel heterogeneity. The *in situ* measurements were done at small and relatively homogeneous areas, while the MERIS sensor recorded much larger areas. The MERIS FR data has a spatial resolution of 300 m by 300 m, while the MERIS RR data has a spatial resolution of 1200 m by 1200 m. As has been mentioned in the IOCCG Report (2006), the lack of correspondence between the match-up field data and satellite data is due to the environmental mismatch in scales; the field data usually describe an area of around 1–10 m, while the satellite spatial scale is often 100 – 1000 m (IOCCG, 2006). Other researchers (Sathyendranath & Platt, 1989; Zaneveld *et al.*, 2005) argued that satellite measurements represent a water column's weighted average, while *in situ* measurements of concentrations are taken at a discrete depth.

The Berau estuary contains several coral reefs, sand bars and islands like Derawan, Samama, Sangalaki, Kakaban and Maratua (Figure 2.4). Water pixels in the proximity of these reefs and islands can be contaminated with light emanating from adjacent pixels of the coral reefs and bottom reflectance in these shallow waters. This study applied MERIS reduced resolution data with a pixel size of 1200 m by 1200 m and so, the area covered by a pixel was sufficiently large. This adjacency effect may appear for certain pixel values in the transition zone for MERIS FR data.

6.6. Conclusions

Spectral unmixing, combined with a coupled water-atmosphere radiative transfer model provides an efficient mechanism for deriving TSM concentration from remote sensing data (e.g. from MERIS) under spatially variable haze conditions. A spectral projection method transforms the given TOA radiance spectra into spectra which correspond to a standard atmospheric condition with a visibility of 50 km. These transformed spectra resemble those for the real 50 km visibility case quite well, and multispectral images of similar data can next be used as an input for a simple atmospheric correction procedure with a standard visibility of 50 km, assuming a homogeneous atmosphere. The present results are partly dependent on the choice of basis vectors. It should also be possible to apply the method with varying basis vectors by using the data from a more extensive look-up table.

In this study, it was shown that the proposed approach increases the accuracy and the correlation between TSM concentration measured and TSM concentration derived from MERIS data compared with other methods used in this study such as C2R, FUB, and MERIS L2. This improvement appears especially in terms of the RMSE, which decreased significantly with this method.

CHAPTER 7

SYNTHESIS

7.1. Introduction

Remote sensing of ocean colour is a very important tool for monitoring the coastal and ocean waters in Indonesia, since Indonesia is an archipelagic country and 70% of its area is occupied by water. Traditional ways to map this large area are time-consuming and expensive. Actually, this traditional way is still used as a main monitoring tool in this developing country. On the other hand, remote sensing techniques have been used in many parts of the world for monitoring marine and coastal waters. Many algorithms and models as well as data bases of IOP and SIOP have been established for Case-2 and Case-1 waters around the world. Unfortunately, limited study was conducted in equatorial tropical waters such as Indonesia. As a consequence, there is a gap between the data availability and the need for monitoring this large tropical archipelagic country. In this study, the calibration and validation of MERIS data as well as algorithm validation was a first step to start utilizing remotely sensed data for monitoring the very large area of the Indonesian tropical waters.

In general, the water constituent retrieval techniques from remote sensing data that have been developed are empirical and semi-analytical. The empirical algorithm focuses mostly on a single constituent concentration. An advantage of this empirical algorithm is that it is simple and straightforward. However, these algorithms can only be applied for local situations, and they require recalibration for each location and time. The semi-analytical method in principle is capable of retrieving more water constituents simultaneously. In this study, we focused on semi-analytical approaches for estimating water constituents, based on the bio-optical model, the semi-empirical Kubelka-Munk model, artificial neural network models and a modification of the Garver-Siegel-Maritorena model.

Testing the new approaches in a coastal environment with spatially variable haze conditions also forms a contribution of this research, since in this equatorial zone the climatic conditions usually limit the application of optical remote sensing imagery. The IOP and SIOP output from this study can be used

as a preliminary benchmark for further study in Indonesia and even, with some adaptation, for other equatorial tropical waters.

This chapter is dedicated to interpreting the results of this research further, its position in the state of knowledge and the contribution of this research in the remote sensing of tropical regions. In this chapter, the main results will be summarized first, followed by the analysis of the interrelationships between the different chapters of this research. Lastly, based on the result acquired, this chapter will recommend future works in this domain.

7.2. Main results

(1) Inherent optical properties and specific inherent optical properties can be determined by using direct in situ optical and constituent measurements in the coastal waters.

This study was first motivated by the absence of information about two sets of important bio-optical parameters, IOP and SIOP, for Indonesian coastal waters, whereas these parameters are the key to improve the accuracy of derived water constituents from remote sensing ocean colour data. The question arising is then: are there any easy-access parameters susceptible to be used to derive SIOP in this complex tropical environment? After several trials, the results of this study indicate that in the study area the lack of IOP/SIOP data for directly using remote sensing data, can be minimized by inversion of a bio-optical model using optical *in situ* and water constituent measurements. It should be noted however, that the quality of IOP and SIOP resulting from such approach depends on the quality of the optical measurement, the water constituent measurement, as well as the model used. Application of this method to the MERIS data in this research indicates that using this approach can improve the estimation of TSM and Chl-*a* concentration.

In Chapter 3 we used the inverse bio-optical model to derive IOP and associated SIOP from *in situ* measurements of AOP and water constituents. The AOP of the Berau estuary was represented by the subsurface irradiance

reflectance, *R(0-)* that was calculated from *in situ* measurement of optical parameters by using a field spectrometer. The *R(0-)* of Berau coastal waters was extensively discussed in this chapter. These reflect the spectral characteristics of coastal waters, ranging from highly turbid estuary to clear ocean waters. The sub-surface irradiance reflectance measured and the model-best-fit spectra are correlated well ($R^2 = 0.74$). A mismatch was apparent in the short wavelengths (blue band) and in the long wavelength region (NIR band) of the spectrum. The wavelengths of 509 nm, 559 nm and 619 nm were the bands where *R(0-)* resulting from *in situ* measurement matched best with the *R(0-)* obtained by the model.

As has been mentioned by Gordon (1975), the *R(0-)* can be correlated with IOP by using a radiative transfer model for water, the bio-optical model. Using this approach, it was found that the SIOP derived for the Berau estuary were sufficiently good, with correlations found between the known SIOP and the derived ones of $R^2 = 0.87$ for specific backscattering of TSM and $R^2 = 0.85$ for specific absorption of Chl-*a*. The results also indicated that the $b^*_{b,TSM}$ was higher in the turbid coastal water than in the offshore area. In the Berau estuary, the values of a^*_{Chl} were almost similar for the turbid and more clear ocean waters, near the continental shelf edge. The value of a_Chl obtained in the coastal water of the Berau estuary is similar to the one found in the North Sea water observed by Astoreca *et al*. (2006), while the value in the offshore water of the Berau estuary was lower than one in the North Sea waters. In the case of the $b_{b,TSM}$, the value in the coastal area of Berau estuary ranges between 0.180 to 0.995 m^{-1}. In the offshore area, the values range from 0.020 to 0.036 m^{-1}, while in the transition zone the values range from 0.033 to 0.527 m^{-1}.

This approach was successfully extended and applied to MERIS data. The result of TSM and Chl-*a* concentration derived from MERIS data using the inverse model are promising. The TSM estimation as well as Chl-*a* concentrations have a high R^2 and low RMSE (*see* section 3.4.4). This result offers good prospects for future work. It will be possible in the future to obtain estimates of TSM and Chl-*a* concentration directly from remote sensing observations, since establishing a bio-optical model for coastal and marine water using image data

is more stable than directly done from water constituents. By knowing bio-optical properties of the water in the coastal and marine environment, we can use it for other MERIS data. The results contribute also in providing original IOP and SIOP data, which were so far almost unavailable for these tropical equatorial regions.

(2). MERIS offers the possibility to assess optical water quality (TSM and Chl-a concentrations) in turbid Case-2 coastal waters

The potential of remote sensing to assess water quality parameters has been studied by many researchers since the Coastal Zone Colour Scanner (CZCS) was launched by NASA in 1978. Following the CZCS, many sensors were put into orbit for monitoring ocean and coastal waters; one of them is the MERIS sensor. With the availability of the sensor, a variety of techniques and algorithms to extract water quality from ocean color sensor became also available. Regular monitoring of coastal water is however hampered by the complexity at each location, especially by the dynamic atmospheric conditions. However, the potential of remote sensing data such as from MERIS has rarely been explored for equatorial tropical waters characterized by a high haze variability such as the Berau estuary.

Chapter 4 explored the capabilities of MERIS data for quantitative and qualitative retrieval of water quality in tropical coastal waters. In this study, Case-2 regional algorithms (C2R and FUB) as well as a global algorithm (MERIS L2) for retrieving TSM and Chl-*a* concentration were tested in order to evaluate their use in these regions. We found that these algorithms were robust under certain conditions for estimating water quality, especially Chl-*a* concentration. The very high dynamics of haze coverage as well as coastal estuary dynamics have caused the algorithms to appear however less appropriate for quantitative water quality concentration retrieval in this tropical equatorial area. This was shown especially for the result of TSM concentration retrieval. TSM values derived from MERIS do not show good correlation with *in situ* measurements. In the case of Chl-*a* concentration however, it was shown that there is a better agreement between Chl-*a* derived from the model and ones resulting from *in*

situ measurements. This indicates that at least, Chl-*a* retrieval will be possible with MERIS, based on the algorithms used. For TSM concentration, research in the future should be done to find the most appropriate algorithm. In this research, the C2R algorithm gave the most appropriate results for deriving Chl-*a* concentrations (R^2 = 0.75 and RMSE 0.33 μgl^{-1}).

Chapter 4 was also dedicated to remote sensing reflectance data measured in the field and the inter-comparison with similar data derived from MERIS. The C2R and MERIS L2 algorithms produce water leaving radiance reflectance; on the other hand, FUB produces remote sensing reflectance. We found that the R_{rs} derived with C2R has the highest correlation with the R_{rs} measured *in situ*, with a sufficiently high R^2 (0.72) and the lowest RMSE, compared to the other two algorithms (FUB and MERIS L2). We also discovered that the highest correlations between R_{rs} measured and R_{rs} derived with C2R, FUB and MERIS L2 were obtained at the wavelengths of 490, 510, 560 and 620 nm. One may suggest that these wavelengths are the most suitable ones for retrieving TSM concentration due to the maximum scattering at 560 nm and 620 nm, as well as maximum absorption by Chl-*a* at 490 nm. For comparison, a previous study by Ohde *et al.* (2007) also found that bands 3 to 6 (490, 510, 560 and 620 nm) were the most suitable ones for retrieving TSM concentration.

In this study, a diffuse light attenuation coefficient (K_d) was derived from a combination of *in situ* R_{rs} measurements and water transparency measured in the field and R_{rs} derived from MERIS data. From the K_d measured, it was found that the best fit between R_{rs} band ratios and ln [$K_d(490)$– K_dw] was achieved for the band ratio of 490 to 620 nm. The best model between $K_d(490)$ derived from MERIS data and the distance from the river mouth was an exponential model, where the highest R^2 was achieved when using the FUB algorithm processor, compared to C2R and MERIS L2. Using the FUB algorithm, we obtained R^2 = 0.77 and RMSE = 0.62.

(3). MERIS data has potential for retrieval of TSM concentration when coupling the radiative transfer model MODTRAN to a semi-analytical model approach

The standard regional Case-2 algorithms processors (C2R and FUB) and the global algorithm (MERIS L2) were evaluated in Chapter 4. It was found that the TSM retrieval from MERIS data gave an unsatisfactory result: we found poor correlation between TSM concentrations retrieved from satellite data with *in situ* measurements. This can be due to the atmospheric correction method which did not seem to work properly in this region of very high haze variability. This shows the need for improvement of the atmospheric correction step for satellite retrieval of water constituents in these regions. Chapter 5 is dedicated to this subject.

In Chapter 5 we tested a more advanced atmospheric correction combined with a semi-analytical model to retrieve TSM concentrations. The radiative transfer model MODTRAN and the semi-analytical model, based on Kubelka-Munk (K-M) theory, were applied for retrieving TSM concentration in this coastal water. We found that this coupling of models was more suitable in this study area compared to the automated plug-in algorithms (C2R, FUB as well MERIS L2), which use standardized atmospheric corrections. In our research, the K-M model was calibrated by using optical *in situ* measurements and it was found that the wavelength of 620 nm (corresponding to band 6 of MERIS) was the best for estimating TSM concentrations. Using this method, the TSM concentrations predicted from measured *in situ* R_{rs}, showed a good agreement with the measured TSM values.

In this research, the inverse K-M model was successfully applied to the atmospherically corrected MERIS data. The TSM concentration estimated from corrected MERIS data by using the empirical and the K-M model appeared to have moderate agreement with the TSM measured in the field. However, this study found that the K-M model improved the accuracy of estimating TSM concentration compared to the empirical as well as the standard algorithms discussed in Chapter 4. Nevertheless, this study observed that there are still discrepancies between TSM derived from MERIS data and TSM *in situ*

measurement. This mismatch can be attributed to within-pixel heterogeneity and spatial haze variations in the MERIS image. Haze variability should be taken into account in order to improve the accuracy of TSM retrieval.

(4). Integration of spectral unmixing with a semi-analytical model could contribute to improvement of TSM concentration retrieval from MERIS data

Studying water quality concentration such as TSM concentration in coastal water from MERIS data is often hampered by atmosphere dynamics and optical complexity of the coastal waters. Satellite images in equatorial tropical regions are frequently contaminated with spatially variable amounts of atmospheric haze, making atmospheric correction methods based on the assumption of a homogeneous atmosphere of limited use. Using this information, in Chapter 6 a combined forward and inverse modelling approach was applied to a semi-analytical model for solving the problems of haze and TSM spatial variability in this study area.

From previous chapters, it was concluded that the vertical mixing of sediment and haze in the atmosphere was a major source of uncertainty. In order to solve this problem, a spectral unmixing model was applied in this study for decomposing the coastal water spectrum into haze and sediment components. Several steps were carried out in the method developed. Firstly, a look-up table of top-of-atmosphere radiance spectra was generated by the coupled forward models. Endmembers were selected from the LUT. The spectral unmixing algorithm was then applied to the MERIS data for decomposing the MERIS image into haze and sediment components. Subsequently, the MERIS data were transformed into images of a constant haze level corresponding to 50 km visibility. Next, atmospheric correction was applied for this standard 50 km visibility and the inverse semi-analytical K-M model was used for retrieval of TSM concentration. The result of this study indicated that this integrated approach improved the correlation between TSM measured and TSM derived from MERIS data. The new approach improved the accuracy of TSM retrieval from MERIS data compared to retrievals with the standard algorithms such as C2R, FUB and MERIS L2.

7.3. Research contributions

7.3.1. Contributions on the knowledge of tropical water remote sensing.

1. First, this research fills a gap by providing the IOP and associated SIOP for equatorial tropical waters. These can be used then for validating ocean colour remote sensing data in these regions. Providing these parameters can be an important step in future development of algorithms applicable in tropical equatorial regions.

2. Secondly, this research contributes to the calibration and validation of MERIS data and Case-2 algorithms for retrieving water quality parameters. Such calibration and validation activities in complex tropical coastal environments have rarely been done before.

3. Thirdly, this study contributes in developing a new method for retrieving TSM concentration under high spatial variations of atmospheric haze. This method was based on a coupled radiative transfer model of water turbidity and atmospheric haze.

4. Lastly, this study contributes in testing the spectral unmixing approach for separating haze from sediment in the water pixel. The top-of-atmosphere radiance signal of ocean scenes in coastal areas can often be decomposed in two major constituents, atmospheric haze and sediment in the water. Both have a different spectral signature, so in principle it is possible to apply spectral unmixing to given spectra in order to separate the signal variations into contributions from two components, haze and sediment. The result of successful application of this method will be useful: more remote sensing images can be used for water quality retrieval, otherwise many images have to be rejected because of haze variations in the image, which is a frequent problem in equatorial regions.

7.3.2. Contribution in the WOTRO – NWO program in the East Kalimantan Program

The East Kalimantan Program is one of the major projects of WOTRO, with the main mission to develop a collaborative research between Indonesian and Dutch institutions in coastal and marine research. As has been mentioned in Chapter 1 (*see* subsection 1.3), there are three research objectives in the program of the Berau Research Cluster. In order to achieve the objectives, the Berau Research Cluster was divided into 6 working groups that involved physical, biological and socio-economical aspects.

Remote sensing of tropical coastal waters is one of the subjects dedicated to mapping of ocean colour parameters such as total suspended sediment concentration and Chl-*a* concentration from remote sensing data and *in situ* observations. For this, several approaches and methods have been applied in this study, in order to find the more appropriate algorithms and models for retrieving TSM and Chl-*a* from MERIS data. The results will contribute to the objectives of the whole research program.

7.3.3. Contribution in the management of the Berau Marine Protected Area

In order to maintain the Berau MPA, coastal managers need information on the bio-physical properties of the coastal and marine waters in this region. Up to now, such information is usually obtained from limited manual observation, which is time and cost consuming. Results of the *in situ* measurements in this research will contribute to the actual database of the region. Moreover, several findings on the application of remote sensing techniques in this area can be directly used as new approaches for retrieving several important parameters. Monitoring water quality and the environment in this Berau MPA will be facilitated in the future.

7.4. Future works

For monitoring water quality using MERIS data in equatorial tropical regions, several interconnected issues were addressed in this study. This study could not cover, of course, all aspects related to MERIS data in Case-2 waters and in this area with very high cloud cover, but at least several aspects have been investigated in this study such as establishing the IOP and SIOP, testing the existing algorithms for Case-2 waters, applying the radiative transfer model for atmospheric correction, a semi-analytical model for estimating water quality and lastly a spectral unmixing approach to suppress spatial haze variations. However, there are some important issues that still need further investigation in the future. These are summarized as follows:

(1). Inversion and forward model of Bio-optical properties

This study established an inverse bio-optical model for retrieving IOP and SIOP. However, these parameters were not validated yet due to the unavailability of sufficient *in situ* measurements of IOP. Thus, in future studies, more *in situ* measurements of IOP have to be done. With such *in situ* IOP data, more research could be undertaken on the subject related to the bio-optical modelling in these regions.

(2). Effect of bottom reflectance on the ocean colour remote sensing data

So far, the atmospheric correction by using the radiative transfer model MODTRAN was tested in this study. The result was only partly successful: several results of modelling were not properly in accordance with the *in situ* data. One of the reasons for this may come from the fact that there are some important factors which were not taken into account yet in the modelling. One of these important factors is the sea bottom effect in clear water. In several studies, it was discovered that the bottom effect may contribute to changes in observed radiance or reflectance of the water. In future work, the bottom types should be investigated and should be integrated in the analysis.

(3). Integrating remote sensing data and hydrological model

Throughout this study, it appeared that the availability of match-up data between satellite overpass and *in situ* measurements is a bottleneck to obtaining more satisfactory results. The very frequent and dynamic cloud cover in the study area has caused that only few images were usable for match-up with *in-situ* data. This fact, which is caused by local climatic and atmospheric conditions, will always be a problem when using remotely sensed data in this tropical equatorial region. One of the possible ways out for resolving this problem is integrating the limited remotely sensed data with hydrological and hydrodynamic modelling. In the context of this study for example, it should be possible to confront the image indicating the TSM concentration distribution resulting from the image analysis with the result of a hydrological model simulation of the land part. The hydrological model of the land part should be capable to indicate river fluxes and temporal patterns of sediment from land to ocean. Also, coupling of the remote sensing observations to a hydrodynamic model of the estuary may be very useful for explaining the ecosystem dynamics of this important marine protection area. In a future study, implementing land hydrological and/or estuary hydrodynamic models may thus contribute to the validation of satellite data and *vice versa*.

(4). Assessing water turbidity impact on the coral reef life

Coral reefs are very important for fishery and for tourism. An increase of turbidity may have several impacts on coral reef life in this ecosystem. The deforestation in the catchment of the Berau river increases the water turbidity and may thus negatively affect this ecosystem, although we lack old quantitative data and information to confirm this hypothesis. There is reason for concern about the possible environmental impact on the ecology of Berau estuary and the barrier reef systems. So far, the nature and magnitude of the water turbidity impact on the coral reef live remains unknown, especially in this study area. Therefore, an assessment of the impact of increasing water turbidity on this fragile ecosystem, especially on the coral reef life, should become an important topic of research in the future.

7.5. Recommendations

After the completion of this study, some items should be taken into account in future research of remote sensing for ocean colour. In this sub topic, the *in situ* measurements, atmospheric correction and the models for deriving TSM and Chl-*a* concentrations are discussed.

7.5.1. *In situ* measurement

In situ measurement is a very important step in the study of remote sensing of ocean color. It is used for algorithm development, calibration and validation of algorithms and data products. Nevertheless, one should be aware that *in situ* data may also contain some errors that can be related to several aspects of measurement: various instrument errors, human error during measurement, as well as environmental factors which often cannot be controlled during measurements. The *in situ* measurements should follow the appropriate measurement protocol for each parameter and be concurrent with image acquisition.

The radiometric measurements should comprise incoming irradiance, and water leaving radiance above water and below the water surface. The position of the sun as well as the wave direction and ship or boat should be taken into account. Finding locations which are cloud free is another condition which should be considered. In order to establish the IOP and SIOP of the study area, the *in situ* measurements of IOP are needed for validating the IOP/SIOP estimation. The water quality parameters such as TSM concentration, Chl-*a* concentration and CDOM absorption should be collected at the same location as the optical measurements. The field locations should represent the water variability of the study area.

7.5.2. Image data

This study recommends using ocean colour remote sensing data with high spatial resolution and multiple spectral bands. MODIS and MERIS data are suitable enough for monitoring ocean waters. However for coastal waters, at least MERIS FR should be recommended and used for studying water quality, where RR (reduced resolution) is appropriate for large open water and oceans.

7.5.3. Models and algorithms

Based on the result of this study, we recommend to improve the physical basis of the semi-empirical K-M model by integrating Chl-*a* and CDOM in addition to TSM. This is possible by including these components in the ratio b_b/a. (i.e., the ratio of light backscatter to absorption)

Atmospheric correction is a pre-processing step that is very important in the study of water quality from remote sensing. Especially spatial variations of atmospheric haze can be a problem, since they might be wrongly interpreted as water quality variations. The applied spectral unmixing approach to decouple haze and sediment variations over an image was already quite successful, but more study is needed to explore the operational aspects of this new method.

7.6. Conclusion

The estimation of IOP and associate SIOP can be successfully done from *in situ* radiometric measurement of AOP combined with an inverse bio-optical model. This study contributed in providing IOP/SIOP for the waters of a tropical equatorial region. The MERIS RR L1 data can be used for estimating water quality parameters such as TSM concentration, Chl-*a* concentration. The existing algorithms such as MERIS L2, C2R and FUB are straightforward, and easy to execute for huge areas such as the Indonesian waters. The results have however different degrees of accuracy depending on atmospheric and water dynamics. In order to improve the accuracy, the atmospheric correction by

using the MODTRAN radiative transfer model is suggested. This method has been explored in this study, resulting in a sufficiently improved accuracy. The semi-analytical approach, based on the K-M model, and a new spectral unmixing technique were proposed in this study for improving the accuracy of estimating TSM concentrations. Applying these new approaches to the tropical coastal waters of Indonesia was quite successful. However, there is still need for more intensive research in order to make these techniques operational.

Bibliography

Aiken, J., Fishwick, J.R., Lavender, S., Barlow R., Moore, G.F., Sessions, H., Bernard, S., Ras, J. & Hardman-Mountford, N.J. 2007. Validation of MERIS reflectance and chlorophyll during the BENCAL cruise October 2002: preliminary validation of new demonstration products for phytoplankton functional types and photosynthetic parameters. *Int. J. Remote Sens.,* **28**, 497–516.

Albert, A. & Mobley, C.D. 2003. An analytical model for substance irradiance and remote sensing reflectance in deep and shallow case-2 waters. *Opt. Express* 11(22), 2873-2890.

Albert, A. 2004. Inversion technique for optical remote sensing in shallow water. Ph.D. Thesis, University of Hamburg, Department of Earth Sciences. http://www.sub.unihamburg.de/opus/volltexte/2005/2325/.

Alcántara, E., Barbosa, C., Stech, J., Novo, E. & Shimabukuro, Y. 2009. Improving the spectral unmixing algorithm to map water turbidity Distributions Environmental. *Modelling & Software*, **24**, 1051–1061.

Alikas, K. & Reinart, A. 2008. Validation of the MERIS products on large European lakes: Peipsi, Vänern and Vättern. *Hydrobiologia,* **599**, 161–168, doi:10.1007/s10750-007-9212-0.

Antoine, D. & Morel, G. 2005. MERIS Algorithm Theoretical Basis Document (ATBD) 2.7 – Atmospheric correction of the MERIS observation over ocean Case 1 waters. Issue 5, Revision 0.

Arroyo-Mora, J.P., Kalacska, M. & Chazdon, R. 2009. Spectral unmixing of forest canopy recovery in selectively logged units in a tropical lowland forest, Costa Rica. Anais XIV Simpósio Brasileiro de Sensoriamento Remoto, Natal, Brasil, INPE, 2539-2546.

Astoreca, R., Ruddick, K., Rousseau, V., Mol, B.V., Parent, J.Y. & Lancelot, C. 2006. Variability of the inherent and apparent optical properties in a highly turbid coastal area: impact on the calibration of remote sensing algorithms. *EARSeL eProceedings* 5. 1-17.

Babin, M. & Stramski, D. 2004. Variations in the mass-specific absorption coefficient of mineral particles suspended in water. *Limnol. Oceanogr.,* **49**, 756–767.

Babin, M., Stramski, D., Ferrari, G.M., Claustre, H., Bricaud, A., Obolenski, G. & Hoepffner, N. 2003. Variation in the light absorption coefficient of phytoplankton, nonalgal particles, and dissolved organic matter in coastal waters around Europe. *J. Geophys. Res.,* **108**, 3211, doi:10.1029/2001JC000882.

Berk, A., Anderson, G.P., Acharya, P.K., Chetwynd, J.H., Bernstein, L.S., Shettle, E.P., Matthew, M.W. & Adler-Golden, S.M. 2000. MODTRAN4 USER's MANUAL. Hanscom AFB: Air Force Research Laboratory, Space Vehicles Directorate, Air Force Materiel Command, MA 01731–3010, 97 pp.

Bhatti, A.M., Rundquist, D., Schalles, J, Ramirez, L & Nasu, S. 2009. A comparison between above-water surface and subsurface spectral reflectances collected over inland waters. *Geocarto Int.,* **24**, 133–141.

Bricaud A., Morel, A., & Barale, V. 1999. MERIS potential for ocean colour studies in the open ocean. *Int. J. Remote Sens.*, **20**, 1757–1769.

Bricaud, A., Claustre, H., Ras, J., Oubelkheir, K. 2004. Natural variability of phytoplanktonic absorption in oceanic waters: Influence of the size structure of algal populations. *J. Geophys. Res.*, **109**, C11010, doi: 10.1029/2004JC002419.

Brockmann, C. 2009. The BEAM 3 Architecture (online). http://www.brockmann-consult.de/beam/doc/BEAM-Architecture-1.2.pdf [accessed 3 August 2009].

Carder, K.L., Chen, F.R., Lee, C.P., Hawes, S. & Kamykowski, D. 1999. Semi-analytic MODIS algorithms for chlorophyll a and absorption with bio-optical domains based on nitrate-depletion temperatures. *J. Geophys. Res.,* **104(C3)**, 5403-5421.

Chang, C.G., Dickey, T.D., Mobley, C.D., Boss, E. & Pegau, W.S. 2003. Toward closure of upwelling radiance in coastal waters. *Appl. Opt.*, **42**, 1574 – 1582.

Chengfeng, L., Yunmei, L., Yong, Z., Deyong, S., Changchun, H. & Heng, L. 2009. A four-band semi-analytical model for estimating chlorophyll a in highly turbid lakes: The case of Taihu Lake, China. *Remote Sens. Environ.*, **Issue 6**, 1175-1182 doi:10.1016/j.rse.2009.02.005.

D'Sa , E.J., Hu, C., Muller-Karger, F.E. & Carder, K.L. 2002. Estimation of colour dissolved organic matter and salinity fields in Case 2 waters using SeaWiFS: examples from Florida Bay and Florida Shelf. *Earth Planet Science*, **111**, 197-207.

D'Sa, E.J., Miller, R.L, & Del Castillo, C. 2006. Bio-optical properties and ocean color algorithms for coastal waters influenced by the Mississippi River during a cold front. *Appl. Opt.*, **45**, 7410–7428.

Darecki, M. & Stramski, D. 2004. An evaluation of MODIS and SeaWiFS bio-optical algorithms in the Baltic Sea. *Remote Sens. Environ.*, **89**, 326–350.

Dekker, A.G. 1993. Detection of Optical Water Quality Parameters for Eutrophic Waters by High Resolution Remote Sensing. Ph.D. Thesis, Free University, Amsterdam, the Netherlands. pp. 1-240.

Doerffer, R. & Schiller, H. 2007. The MERIS Case 2 water algorithm. *Int. J. Remote Sens.*, **28**, 517–535.

Doerffer, R. & Schiller, H. 2008. MERIS Algorithm Theoretical Basis Document (ATBD)– MERIS regional coastal and lake Case 2 water project atmospheric correction ATBD. Version 1.0.

Doerffer, R., Sørensen, K. & Aiken, J. 1999. MERIS potential for coastal zone applications. *Int. J. Remote Sens.*, **20**, 1809–1818.

Ffield, A. & Gordan, A. L. 1992. Vertical mixing in the Indonesian thermocline. *J. Phys. Oceanogr.*, **22**, 184–195.

Fischer, J. & Fell, F. 1999. Simultaion of MERIS measurements above selected ocean waters. *Int. J. Remote Sens.*, **20**, 1787–1807.

Floricioiu, D., Reidl, C. & Rott, H. 2003. ENVISAT MERIS capabilities for monitoring the water quality of perialphine Lakes. *Proc. of IEEE IGARSS, 2003, 21 – 25 July 2003 Toulouse France.*

Folkestad, A., Pettersson, L.H. & Durand, D.D. 2007. Inter-comparison of ocean colour data products during algal blooms in the Skagerrak, *Int. J. Remote Sens.*, **28**, 569–592.

Gallegos, C.L. & Correl, D.L. 1990. Modelling spectral diffuse attenuation, absorption and scattering coefficients in a turbid estuary. *Limnol. Oceanogr.*, **35**, 1486-1502.

Gege, P. 2005. The Water Colour Simulator WASI. User Manual for Version 3. DLR Internal Report IB 564-01/05. 83 pp.

Glantz, M., Katz, R. & Nicholls, N. (*Eds.*). 1991. Teleconnections Linking Worldwide Climate Anomalies. Cambridge University Press, Cambridge.

Goodman, J. 2004. Hyperspectral Remote Sensing of Coral Reefs: Deriving Bathymetry, Aquatic Optical Properties and a Benthic Spectral Unmixing Classification Using AVIRIS Data in the Hawaiian Island. PhD thesis, University of California.

Gordon, H. R. 1997. Atmospheric correction of ocean color imagery in the Earth Observing System era. *J. Geophys. Res.*, **102**, 17081– 17106.

Gordon, H.R. & Morel, A.Y. 1983. Remote Assessment of Ocean Color for Interpretation of Satellite Visible Imagery: A Review. Springer Press, New York.

Gordon, H.R. & Wang, M. 1994. Retrieval of water-leaving radiance and aerosol optical thickness over the oceans with SeaWiFS: A preliminary algorithm. *Appl. Opt.*, **33**, 443–452.

Gordon, H.R. 1991. Absorption and scattering estimates from irradiance measurements: Monte Carlo simulation. *Limnol. Oceanogr.*, **36**, 769-777.

Gordon, H.R., Brown, O.B. & Jacobs, M.M. 1975. Computed relationship between the inherent and apparent optical properties of a flat homogeneous ocean. *Appl. Opt.*, **14**, 417-427.

Haan, J.F. de, Kokke, J.M.M., Dekker, A.G. & Rijkeboer, M. 1999. Remote sensing algorithm development: operationalisation of tools for the analysis and processing of remote sensing data of coastal and inland waters. NBN 90 54 11 267 0.

Haltrin, V.I. & Arnone, R.A. 2003. An algorithm to estimate concentrations of suspended particles in seawater from satellite optical images. In: I. Levin & G. Gilbert (eds.), Current Problems in Optic Natural Waters. *Proc. of the II International Conference ONW*, St Petersburg, Russia.

Hamre, B., Frette, Ø., Erga, S.R., Stamnes, J.J. & Stamnes, K. 2003. Parameterization and analysis of the optical absorption and scattering coefficients in a Western Norwegian fjord: a case II water study. *Appl. Opt.*, **42**, 883-892.

Hautala, S. L., Sprintall, J., Potemra, J. T., Chong, J. C., Pandoe, W., Bray, N. & Gani Ilahude, A. 2001. Velocity structure and transport of the

136

Indonesian throughflow in the major straits restricting flow into the Indian Ocean, *J. Geophys. Res.*, **106**, 19,527–19,546.

Heege, T. 2000. Flugzeuggestützte Fernerkundung von Wasserinhaltsstoffen im Bodensee," Ph.D. thesis (Institut für Methodik der Fernerkundung, Deutsches Zentrum für Luft- und Raumfahrt Oberpfaffenhofen).

Hendiarti, N., Siegel, H. & Ohde, T. 2004. Investigation of different coastal processes in Indonesian waters using SeaWiFS data. *Deep Sea Res. Part II*, **51**, 85-97. doi:10.1016/J.dsr2.2003.10.003.

Hoogenboom, J. & Dekker, A.G. 1997. Simulation of the medium resolution imaging spectrometer (MERIS) performance for detecting chlorophyll a over turbid inland waters. *SPIE Proc.* 2963, 440–447.

Hooker, S.B. & Maritorena, S. 2000. An Evaluation of Oceanographic Radiometers and Deployment Methodologies. *J. Atmospheric and Ocean Technology*, **17**, 811–830.

Ibelings, B., Vos, R., Boderie, P., Hakvoort, H. & Hoogenboom, E. 2001. The RALLY Project: Remote Sensing of Algal Blooms in Lake IJssel – Integration with *In Situ* Data and Computational Modeling. RIZA report 2001.036, RIZA Institute for Inland Water Management and Waste Water Treatment.

IGOS. 2006. A Coastal Theme for the IGOS Partnership - For the Monitoring of our Environment from Space and from Earth. Paris, UNESCO 2006. 60 pp. (IOC Information document No. 1220).

IOCCG. 2000. Remote sensing of ocean colour in coastal and other optically-complex water. In: Sathyendranath, S (ed), Report of the International Ocean Colour Coordinating Group, No.3, IOCCG, Dartmouth, Canada.

IOCCG. 2006. Remote Sensing of Inherent Optical Properties: Fundamentals, Tests of Algorithms, and Applications. Lee, Z.P. (ed.), Reports of the International Ocean-Colour Coordinating Group, No. 5, IOCCG, Dartmouth, Canada.

Ismuranty, C. 2003. Building the co-management for the conservation and sustainable use of the Derawan Islands, East Kalimantan, Indonesia. Second International Tropical Marine Ecosystems Management Symposium (ITMEMS 2), Manilla, Philippines. March 24-27, 2003.

Jerlov, N. G. 1976. Marine Optics, Elsevier, Amsterdam, 231 p.

Kahru, M. & Mitchell, B.G. 2001. Seasonal and non-seasonal variability of satellite derived chlorophyll and colored dissolved organic matter concentration in the California current. *J. Geophys. Res.*, **106**, 2517-2529.

Kärdi, T. 2007. Remote sensing of urban areas: linear spectral unmixing of Landsat Thematic Mapper images acquired over Tartu (Estonia). *Proc. Estonian Acad. Sci. Biol. Ecol. 56(1)*, 19-32.

Keshava, N. & Mustard, J.F. 2002. Spectral unmixing. *IEEE Signal Processing Magazine*.

Kirk, J.T.O. 1984. Dependence of relationship between inherent and apparent optical properties of water on solar altitude. *Limnol. Oceanogr.*, **29**, 350-356.

Kirk, J.T.O. 1994. Light & Photosynthesis in aquatic ecosystems. University Press., Cambridge UK.

Koponen, S., Attila, J., Pulliainen, J., Kallio, K., Pyhälahti, T., Lindfors, A., Rasmus, K., & Hallikainen, M. 2007. A Case Study of Airborne and Satellite Remote Sensing of a Spring Bloom Event in the Gulf of Finland. *Cont. Shelf Res.*, **27**, 228–244.

Koponen, S., Pulliainen, J., Kallio, K. & Hallikainen, M. 2002. Lake water quality classification with airborne hyperspectral spectrometer and simulated MERIS-data. *Remote Sens. Environ.*, **79**, 51–59.

Kratzer, S., Brockmann, C. & Moore, G. 2008. Using MERIS full resolution data to monitor coastal waters - A case study from Himmerfjärden, a fjord-like bay in the northwestern Baltic Sea. *Remote Sens. Environ.*, **112**, 2284–2300.

Krawczyk, H., Neumann, A., Gerasch, B., Walzel, T. 2007. Regional products for the Baltic Sea using MERIS data. *Int. J. Remote Sens.*, **28**, 593–608.

Lee, Z.P., Carder, K.L., and Arnone, R. 2002. Deriving inherent optical properties from water color: A multi-band quasi-analytical algorithm for optically deep waters. *Appl. Opt.*, **41**, 5755–5772.

LIPI. 1995. Marine survey to support Marine Resources Evaluation and Planning (MREP) in Derawan islands region. Indonesian Scientific Institue – LIPI Jakarta (Indonesia Language).

Longhurst, A. 1993. Seasonal cooling and blooming in tropical oceans, *Deep Sea Res*. Part I, **40**, 2145–2165.

Lu, D., Morana, E. & Batistella, M. 2003. Linear mixture model applied to Amazonian vegetation classification. *Remote Sens. Environ.*, **87**, 456.469.

Lunetta, R. S. 1998. Applications, project formulation, and analytical approach. In *Remote Sensing Change Detection: Environmental Monitoring Methods and Applications* (Lunetta, R.S. & Elvidge, C.D., *eds*), pp. 1-19. Taylor & Francis, London.

Lyon, P. & Hoge, F. 2006. The Linear Matrix Inversion Algorithm. *In*: Lee Z.P. (*ed*.). 2006. Remote Sensing of Inherent Optical Properties: Fundamentals, Tests of Algorithms, and Applications. *IOCCG Report Number 5*, 49–55.

Makassar Strait. *Geophys. Res. Lett.*, **26**, 3325–3328.

Maritorena, S. & Siegel, D.A. 2005. Consistent merging of satellite ocean color data sets using a bio-optical model. *Remote Sens. Environ.*, **94**, 429–440.

Maritorena, S., Siegel, D.A. & Peterson, A.R. 2002. Optimization of a semi-analytical ocean color model for global-scale applications. *Appl. Opt.*, **41**, 2705-2714.

Matsumoto, H. 1997. Portable U-10 Water Quality Checker and WP-100 Water Quality Monitor. Readout Horiba Technical Report.

Matthew, M.W., Adler-Golden, S.M., Berk, A., Richtsmeier, S.C., Levine, R.Y., Bernstein, L.S., Acharya, P.K., Anderson, G.P., Felde, G.W., Hoke, M.P., Ratkowski, A., Burke, H-H., Kaiser, R.D., Miller, D. P. 2000. Status of atmospheric correction using a MODTRAN4-based algorithm. SPIE Proceeding, Algorithms for Multispectral, Hyperspectral, and Ultraspectral Imagery VI, Volume 4049.

Mercado, J. M., Ramı́rez, T. & Corte′s, D. 2007. Changes in nutrient concentration induced by hydrological variability and its effect on light absorption by phytoplankton in the Albora′n Sea (Western Mediterranean Sea). *J. Marine Syst.* doi:10.1016/j.jmarsys.2007.05.009.

Meyer, G., 1996. Variation of Indonesian through flow and ElNiño–Southern Oscillation. *J. Geophys. Res*., **101**, 12255–12263.

Miller, R.L., Del Castillo, C.E. and McKee, B.A., 2005. Remote Sensing of Coastal Aquatic Environments. Springer, Dordrecht.

Mitchell, B.G. & Kiefer, D.A. 1988. Variability in the pigment specific fluorescence and absorption spectra in the northeastern Pacific Ocean. *Deep Sea Res. Part A*, **35**, 665-689.

Mobley, C.D. 1994. Light and Water - radiative transfer in natural waters. *Academic Press, San Diego.*

Morel, A. & Prieur, L. 1977. Analysis of variations in ocean color. *Limnol. Oceanogr.*, **22**, 709-722.

Morel, A. 1974. Optical properties of pure water and pure seawater, in Optical Aspects of Oceanography, edited by N.G. Jerlov and E. Steemann-Nielsen, pp. 1 – 24, Academic, San Diego, Calif.

Morel, A. 1980. In-water and remote sensing measurements of ocean color. *Boundary-Layer Meteorology*, **18**, 177–201.

Mueller, J.L. 2000. SeaWiFS algorithm fort the diffuse attenuation coefficient (Kd490) using water leaving radiances at 490 and 560 nm. *Greenbelt, Maryland: NASA–GSFC*.

Murray, S.P. & Arief, D. 1988. Through flow into the Indian Ocean through the Lombok Strait. *Nature* 333 (6172), 444–447.

Nontji, A. 2000. Coral Reefs of Indonesia: Past, Present and Future. Paper presented at the 9th International Coral Reef Symposium, Bali, Indonesia, 23-27 October 2000.

Novo, E.M. & Shimabukuro, Y.E. 1994. Spectral Mixture Analysis of Inland Tropical Waters *Int. J. Remote Sens.*, **v15**, 1351-1356.

Novo, E.M.L.M., de Farias Barbosa, C.C , de Freitas, R.M., Shimabukuro, Y.E., Melack, J.M., & Filho, W.P. 2006. Seasonal changes in chlorophyll distributions in Amazon floodplain lakes derived from MODIS images. *Limnology*, **7**, 153–161.

P3O-LIPI. 1995. Survey Kelautan untuk menunjang MREP Kawasan Kepulauan Derawan. P3O – LIPI, Ambon.

Ohde, T., Siegel, H. & Gerth, M. 2007. Validation of MERIS Level-2 products in the Baltic Sea, the Namibian coastal area and the Atlantic Ocean. *Int. J. Remote Sens.*, **28**, 609 –624..

Oyama, Y., Matsushita, B., Fukushima, T., Nagai, T. & Imai, A. 2007. A new algorithm for estimating chlorophyll-a concentration from multispectral satellite data in case II waters: a simulation based on a controlled laboratory experiment. *Int. J. Remote Sens*, **28**, 1437–1453.

Pandey, V.K., Bhatt, V., Pandey, A.C. and. Das, I.M.L. 2007. Impact of Indonesian through-flow blockage on the Southern Indian Ocean. *Current Science*, **93**, 399 – 406.

Parente, M. 2004. An investigation of the Properties of Expectation-Maximization and Gauss Mixture Vector Quantization in Density Estimation and Clustering, EE391 Report, Stanford University.

Pope, R.M., &. Fry, E.S. 1997. Absorption spectrum (380– 700 nm) of pure water, II, integrating cavity measurements, *Appl. Opt.*, **36**, 8710– 8723.

Preisendorfer, R.W. 1976. Hydrologic Optics. U.S. Department of Commerce, National Oceanic and Atmospheric Administration, Environmental Research Laboratories, Pacific Marine Environmental Laboratory.

Prieur, L. & Sathyendranath, S. 1981. An optical classification of coastal and oceanic waters based on the specific spectral absorption curves of phytoplankton pigments, dissolved organic matter, and other particulate materials. *Limnol. Oceanogr.*, **26**, 671-689.

Rahman, H. & Dedieu, G. 1994, SMAC: A simplified method for the atmospheric correction of satellite measurements in the solar spectrum. *Int. J. Remote Sens.*, **15**, 123–143.

Rast, M., Bezy, J.L. and Bruzzi, S. 1999. The ESA Medium Resolution Imaging Spectrometer MERIS – a review of the instrument and its mission. *Int. J. Remote Sens.*, **20**, 1681–1702..

Salama, M.S., Dekker, A., Su, Z., Mannaerts, C.M. & Verhoef, W. 2009. Deriving Inherent Optical Properties and Associated Inversion-Uncertainties in the Dutch Lakes. Hydrology and Earth System Sciences, 13, 1113-1121

Salama, M.S., Monbaliu, J. & Coppin, P., 2004, The atmospheric correction of AVHRR images. International Journal of Remote Sensing Vol. 25, No 7-8, 1349-1355.

Salama, M.S., & Shen F. 2010 (a). Stochastic inversion of ocean color data using the cross-entropy method. Optics Express. **18** (2), 479-499.

Salama, M.S. & Shen, F. 2010 (b). Simultaneous atmospheric correction and quantification of suspended particulate matter from orbital and geostationary Earth Observation sensors. Estuarine, Coastal and Shelf Sciences, 86(3), 499-511

Salama, M.S. & Stein, A. 2009. Error decomposition and estimation of inherent optical properties. Applied Optics, **48**, 4947-4962

Sathyendranath, S. & Platt, T. 1989. Remote sensing of ocean chlorophyll: consequence of non uniform pigment profile. *Appl. Opt.*, **28**, 490–495.

Sathyendranath, S., Lazzara, L. & Prieur, L. 1987. Variations in the spectral values of specific absorption of phytoplankton. *Limnol. Oceanogr.*, **32** , 403-415.

Schiller, H. & Doerffer, R. 1999. Neural network for emulation of an inverse model - operational derivation of Case II water properties from MERIS data. *Int. J. Remote Sens.*, **20**, 1735–1746.

Schroeder T., Schaale M. & Fischer, J. 2007. Retrieval of atmospheric and oceanic properties from MERIS measurements: A new Case-2 water processor for BEAM. *Int. J. Remote Sens.,* **28**, 5627–5632..

Schroeder, T. & Schaale, M. 2005. MERIS Case-2 Water Properties Processor, Version 1.0.1, *Institute for Space Sciences, Freie Universität Berlin (FUB)* http://www.brockmann-consult.de/beam/software/plugins/FUB-WeW-Water-1.0.1.zip.

Sharkov, E.A. 1998. Remote Sensing of Tropical Region. John Wiley & Sons in association with Praxis Publishing, Chichester.

Shen, F., Verhoef, W., Zhou, Y.X., Salama, M.S., Liu, X. Satellite estimates of wide-range suspended sediment concentrations in estuarine and coastal waters using MERIS data (*submitted*).

Situmorang, R.L. & Burhan, G. 1995. Peta Geologi Lembar Tanjung Redep, Kalimantan. Pusat Penelitian dan Pengembangan Geologi. Bandung.

Smith, R. C. & Baker, K. S. 1981. Optical properties of the clearest natural waters (200–800 nm). *Appl. Opt.*, **20**, 177–184.

Sørensen, K., Aas, E. & Høkedal, J. 2006. Validation of MERIS water products and bio-optical relationships in the Skagerrak. *Int. J. Remote Sens.*, **28**, 555–568.

Souza, C.Jr., Firestone, L., Silva, L.M. & Roberts, D. 2003. Mapping forest degradation in the Eastern Amazon from SPOT 4 through spectral mixture models. *Remote Sens. Environ.*, **87**, 494-506.

Stramski, D., Sciandra, A. & Claustre, H. 2002. Effects of temperature, nitrogen, and light limitation on the optical properties of the marine diatom Thalassiosira pseudonana. *Limnol. Oceanogr.*, **47**, 392–403.

Susanto, R. D., Moore II, T.S., & Marra, J. 2006. Ocean color variability in the Indonesian Seas during the SeaWiFS era. Geochem. Geophys. Geosyst., **7**, Q05021, doi:10.1029/2005GC001009.

Thiemann, S. & Kaufman, H. 2000. Determination of chlorophyll contentand tropic state of lakes using field spectrometer and IRS – IC satellite data in the Mecklenburg Lake Distract Germany. *Remote Sens. Environ.*, **73**, 227 - 235.

Tilstone, G.H., Moore, G.F., Sorensen K., Ruttgers, R., Viskum, P.Y., Martinez-Vicente, V. & Ruddick, K.G. 2004. Regional Validation of MERIS Chlorophyll products in North Sea coastal waters: MAVT Inter-calibration report paper presented at Proceedings of the ENVISAT validation workshop European Space Agency, Frascati, Italy.

Tyler, A.N., Svab, E., Preston, T., Présing, M. & Kovács, W.A. 2006. Remote sensing of the water quality of shallow lakes: A mixture modelling approach to quantifying phytoplankton in water characterized by high suspended sediment, *Int. J. Remote Sens.*, **27**, 1521–1537.

UNESCO. 2002. The Hanoi Statement http://whc.unesco.org/uploads/events/documents/event_501_1.pdf.

Van der Meer, F. & De Jong, S.M. 2000. Improving the results of spectral unmixing of Landsat Thematic Mapper imagery by enhancing the orthogonality of end-members, *Int. J. Remote Sens.*, **21**, 2781–2797.

Van der Woerd, H.J. & Pasterkamp, R. 2008. HYDROPT: A fast and flexible method to retrieve chlorophyll-a from multi-spectral satellite observations of optically complex coastal waters. *Remote Sens. Environ.*, **112**, 1795–1807.

Verhoef, W. & Bach, H. 2003. Simulation of hyperspectral and directional radiance images using coupled biophysical and atmospheric radiative transfer models. *Remote Sens. Environ.*, **87**, 23–41.

143

Vermote, E.F., El Saleoql, N., Justice, C.O., Kaufman, Y.J., Privette, J.L., Remer, L., Roger, J.C., & Tank, D. 1997. Atmospheric correction of visible to middle-infrared EOS-MODIS data over land surfaces: Background, operational algorithm and validation. *J. Geophys. Res*., **102**, 17,131–17,141.

Veron, J. E. N. 1995. Corals in Space and Time: Biography and Evolution of the Scleractinia, 321 pp., Cornell Univ. Press, Ithaca, N. Y.

Westland, S., Lovine, L. & Bisshop, J.M. 2002. Kubelka-Munk or Neural Networks for Computer Colorant formulation. 9th Congress of the International Colour Association, *Proc. of SPI Vol. 4421.*

Wiryawan, B., Stanley, S.A., Yulianto, I., Susanto, H.A. 2004. Derawan Island Profile, Berau Regency, East Kalimantan. The Nature Conservancy, and Pemerintah Kabupaten Berau, Tanjung Redeb- Kalimantan, Indonesia, 71pp.

WWF. 2006. Berau Marine Protected Area. http//assets.panda.org/downloads/mpaberau_map.doc [accessed 30 October 2006].

Wyrtki, K. 1987, Indonesian through-flow and associated pressure gradient. *J. Geophys. Res*., **92**, 12941–12946.

Yang, L. & Kruse, B. 2004. Revised Kubelka-Munk theory: I. Theory and Application. Linköping University , Sweden . *J. Opt. Society of America,* A21, 1933–194141, doi:10.1364/JOSAA.21.001933.

Zaneveld, J.R.V., Barnard, A.H., & Boss, E. 2005. Theoretical derivation of the depth average of remotely sensed optical parameters. *Optic Express*, **13**, 9052–9061.

Summary

The coastal zone is a shallow area where land, ocean and atmosphere strongly interact. It is covering approximately 7% of the surface of the global ocean. The coastal zones are increasingly attracting interest because they are the most populated and utilized areas on earth. Despite of its relatively small surface area, the coastal zone plays a considerable role in the biogeochemical cycles because virtually all land-derived materials (water, sediments, dissolved and particulate nutrients, pollutants) enter this region through surface runoff or groundwater flow. Thus, preservation of the ecological quality status of these zones including the quality of the coastal waters is a key issue of coastal zone management. Monitoring this zone requires approaches that can monitor their complex and heterogeneous processes and rapid changes. Remote sensing is one approach that can be used to monitor effectively the dynamics of the coastal zone.

Many coastal zones in Indonesia and in the world are characterized by a high concentration of suspended matter which is transported by rivers into the sea. There are many approaches and algorithms available for monitoring the Case-1 waters (open ocean). Those algorithms fail however, when applied to Case-2 waters (coastal and inland waters). Recently, many studies have been done in development of algorithms for Case-2 waters by using empirical, semi-empirical, as well as analytical approaches. However, most of the algorithms were developed and validated in high-latitude coastal and inland waters, and only few have been tested in equatorial tropical regions. In order to fill this gap, this research focused on the study of ocean colour remote sensing for monitoring water quality parameters in the tropical equatorial region with frequent cloud cover.

This thesis used explorative approaches and algorithms in the monitoring of water quality in the Case-2 waters. The research was driven by field observations, MERIS satellite data analysis and application of algorithms for quantifying the water quality parameters. In order to achieve the objective, the methodology is divided into 4 steps: (1) establishing an inverse bio-optical

model for estimating IOP and SIOP from *in situ* measurement of AOP and biogeochemical parameters and then applying the approach to the MERIS data for retrieving water quality parameters; (2) a semi-analytical approach, especially a neural network analysis and validated with *in situ* measurements; (3) a coupled radiative transfer model for atmospheric correction and a semi-analytical approach, based on the Kubelka-Munk model for estimating TSM concentration, and (4) a spectral unmixing model combined with the inverse K-M model which was applied for retrieval of TSM concentration.

The methods were developed for particular conditions of the Berau estuary, but they can be applied to other Case-2 waters in Indonesia or other environments, since the research location was chosen based on its representativeness for the major phenomena in Indonesian waters. A series of field observations were done in the period of 2006 into 2008. Totally, more than 100 field locations were measured, although not all of the *in situ* measurements were in concordance with satellite overpasses.

The results showed that estimating water qualities parameters (e.g. TSM and Chl-*a* concentrations) can be done by following a simple empirical approach and by more complex semi-empirical approaches. It was concluded that a semi-analytical bio-optical model via estimation of IOP and associate SIOP give a better estimation TSM and Chl-*a* concentration.

The existing Case-2 algorithm regional processors (e.g. C2R and FUB) and the global algorithm (MERIS L2), as well as a purely empirical approach can be used to understand the spatial distribution of water quality in a more quantitative way. However, these are only partly successful because the standard atmospheric corrections in these algorithms do not work properly under conditions of partial cloud cover and highly complex turbid waters. In this study it was found that application of a spectral unmixing algorithm helped in reducing the effects of haze variations while leaving the spectral effects of sediment variation intact. Combined with a standard atmospheric correction based on the MODTRAN radiative transfer model, the inverse semi-empirical K-M model was next applied for estimating TSM concentration. This methodology proved to be quite robust, although for TSM concentrations below 50 mg l^{-1} the standard Case-2 algorithms are equally successful.

Samenvatting

De kuststroken van oceanen bestaan uit ondiep zeewater waar land, zee en de atmosfeer voortdurend in met elkaar in wisselwerking zijn. Zij beslaan ongeveer 7% van het totale zeeoppervlak. Kustzones trekken meer en meer de aandacht omdat zij de dichtst bevolkte en meest intensief gebruikte gebieden op aarde vormen. Ondanks hun relatief geringe oppervlak spelen kustgebieden een aanzienlijke rol in de biogeochemische cycli, omdat praktisch alle van het land afkomstige stoffen (water, sediment, al dan niet opgeloste voedingsstoffen, afval) deze gebieden binnenkomen door rivierafvoer en grondwaterstroming. Het verbeteren van de ecologische kwaliteit en de waterkwaliteit in deze gebieden is daarom van groot belang voor het beheer van de kustzones. Monitoring van deze zone vereist een benadering waarbij goed wordt gelet op heterogene processen en snelle veranderingen, en aardobservatie technieken zijn hiervoor zeer geschikt.

Veel kustgebieden in Indonesië en elders in de wereld worden gekenmerkt door hoge concentraties van zwevende stof in het water dat door rivieren naar zee wordt getransporteerd. Er zijn veel benaderingen en algoritmes beschikbaar voor het monitoren van Case-1 wateren (oceanen). Deze algoritmen falen echter als ze worden toegepast op Case-2 wateren (kust- en binnenwateren). In het recente verleden zijn veel studies uitgevoerd om algoritmen te ontwikkelen voor Case-2 wateren door het gebruik van empirische, semi-empirische en analytische methodes. Echter, de meeste van deze algoritmen zijn ontwikkeld en gevalideerd voor kust- en binnenwateren in gebieden op hogere geografische breedte, en slechts weinig zijn er getest voor gebieden in de tropen. Om deze leemte op te vullen is het onderhavig onderzoek gericht op aardobservatie technieken voor het bepalen van waterkwaliteit in tropische gebieden met frequente bewolking.

Dit proefschrift beschrijft verschillende benaderingen en algoritmen welke zijn getest voor het monitoren van waterkwaliteit in Case-2 wateren. Het onderzoek steunt op veldwaarnemingen, MERIS satelliet data analyse, en de toepassing van algoritmen voor het bepalen van waterkwaliteitsparameters. Om de doelstelling te bereiken zijn vier stappen gevolgd: (1) het vaststellen van een

lokaal invers bio-optisch model voor het schatten van inherente optische eigenschappen (IOP)en specifieke inherente optische eigenschappen (SIOP) uit *in situ* metingen van schijnbare optische eigenschappen (AOP), en vervolgens het toepassen hiervan op MERIS data voor het bepalen van waterkwaliteitsparameters; (2) een semi-analytische benadering, in het bijzonder een op een neuraal netwerk gebaseerde benadering, gevalideerd met *in situ* metingen; (3) een gekoppeld model voor stralingsoverdracht in water en in de atmosfeer, waarbij voor het water een semi-empirisch Kubelka-Munk (K-M) model is gebruikt voor het verband met het sedimentgehalte; en (4) een spectraal decompositiemodel gecombineerd met het inverse K-M model om het sedimentgehalte te bepalen.

De ontwikkelde methodes gelden voor de speciale omstandigheden van het Berau estuarium, maar kunnen ook worden toegepast op andere Case-2 wateren in Indonesië en elders, aangezien de onderzoekslocatie is gekozen op grond van representativiteit voor de voornaamste verschijnselen in de Indonesische wateren. Locale veldmetingen zijn verricht in de periode 2006-2008. In totaal is er op meer dan 100 locaties gemeten, hoewel niet alle *in situ* metingen samenvielen met satellietoverkomsten onder geschikte condities.

De resultaten tonen aan dat het schatten van waterkwaliteitsparameters (bijv. zwevende stof en chlorofylgehalte) kan worden uitgevoerd via een simpele empirische benadering en tevens via wat ingewikkelder semi-empirische benaderingen. Geconcludeerd is dat een semi-analytisch bio-optisch model via het schatten van IOP en bijbehorende SIOP een betere schatting kan geven van zwevend stof en chlorofyl-a concentratie.

De bestaande Case-2 algoritmen voor regionale toepassing (bijv. C2R en FUB) en het globale algoritme (MERIS L2), evenals a puur empirische benadering kunnen worden gebruikt om de ruimtelijke verdeling van de waterkwaliteit op een kwantitatieve wijze inzichtelijk te maken. Echter, deze zijn slechts matig succesvol omdat de standaard methoden voor atmosfeercorrectie in deze algoritmen niet goed werken bij gedeeltelijke bewolking en voor zeer troebel water. In deze studie is geconstateerd dat het toepassen van een spectraal decompositie algoritme de effecten van ruimtelijke variaties van heiigheid in de atmosfeer kan onderdrukken, terwijl de variaties ten gevolge van zwevende

stof intact bleven. Gecombineerd met een standaard atmosfeercorrectie op basis van berekeningen met het MODTRAN model, is vervolgens het inverse K-M model toegepast om het gehalte zwevende stof te bepalen. Deze methode blijkt heel robuust te werken, hoewel voor zwevende stof concentraties beneden de 50 mg per liter de standaard Case-2 algoritmen even goed presteren.

Curriculum Vitae

Wiwin Ambarwulan was born on June 29, 1960 in Jakarta, Indonesia. She spent her elementary and junior high school years in Jakarta, and graduated in 1980 from senior high school in the same city. Then, she continued her study at Bogor Agricultural University (IPB), from where a Bachelor of Soil Science was earned in March 1986. In 1987 she joined the National Coordinating Agency for Surveys and Mapping (BAKOSURTANAL), Indonesia, as a researcher. Under financial sponsorship of the Netherlands government, from August 1990 to Mei 1991 she joined Postgraduate Course in Geographical Landscape Analysis for Indonesian Resources with emphasis on Applied Geomorphologic Survey at International Institute for Aerospace Survey and Earth Sciences (ITC), Enschede, The Netherlands and obtained a Diploma. In the period of 1991 to 2000 she was as researcher and lecturer staff in the field of remote sensing and GIS at BAKOSURTANAL. From September 2000 to March 2002, she got the second scholarship from the Netherlands government to continue her study at International Institute for Geo-information Science and Earth Observation (ITC), Enschede, The Netherlands. She obtained Master of Science in Earth Resources and Engineering Geology (EREG) program in the specialization of Coastal Zone Studies, *with distinction*. Her MSc thesis topic was Mapping of TSM Concentrations from SPOT and Landsat TM Satellite Images for Integrated Coastal Zone Management in Teluk Banten, Indonesia. Beginning February 2006, she obtained the third time scholarship from the Netherlands government and she started her PhD studies in Department of Water Resources, Faculty of Geo-Information Science and Earth Observation (ITC), University of Twente, the Netherlands. Her PhD research was part of the Berau Research Cluster under East Kalimantan Program (EKP) and funded by WOTRO, the Netherland.

Publication

1. **ISI Journal**
    -   **Ambarwulan**, W., Salama, M.S., Mannaerts, C.M.M, Verhoef, W. Estimating the specific inherent optical properties of tropical coastal water using bio-optical model inversion in the Berau coastal waters, Indonesia. Hydrobiology Journal. *Accepted with revision*.
    -   **Ambarwulan,** W., Mannaerts, C.M.M, van der Woerd, H.J., Salama, M.S. MERIS data for monitoring tropical coastal waters: a case study of Berau estuary, East Kalimantan, Indonesia. Geocarto International. *In Press*.
    -   **Ambarwulan**, W., Verhoef, W., Mannaerts, C.M.M, Salama, M.S. Estimating total suspended matter concentration in tropical coastal waters of the Berau estuary, Indonesia. International Journal of Remote Sensing. *Accepted with revision.*
    -   **Ambarwulan, W.**, Verhoef, W., Mannaerts, C.M.M. Spectral unmixing applied to MERIS images of East Kalimantan coastal waters to separate atmospheric haze from water sediment effects. Hydrology and Earth System Sciences (HESS) Journal. *Prepared for Submission*.

2. **M.Sc. Thesis**
    -   **Ambarwulan,W.**, 2002. Mapping of TSM concentrations from SPOT and Landsat TM satellite images for integrated coastal zone management in Teluk Banten, Indonesia. ITC. 2002. 129 p.

ITC Dissertation List

http://www.itc.nl/research/phd/phd_graduates.aspx